AD-A201 993

NAVAL POSTGRADUATE SCHOOL
Monterey, California

UNITED STATES NAVY · NAVAL POSTGRADUATE SCHOOL·

THESIS

AN EXPERIMENTAL INVESTIGATION OF A
FIGHTER AIRCRAFT MODEL AT
HIGH ANGLES OF ATTACK

by

David Humbert Leedy

September 1988

Thesis Advisor: S. K. Hebbar

Approved for public release; distribution is unlimited

89   1   09   198

REPORT DOCUMENTATION PAGE

1a REPORT SECURITY CLASSIFICATION UNCLASSIFIED		1b RESTRICTIVE MARKINGS			
2a SECURITY CLASSIFICATION AUTHORITY		3 DISTRIBUTION/AVAILABILITY OF REPORT Approved for public release; distribution is unlimited			
2b DECLASSIFICATION/DOWNGRADING SCHEDULE					
4 PERFORMING ORGANIZATION REPORT NUMBER(S)		5 MONITORING ORGANIZATION REPORT NUMBER(S)			
6a NAME OF PERFORMING ORGANIZATION Naval Postgraduate School	6b OFFICE SYMBOL (If applicable) 67	7a NAME OF MONITORING ORGANIZATION Naval Postgraduate School			
6c ADDRESS (City, State, and ZIP Code) Monterey, CA 93943-5000		7b ADDRESS (City, State, and ZIP Code) Monterey, CA 93943-5000			
8a NAME OF FUNDING/SPONSORING ORGANIZATION	8b OFFICE SYMBOL (If applicable)	9 PROCUREMENT INSTRUMENT IDENTIFICATION NUMBER			
8c ADDRESS (City, State and ZIP Code)		10 SOURCE OF FUNDING NUMBERS			
		PROGRAM ELEMENT NO	PROJECT NO	TASK NO	WORK UNIT ACCESSION NO

11 TITLE (Include Security Classification)

AN EXPERIMENTAL INVESTIGATION OF A FIGHTER AIRCRAFT MODEL AT HIGH ANGLES OF ATTACK

12 PERSONAL AUTHOR(S)
Leedy, David H.

13a TYPE OF REPORT Master's Thesis	13b TIME COVERED FROM _____ TO _____	14 DATE OF REPORT (Year, Month, Day) 1988, September	15 PAGE COUNT 168

16 SUPPLEMENTARY NOTATION The views expressed in this thesis are those of the author and do not reflect the official policy or position of the Department of Defense or the U.S. Government

17 COSATI CODES			18 SUBJECT TERMS (Continue on reverse if necessary and identify by block number)
FIELD	GROUP	SUB-GROUP	High Angle of Attack Aerodynamics Flow Visualization, Laser Sheet Balance Measurements

19 ABSTRACT (Continue on reverse if necessary and identify by block number)

>A low speed wind tunnel investigation was conducted to examine the aerodynamic characteristics of the flowfield around a three percent scale YF-17 lightweight fighter prototype model at high angles of attack using flow visualization and force and moment measurements. Smoke filaments, injected into the wind tunnel test section, were illuminated by a laser sheet to highlight flow phenomena about the model. Force and moment measurements were made using a precision six-component strain gage balance. The investigation marked the first attempt at qualitative flow analysis using the laser sheet flow visualization system recently installed in the Naval Postgraduate School low speed wind tunnel facility. The investigation was undertaken to specifically identify flow phenomena

20 DISTRIBUTION/AVAILABILITY OF ABSTRACT ☒ UNCLASSIFIED/UNLIMITED ☐ SAME AS RPT ☐ DTIC USERS	21 ABSTRACT SECURITY CLASSIFICATION UNCLASSIFIED	
22a NAME OF RESPONSIBLE INDIVIDUAL S. K. Hebbar	22b TELEPHONE (Include Area Code) 408/646-2997	22c OFFICE SYMBOL 67Hb

DD FORM 1473, 84 MAR 83 APR edition may be used until exhausted
All other editions are obsolete

and/or regions of interest that may have bearing on the design and performance of supermaneuverable aircraft. The data indicate a good correlation between the observed flow phenomena and force and moment measurements at various angles of attack, thus establishing the credibility of such experimental investigations for high angle of attack aerodynamic research.

Accession For	
NTIS GRA&I	X
DTIC TAB	☐
Unannounced	☐
Justification	
By	
Distribution/	
Availability Codes	
Dist	Avail and/or Special
A-1	

DTIC
COPY
INSPECTED
4

An Experimental Investigation
of a Fighter Aircraft Model
at High Angles of Attack

by

David H. Leedy
Lieutenant Commander, United States Navy
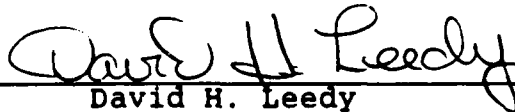B. S., University of Cincinnati, 1974

Submitted in partial fulfillment of the
requirements for the degree of

MASTER OF SCIENCE IN AERONAUTICAL ENGINEERING

from the

NAVAL POSTGRADUATE SCHOOL
September 1988

Author: _____
                    David H. Leedy

Approved By: _____
                    S. K. Hebbar, Thesis Advisor

_____
E. Roberts Wood, Chairman,
Department of Aeronautics and Astronautics

_____
Gordon E. Schacher,
Dean of Science and Engineering

iii

ABSTRACT

A low speed wind tunnel investigation was conducted to examine the aerodynamic characteristics of the flowfield around a three percent scale YF-17 lightweight fighter prototype model at high angles of attack using flow visualization and force and moment measurements. Smoke filaments, injected into the wind tunnel test section, were illuminated by a laser sheet to highlight flow phenomena about the model. Force and moment measurements were made using a precision six-component strain gage balance. The investigation marked the first attempt at qualitative flow analysis using the laser sheet flow visualization system recently installed in the Naval Postgraduate School low speed wind tunnel facility. The investigation was undertaken to specifically identify flow phenomena and/or regions of interest that may have bearing on the design and performance of supermaneuverable aircraft. The data indicate a good correlation between the observed flow phenomena and force and moment measurements at various angles of attack, thus establishing the credibility of such experimental investigations for high angle of attack aerodynamic research.

TABLE OF CONTENTS

ACKNOWLEDGMENT

I. INTRODUCTION

A. BACKGROUND

The survivability and tactical effectiveness of a modern fighter aircraft must be evaluated in a great many scenarios ranging from engagements which occur beyond the visual range of the pilots, to close-in, air-to-air combat or "dogfighting". In the close-in engagement, maneuverability becomes one of the most important factors in deciding the outcome of aerial combat [Ref. 1 and 2]. Maneuvering aggressively can rapidly deplete an aircraft's energy and result in rapid deceleration to low speeds and high angles of attack. Flight in this regime often results in exceeding the aircraft performance capabilities producing stalls and loss of control. Expanding the maneuvering envelope boundaries of tactical aircraft to include controlled flight in the low speed, high angle of attack regime is a primary concern of today's aircraft designers. Studies have shown that the ability to perform rapid, transient maneuvers, even into post-stall flight, can greatly enhance an aircraft's air combat capability and significantly improve mission success. These capabilities are highly dependent upon maintaining a high degree of control effectiveness throughout the maneuvering angle of attack range and about all aircraft axes [Ref. 3].

1

The optimum and maximum angles of attack are highly dependent on the scenario and vary greatly between offensive and defensive maneuvering. Offensive maneuvering requires the pilot to accurately position himself for employment of the specific weapon he has chosen to use in the engagement. This may require absolutely smooth tracking and precise control response in the case of guns or a momentary point and shoot maneuver in the case of IR missiles. Defensive maneuvers, on the other hand, are more commonly carried out at higher angles of attack which are usually past the point of airframe buffet where the concern is not handling accuracy but radical maneuvering to deny the enemy a weapons solution. Defining and expanding the maneuvering envelope at high angles of attack can provide the modern combat pilot the tactical flexibility needed to achieve superiority [Ref. 2].

The drive to obtain supermaneuverability has begun in great earnest. Post-stall (PST) capability up to at least 70 degrees angle of attack and direct force (DFM) control to allow yaw and pitch control independent of flight path have been identified as two related capabilities which hold the greatest promise. PST is seen as a capability required to maneuver the aircraft into an either offensive or defensive position as the situation dictates. DFM would be used primarily to obtain weapons firing solutions once the advantage had been gained [Ref. 4]. In a recent study using numerical optimization techniques it was shown that PST

2

capability enabled large turn rates and reduced the area required for maneuvering [Ref. 5]. The X-31 aircraft has been designated the first supermaneuverable aircraft and will attempt to exploit these two concepts.

Though not designed for supermaneuverability, many recently developed aircraft have achieved improved high angle of attack performance by incorporating innovative aerodynamic design features. The Northrop Corporation developed the hybrid wing concept in the late 1960's and applied it to the YF-17 lightweight fighter prototype in 1972 in direct response to the challenge of achieving maximum lift and angle of attack while maintaining positive stability and control. The hybrid wing planform of the YF-17 results from the combining of a conventional wing with moderate sweepback and aspect ratio with a wing root leading edge extension (LEX), also known as a strake. Figure 1 illustrates these two concepts in their combined form. The conventional wing maintains attached flow to moderate angles of attack where the flow separates resulting in buffet and eventual stall. The LEX induces a vortex flow which increases in strength with increasing angles of attack. The stable vortex flow creates an area of high negative pressure on the wing upper surface which increases lift and delays separation of laminar flow on the basic planform. The flight envelope of the aircraft is expanded by the improved stability and control of the aircraft in the high angle of attack regime. [Ref. 6]

3

BASIC PLANFORM
Attached flow
Moderate sweep and aspect ratio

WING ROOT LEADING EDGE EXTENSION
Separation induced vortex flow
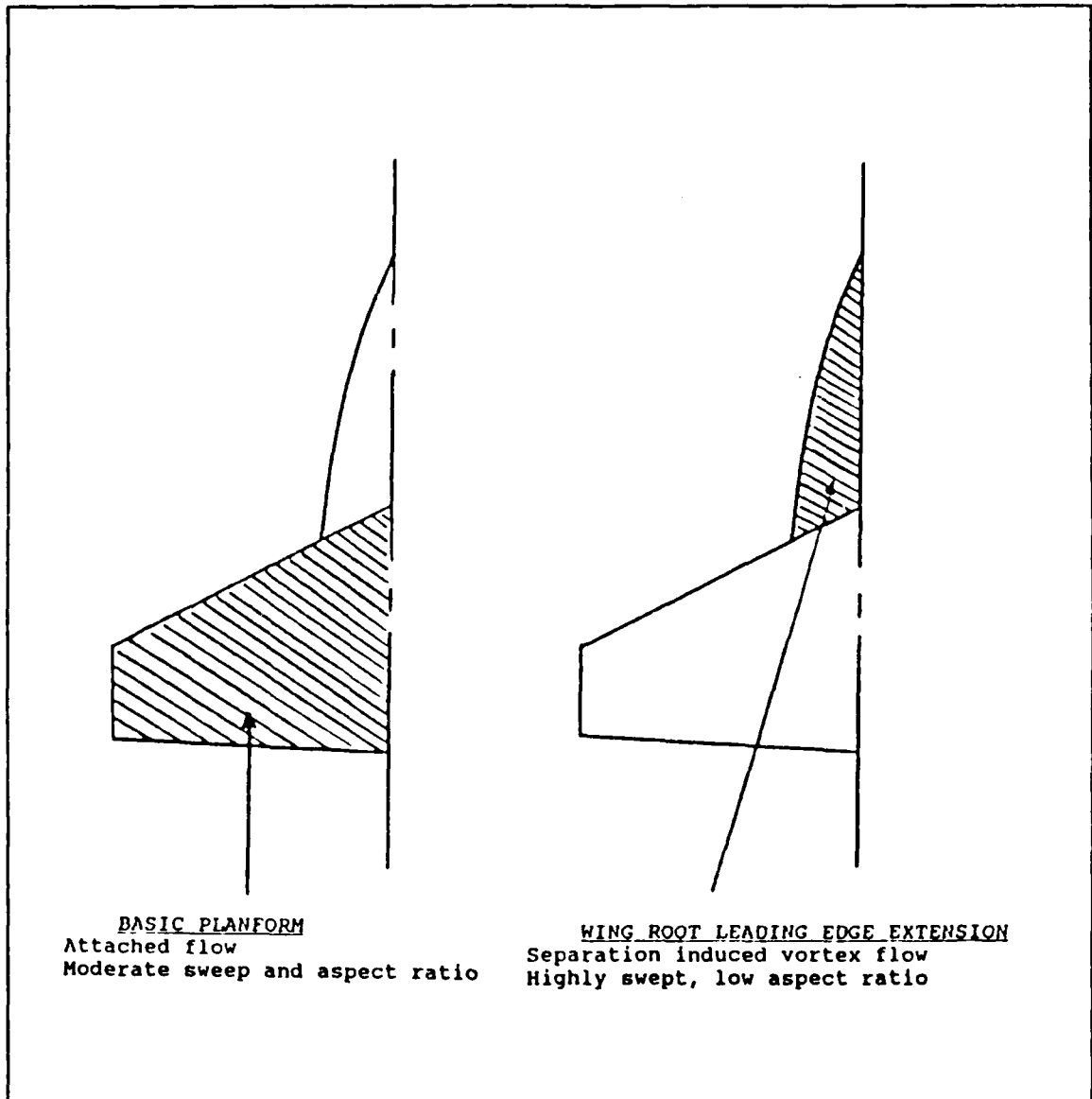Highly swept, low aspect ratio

Figure 1.   Hybrid Wing

As a prelude to engaging in supermaneuverability research at the Naval Postgraduate School, this investigation was undertaken to characterize the flowfield around a fighter aircraft model, specifically, the YF-17. The capabilities of the recently installed laser sheet flow visualization system [Ref. 7] in the low speed wind tunnel facility of the Department of Aeronautics and Astronautics, were adapted for extensive flow visualization of the flowfield about the model. In addition to flow visualization data, measurements were made to obtain force and moment data on the model and the correlation between these two data sets examined to provide insight into areas of aerodynamic interest.

The focus of the current experimental investigation of high angle of attack aerodynamics included:

1. Flow visualization to enhance understanding of the basic aerodynamic phenomena

2. Force and moment measurements at high angles-of attack and moderate roll and yaw angles

3. Study of the correlation between the observed flow and measured forces and moments

Much of the research to date has been concerned with the effect of isolated aerodynamic mechanisms in an attempt to predict and examine their effect. The intent of this investigation was to gain insight into the high angle of attack behavior of a current fighter aircraft as a whole, not just concentrating on the effect of singular concepts at work

5

in the design such as the hybrid wing. Once a complete mapping of the flow over the aircraft has been accomplished the interaction of the various lift and drag generating devices can be interpreted and a methodology created to design for enhanced high angle of attack performance. Particular attention has been paid to the effect of forebody generated vortices and their effect on the forces and moments which were measured. A great deal of work has been done on this phenomena, especially in regard to missiles. The results achieved thus far have been far from conclusive and it is hoped this investigation will add to the available literature in a positive manner.

Expected observations include:

1. Increased asymmetrical vortex shedding from the nose section forward of the LEX's as the angle of attack increases. This should be recognizable by an increase in generated side forces.

2. LEX generated vortices should increase in strength through moderate to high angles of attack eventually bursting thus losing their lift enhancing effect.

3. Flow over the wing should remain attached through moderate angles-of attack separating first at the wingtips then moving in gradually with increasing angle of attack. The LEX induced vortices should keep the inboard flow attached until higher angles of attack are

reached where the vortices will burst and lose their effectiveness.

Although the experimental work accomplished in this thesis has been substantial, it is by no means complete. A continuing effort at the Naval Postgraduate School will examine the flowfield characteristics and behavior at high angles of attack using laser Doppler velocimetry (LDV) and hotwire anemometry. This should lead to a thorough investigation and a better understanding of the effects of high angle of attack flight.

B. HIGH ANGLE OF ATTACK AERODYNAMICS

The separation of flow from the body of an aircraft exerts considerable aerodynamic forces that must be understood and controlled if true supermaneuverability is to be realized in our next generation of tactical aircraft. The increasing design complexity of modern aircraft, which includes vortex generating strakes, forward swept wings, canards and leading edge wing snags complicates the flow behavior in ways that are often not understood until well after an aircraft has entered service. This is so, in spite of knowing the high angle of attack characteristics of fighter aircraft are highly configuration dependent [Ref. 3].

Conventional aircraft controls have limited capability at high angles of attack. The yaw control provided by a conventional rudder decreases with increasing angle of attack as the tail becomes blanketed by the stalled flow from the

7

wing. Previous studies show that improvement of rudder effectiveness may not be possible. Reduced maneuvering capability results from inadequate yaw control just when maximum effectiveness is required. The long, slender nose of the modern fighter aircraft also contributes to the problem by producing powerful vortex flowfields at high angles of attack. The side forces generated by the asymmetric shedding of these vortices coupled with the long moment arm from the nose to the aircraft's center of gravity present a control problem of significant proportion. [Ref. 3 and 8]

The aerodynamics of vortex generation from slender bodies is well documented [Ref. 9, 10 and 11]. Reding and Ericsson [Ref. 11] describe the phenomena as consisting of four regions in which characteristic vortices induce angle of attack dependent forces and moments. At very low angles of attack the flow is vortex free. As the angle of attack increases symmetric vortices are formed at the nose which gain strength as the angle of attack gets higher and higher. Eventually the angle of attack reaches a point at which the vortices become asymmetric which create side forces on the body. These vortices are relatively steady but can alternate positions near the point of maximum side force generation. Finally, the angle of attack increases to the value where the flow separation becomes unsteady. The side forces decrease to zero while the normal force becomes nearly constant [Ref. 12]. Figure 2, reproduced from [Ref. 13], illustrates the
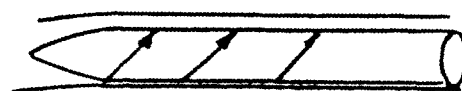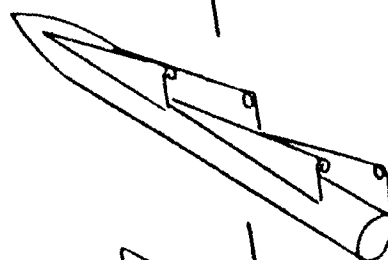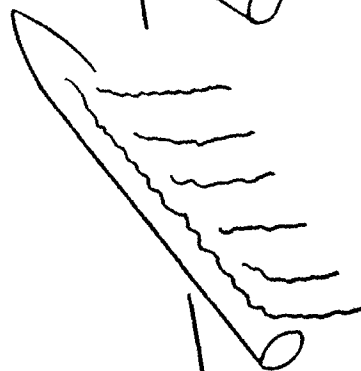
Figure 2. Vortex Generating Regimes

9

various regimes as they affect a slender body of rotation with an ogive nose. Forebody vortex management has been suggested as a means of yaw control for aircraft operating at high angles of attack. Strakes, conformally attached in the nose section, would deploy to generate asymmetric vortex shedding thus providing controlled yaw [Ref. 14].

The lifting surfaces of an aircraft influence the actual effect shedding vortices have. Flow around the sharp leading edge of a delta wing forms vortices which increase in strength with increasing angle of attack (see Figure 3). LEX's, discussed previously, are merely highly swept delta wings purposely designed to take advantage of the increased lift generated by these vortices. The body vortices also interact with the LEX's up to certain angles of attack to improve the lift performance of the basic planform. [Ref. 13]

C. FLOW VISUALIZATION

Flow visualization has been an important tool in the understanding of fluid dynamics for many years. As early as 1883, when Osborne Reynolds used dye in water to visualize flow through a glass tube, scientists have realized the value of visual cues in unraveling the physical mysteries of fluid mechanics [Ref. 15]. There are numerous techniques by which flow is made visible. Flow visualization by laser sheet and water tunnel dye injection are two of the most recent developments which are proving most valuable in high angle of attack research. Sophisticated water tunnels with dye

10
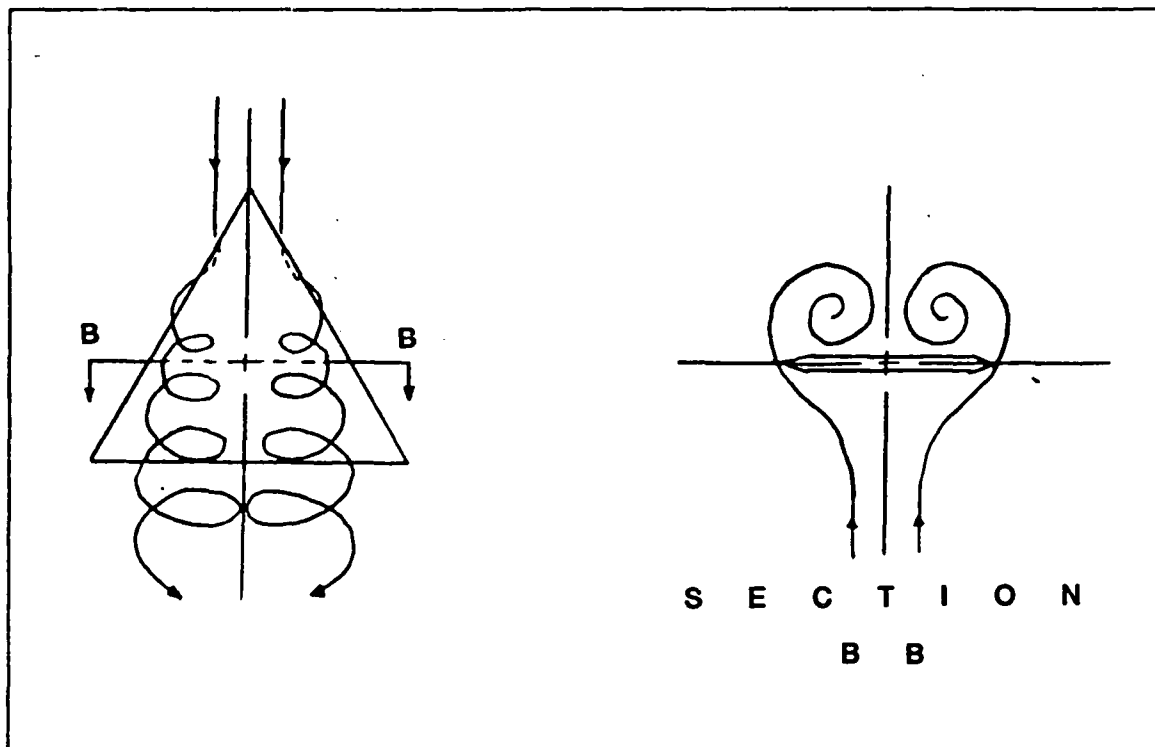
Figure 3.   Vortex Flow about a Delta Wing

ejecting   models   provide   the   researcher   with   a   three
dimensional view of flow phenomenon. Observation of the flow
as it reacts to aircraft movement, offers the capability to
understand the dynamics of flow around the entire body of an
aircraft.   The vortex dominated flows typically generated by
the new missile and aircraft designs of the early 1970's were
responsible for the increasing use of water tunnels because
wind tunnels lacked the capability to provide the required
definition [Ref 16].

Figures   4   and   5   illustrate   the   details   of   complex
flowfields available through water tunnel flow visualization.
The vortices generated by the forebody of the aircraft are

Figure 4. Pitch = 50°

Figure 5. Pitch = 70°

clearly visible as are the differences between the flow patterns at the two angles of attack. These are typical water tunnel flow visualization results achieved in the Naval Postgraduate School water tunnel flow visualization facility with a 1/48 scale model of an F/A-18 aircraft.
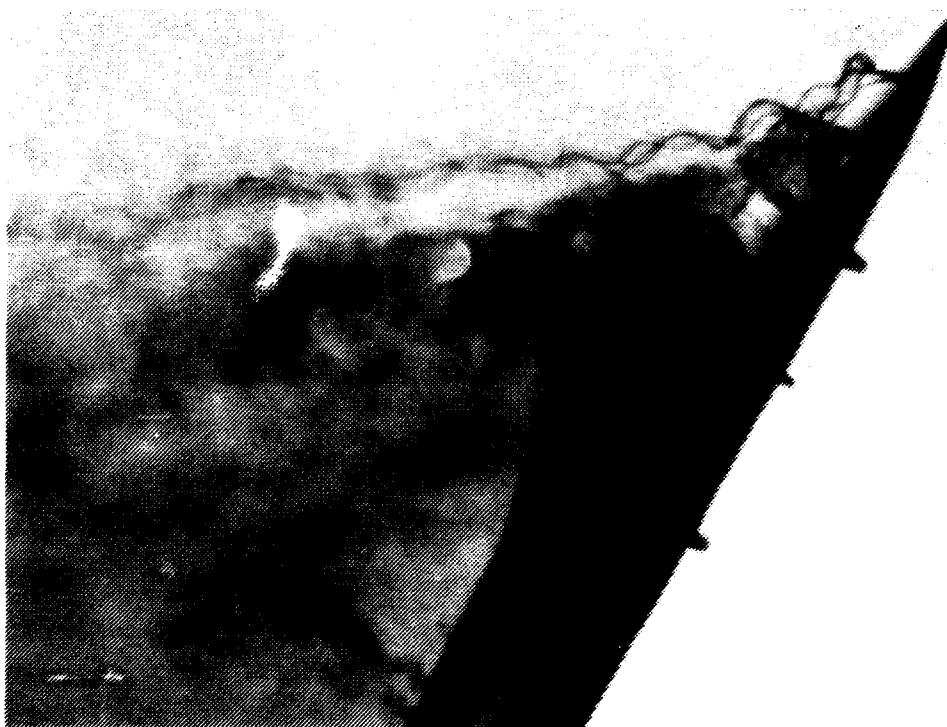
Flow visualization by laser sheet combines a tracer material in the flow with a thin sheet of laser light to provide a two dimensional representation of local flow behavior. Laser light has been a proven method of illumination for years and continues to be used in various capacities for flow research [Ref. 17]. This was the flow visualization method employed in this investigation and will be discussed in detail in the following section.

A recent study by Malcolm and Nelson [Ref. 18] addressed the relationship between the results obtained in testing in both wind tunnels and water tunnels. Using identical models and operating both tunnels at the same Reynolds number, the results showed the vortex characteristics to be almost identical. The study goes on to compare results with both tunnels running at different Reynolds number. For low speeds, vortex behavior exhibited only minor differences between the two mediums. It is concluded that both techniques are eminently suitable for the study of vortex flowfields.

Detailed study of the flowfield cross sections, accomplished for specified flight regimes in this

experimental investigation, is the first step toward understanding the physics of the phenomena and ultimately achieving true supermaneuverability in combat aircraft. Controlled flight at high angles of attack will require the designer to be innovative and resourceful to fully utilize the ever changing flowfield about the aircraft. True supermaneuverability will, no doubt, involve a combination of vectored thrust and active aerodynamic controls.

II. EQUIPMENT AND PROCEDURE

A. APPARATUS

Major equipment required to complete the experimental portion of this thesis included:

1. A low-speed wind tunnel

2. A fighter aircraft model and necessary support structures

3. A flow visualization system

4. A six-component strain gage balance

5. Data acquisition hardware/software

Information concerning the specifications, construction and configuration of all equipment used is provided in this section.

1. Wind Tunnel

Experimental investigations were carried out at the Naval Postgraduate School wind tunnel test facility. The tunnel is a horizontal flow low-speed design from the Aerolab Development Company of Pasadena, California, installed in the mid-1950's. It is a single return tunnel which measures 64 feet in length and varies between 21.5 and 25.5 feet in width (see Figure 6). The wind tunnel is powered by a 100 horsepower electric motor which drives a three-blade variable pitch fan through a four-speed transmission. Turning vanes located in all four corners and a set of stator blades directly downstream of the fan straighten and smooth the
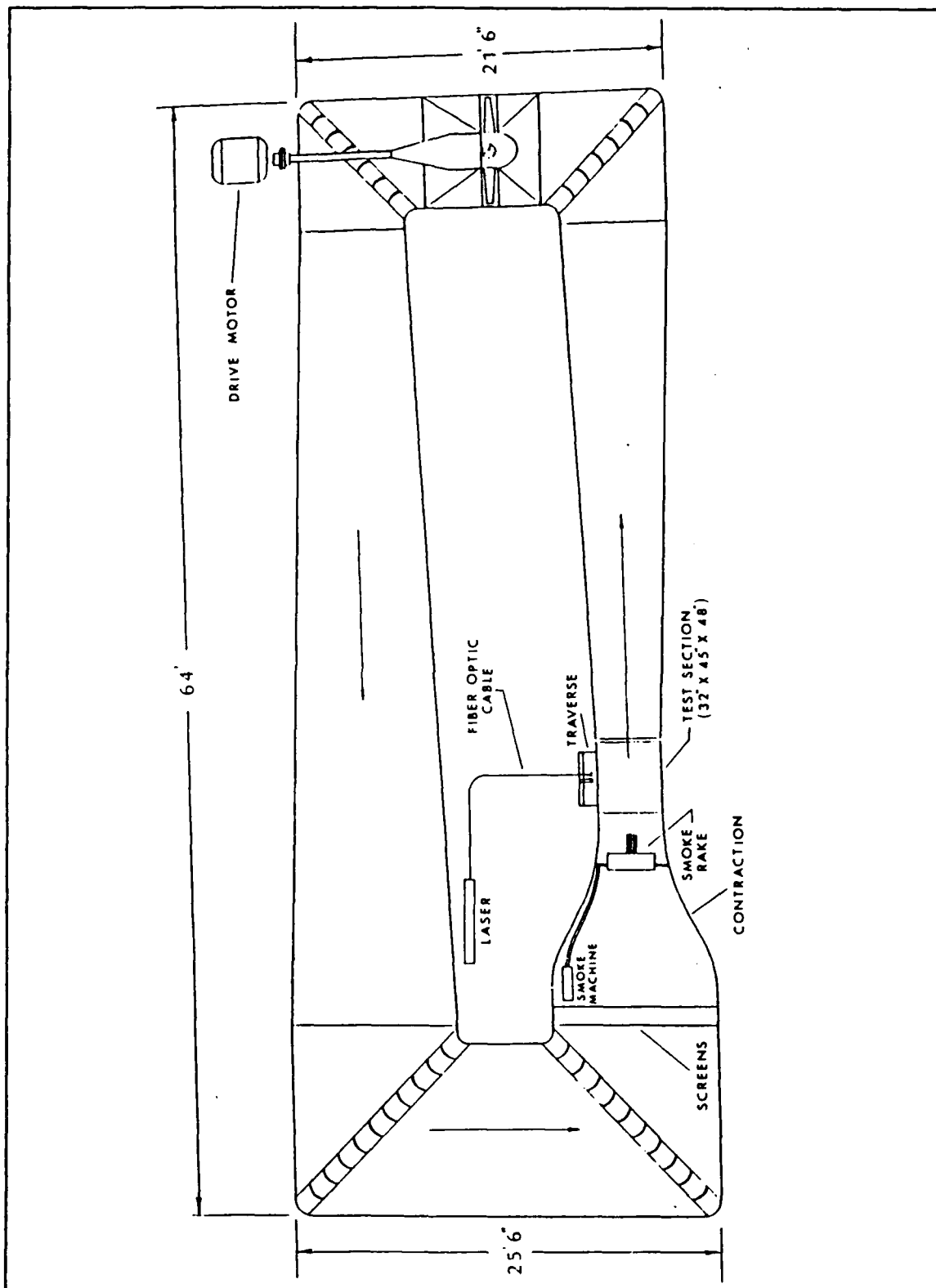
Figure 6.   Low Speed Wind Tunnel

16

airflow. Two fine-mesh wire screens immediately prior to the settling chamber breakdown any remaining turbulent fluctuations. The contraction ratio between the settling chamber and the test section is approximately 10:1. A heavy wire mesh screen at the end of the test section diffuser guards against foreign object damage to the fan blades. [Ref. 19]

The test section of the tunnel operates at atmospheric pressure and measures 45 inches wide by 32 inches high, with corner fillets that contain the test section lighting and alleviate boundary layer effects at the wall intersections. The walls of the test section also diverge slightly to compensate for contraction effects due to boundary layer growth. Breather slots located immediately downstream of the test section allow air to enter the tunnel circuit to make up for losses due to leakage and ensure the test section pressure remains uniform. Available test section height is reduced to 28 inches by a horizontal reflection plane located in the middle of the test section floor. A remotely controlled turntable in the center of the reflection plane allows for model mounting and variable pitch angles. Access to the test section is through hinged windows located on either side or through a removable plexiglass insert on top. [Ref. 19]

Flow measurement components integral to the wind tunnel are a dial thermometer, a water manometer and a test

17

section pitot static tube. The dial thermometer measures temperature in the settling chamber. The water-filled manometer is used to measure the static pressure difference between the test section and the settling chamber. Each section has four static pressure taps, one on each wall, connected to a common manifold. The manifolds feed into the manometer where the pressure difference in centimeters of water gives the test section dynamic pressure. The taps in the test section are located at the entrance to preclude any induced errors from model interference. Actual test section velocity is determined by the following equation: [Ref. 19]

$$U_m = [(2*2.046*cm \ H_2O)/(0.93*\rho)]^{.5}$$

where:

U_m = measured velocity (ft/sec)

2.046 = conversion factor

cm H_2O = manometer reading in cm of H_2O

0.93 = settling chamber total pressure correction

ρ = air density (lb_m/ft^3)

A digital readout of the test section dynamic pressure is provided through a pressure transducer circuit connected to the manometer. Greater accuracy is available with the digital readout once it has been calibrated. The test section pitot tube system provides only approximate velocity readings through an airspeed indicator starting at 40 knots.

2. Fighter Model

The fighter model is a three percent scale model of the Northrop Corporation's YF-17 lightweight fighter prototype (see Figure 7 and 8). The model was fabricated by the company's Aero Sciences branch in the early 1970's from steel and aluminum and has provisions for variable flap settings and wingtip missiles. The balance block section of the model accommodates a one-inch precision balance and contains the balance attachment and locating pin.

The YF-17 was the prototype aircraft from which the McDonnell Douglas F/A-18 evolved. The model was utilized by Northrop for extensive subsonic and supersonic wind tunnel testing of the hybrid wing concept discussed earlier. Key dimensions of the model are listed below: [Ref. 20]

1. Total length = 19.125 in.

2. Wing span   = 12.60 in.

3. Wing area   = 45.36 in.^{2}

4. Wing MAC   = 3.88 in.

5. Frontal area = 2.88 in.^{2}

6. Planform area = 89.28 in.^{2}

7. Side area   = 53.42 in.^{2}

The longitudinal axis scaling in Figure 7 is included to provide a visual reference for discussion of the flow visualization results.
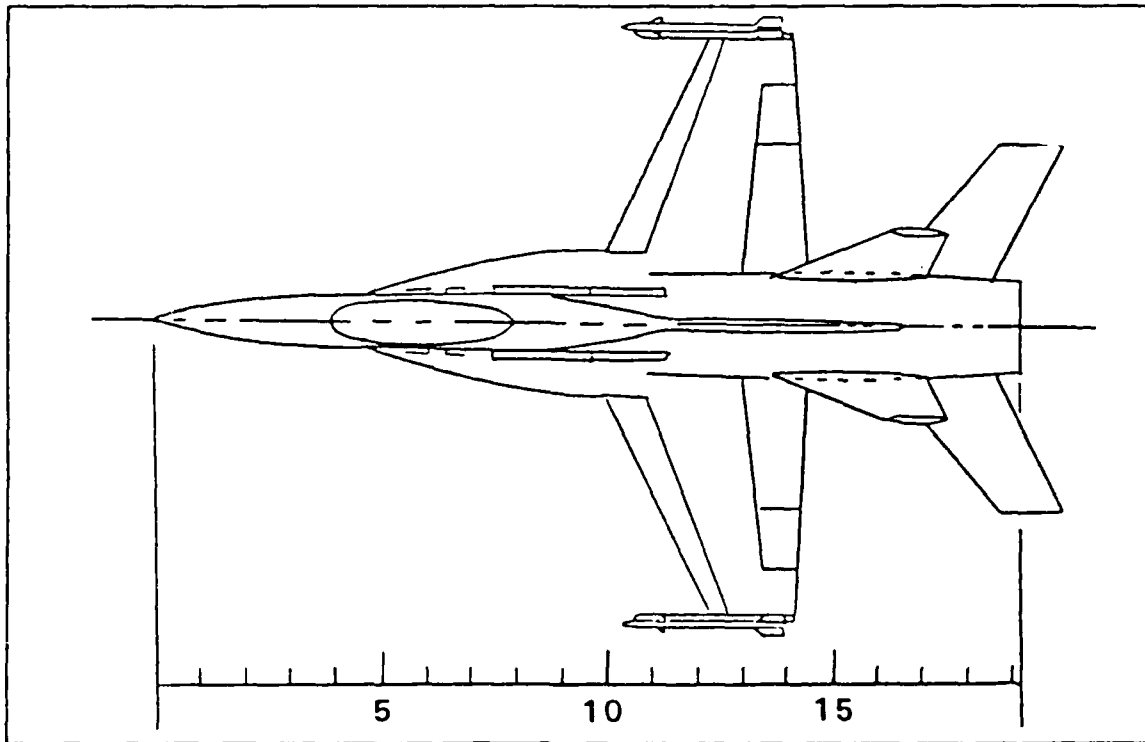
19

Figure 7.   YF-17 Scaled Planform View (TOP)
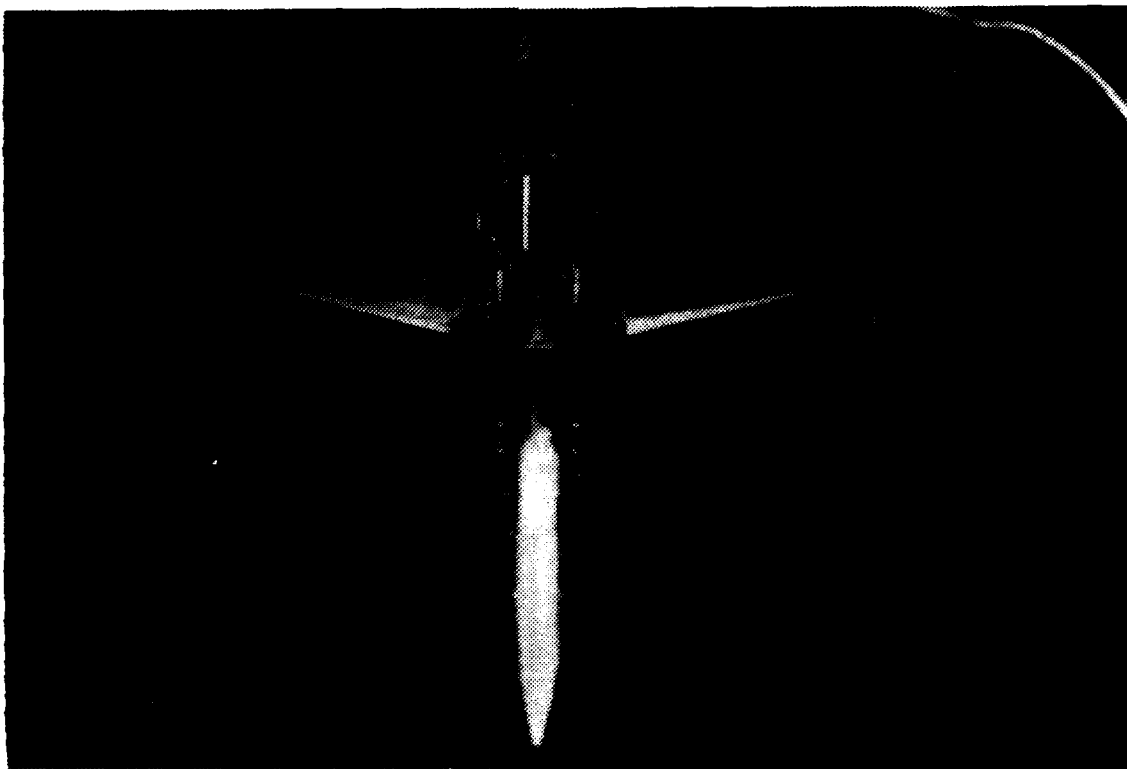
Figure 8.   YF-17 Lightweight Fighter Prototype Model

3. Balance

A one-inch diameter Task Corporation balance was use for force and moment measurements (see Figure 9). The six component strain gage precision balance was on loan to the Naval Postgraduate School from the NASA-Ames Research Center under provisions of the Navy-NASA Joint Institute of Aeronautics. The balance calibration data and data conversion values were provided by NASA and are listed in Appendix A [Ref. 21]. Two strain gages each are dedicated to normal and side force measurements while axial force and rolling moment utilize one gage apiece. Each gage has a separate channel for excitation and output. Table 1 lists

Figure 9. Task Corporation One-Inch Balance

21

the balance channel capacities and accuracies. All accuracies are based on maximum load.

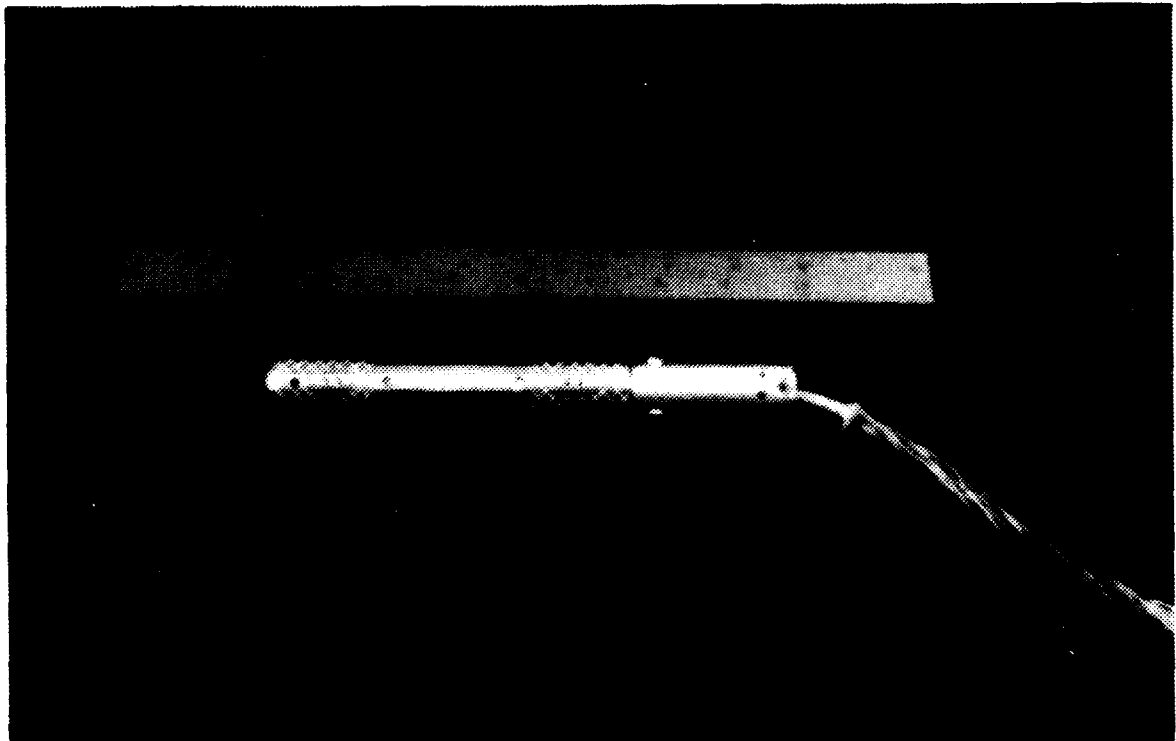The model was constructed with a close tolerance machined channel specifically designed for use with the Task balance. A locating pin through the top of the model secures the model to the balance and locates the balance center with the approximate center of pressure of the model.

4. Model/Balance Support

The model is supported by the balance which is connected to a balance support or sting. The sting extends aft of the model and fits securely into a rigid vertical swinging arm assembly which is securely fixed to the reflection plane turntable at the base and supported by a one-inch steel pin through the three-quarter-inch thick plexiglass viewing window on top (see Figures 10 and 11).

TABLE 1. BALANCE CHANNELS

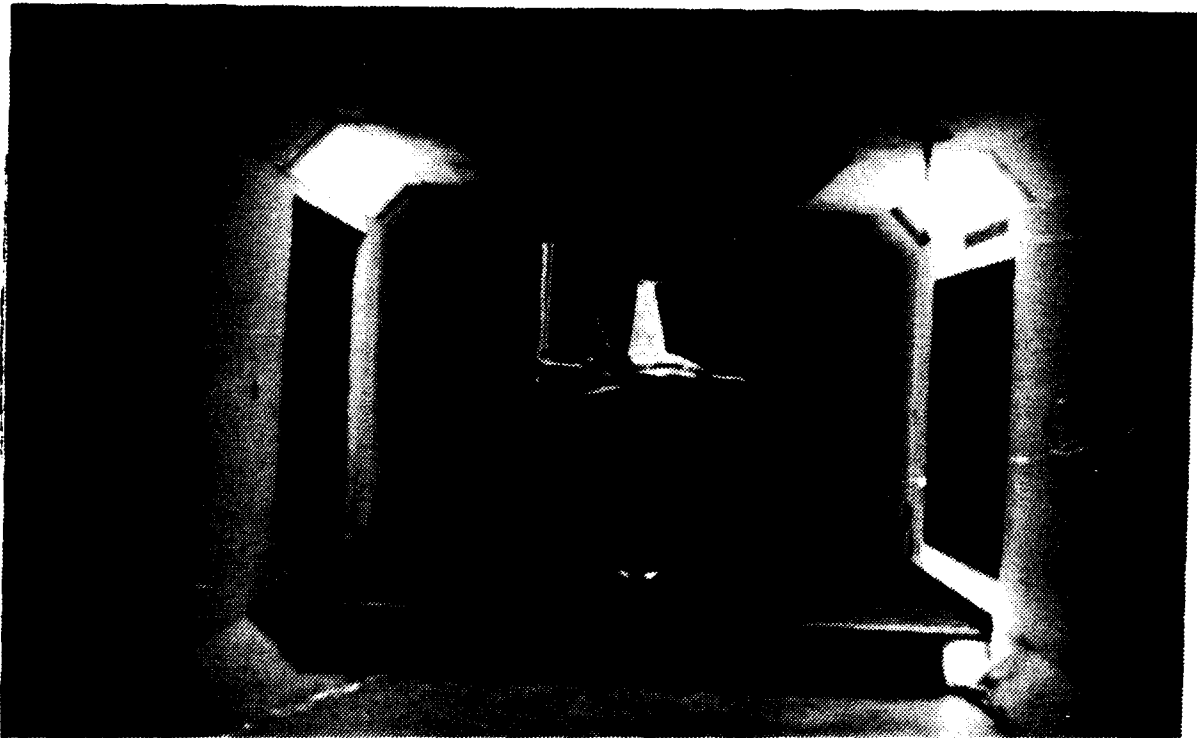| Channel	Component	Maximum Load	%Accuracy
N1	Normal Force	400 lbs.	0.056
N2	Normal Force	400 lbs.	0.049
S1	Side Force	200 lbs.	0.115
S2	Side Force	200 lbs.	0.132
A	Axial Force	100 lbs.	0.153
R	Roll Moment	21 ft-lbs.	0.204

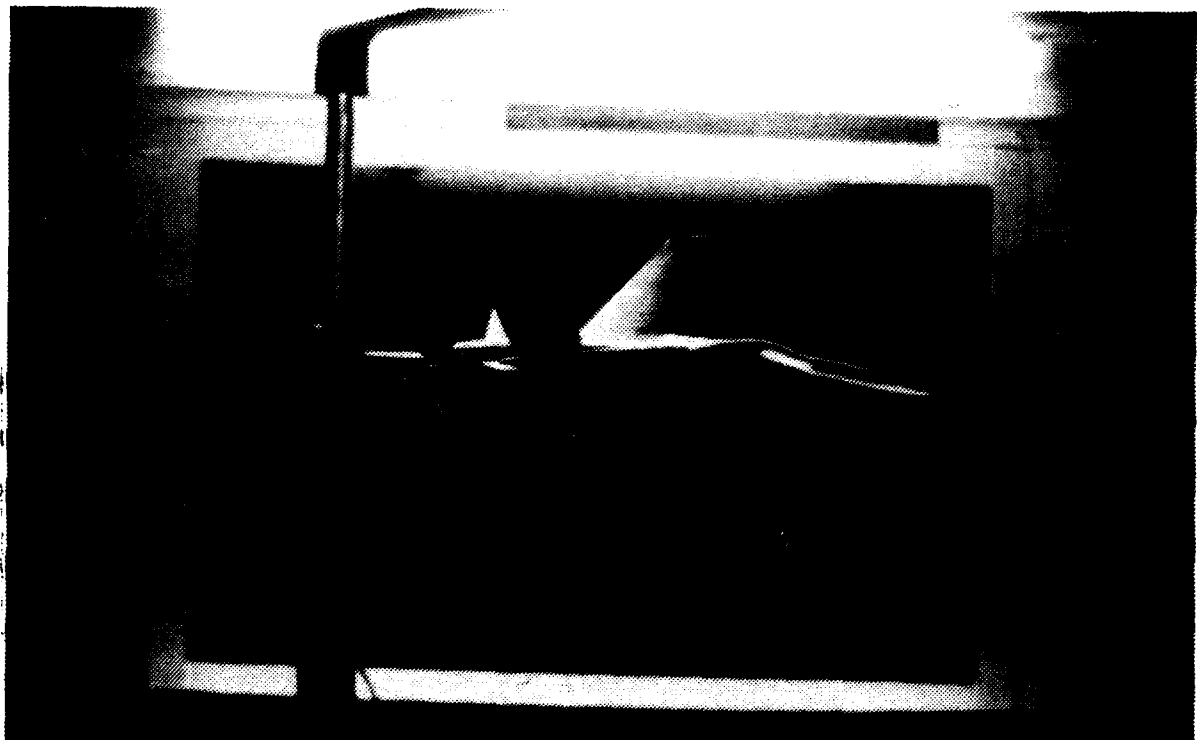Figure 10.   Fighter Model in Wind Tunnel

Figure 11.   Fighter Model Viewed From Side Window

The sting mount and swinging arm assembly permit pitch angles of -35 degrees to +90 degrees, yaw angles of plus or minus 5, 10 or 15 degrees, and 360 degrees of roll. The arm assembly pivot point, model center of pressure and balance center all coincide. The effects of vibration are kept to a minimum by heavy duty construction and the cross sectional areas of the mount assemblies are such that the effect on the test section airflow is minimal. The turntable is supported by a heavyweight pedestal that rotates via an electric motor powered chain drive gear assembly. Pitch angle and pitch rate can be controlled manually or through the computerized data acquisition system. Pitch angles are read to an accuracy of 0.1 degrees through a ring scale located on the pedestal.

5. Flow Visualization System

A flow visualization system using smoke and a laser sheet for illumination was installed in the low speed wind tunnel [Ref. 7]. Major components of the system include a portable smoke generating machine, a portable smoke rake and smoke tube, a 5W Argon-ion laser and associated optics mounted on a traverse mechanism to permit complete coverage of the wind tunnel test section. Each major component is briefly discussed below. The reader is directed to Reference 7 for detailed information on the entire flow visualization system.

A Rosco model 1500 Fog/Smoke machine, originally intended for theatrical use provides smoke through the vaporization of fluid specifically designed for use with the machine. The operating temperature, pressure and exit nozzle are factory set and not adjustable. The volume of smoke produced is adjustable and can be controlled via a 25-foot remote control. The smoke has proven to be safe to use and suitable for illumination by laser sheet. [Ref. 7]

The smoke is injected into the wind tunnel airstream through either a 21-tube smoke rake or a single outlet smoke tube. The smoke is fed to the injection device via a three-inch diameter flexible hose. The smoke rake tubes are 3/16 inch in diameter, 18 inches in length and spaced one and one-half inches apart along the trailing edge of the rake airfoil. The single outlet smoke tube also attaches to the three-inch smoke feed hose. The smoke enters a cylindrical settling chamber, passes through a honeycomb flow straightener and then exits a one-inch diameter tube after going through a 10:1 contraction section. Both injection devices are designed to allow positioning at varying locations in the tunnel to ensure adequate coverage for all anticipated model configurations and pitch angles.

A Spectra Physics, Model 164, 5W Argon-ion laser provides illumination of the smoke. Laser output is routed to the light sheet optics through a ten-meter long fiber optics cable which simplifies the physical set-up of the

system and greatly enhances the safety. The light conversion optics, which consist of a collimator, a beam expander and a plano-cylindrical lens create a laser sheet which is approximately two millimeters thick. The entire optics set is mounted on a six-inch rail which is attached to a traverse mechanism designed to provide horizontal and vertical travel through the entire test section.

6. Data Acquisition Hardware

Figure 12 shows the data acquisition system hardware components required to support the use of the Task balance [Ref. 13]. In addition to the thermometer and manometers discussed earlier a data acquisition circuit is necessary to utilize the balance output. A signal conditioning circuit for each individual strain gage in the balance supplies voltage for calibration and zeroing. The signal conditioner output is fed to a Hewlett-Packard relay multiplexer which sequentially cycles through each balance channel as specified by the data acquisition software. An amplifier (1000 gain, low noise) boosts the output signal to improve resolution after which the analog voltage signal is converted to a digital signal by a Hewlett-Packard digital multimeter for use in the data acquisition software program. An IBM-AT microcomputer controls data acquisition and model positioning during the experiment and stores the collected data.
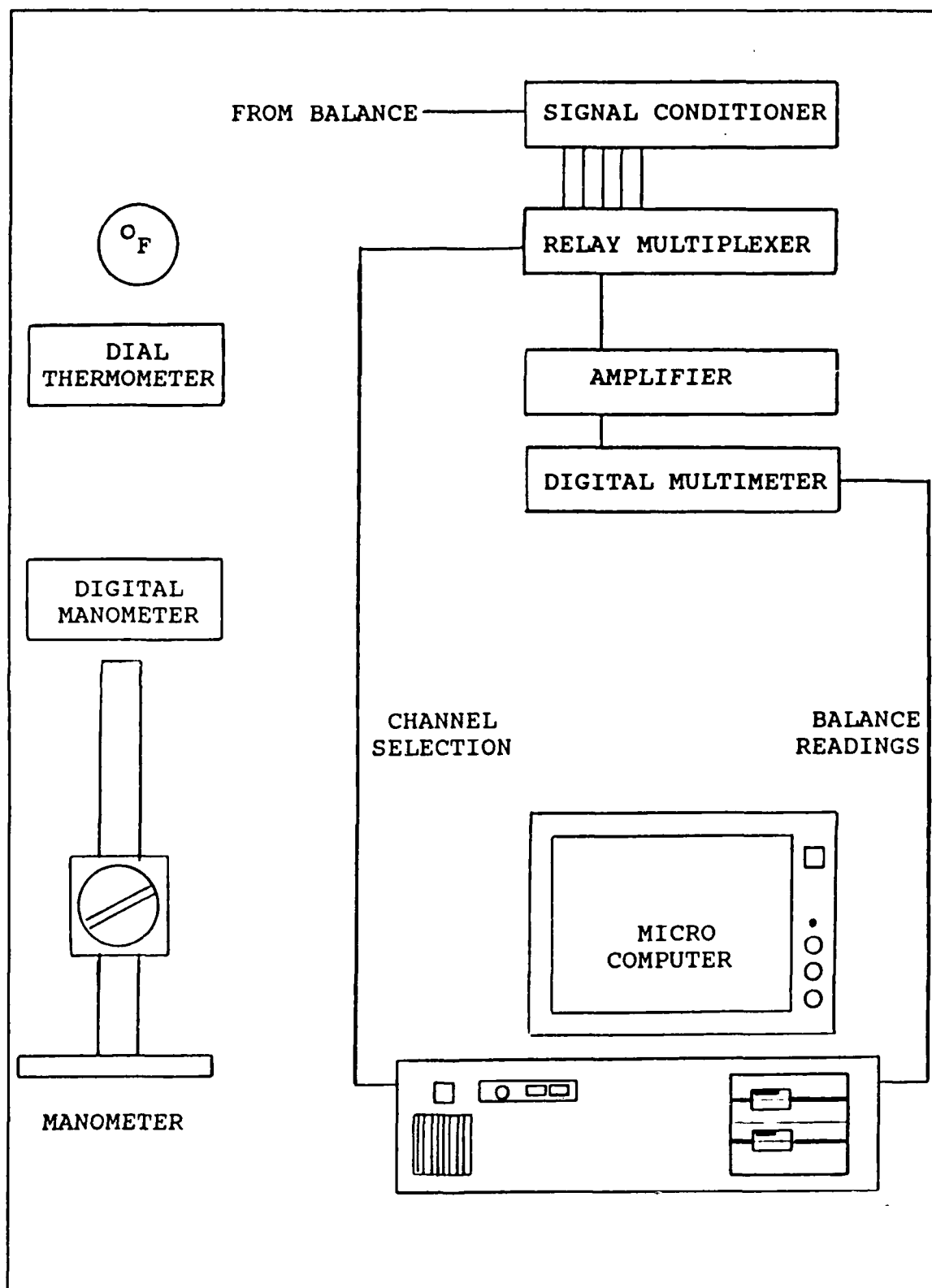
Figure 12. Data Acquisition Hardware

7. Data Acquisition Software

The data acquisition program is listed in Appendix B. A shell program controls the Hewlett-Packard instrument package and a data collection/conversion program transforms each balance channel's output into a compatible format. The balance readings are time averaged and combined with the appropriate calibration constants (Appendix A), to present normal, side and axial force values in pounds and pitching, rolling and yawing moments in foot-pounds. The two balance channels for normal force and two balance channels for side force are combined in this process to give but one reading for each. These readings are then converted to coefficient form by the computer program listed in Appendix C for ease of data comparison. Conversion of the data to coefficient form allowed comparison of data among the various angles of attack taking into account the test section differences due to model blockage. The force coefficients were obtained by nondimensionalizing forces with the free stream dynamic pressure and the frontal area of the model. Moment coefficients were calculated using the above parameters and a balance reference length of one.

B. EXPERIMENTAL CONDITIONS

The goal of the experiment was to measure the effects of low speed, high angle of attack flight on the aircraft as a whole and gain an understanding of the physics involved through flow visualization.

28

To meet this goal, the experiment was carried out in two phases. The first phase involved the measurement of forces and moments on the model for angles of attack varying from -35 degrees to +85 degrees at speeds of 10 m/s, 35 m/s and 50 m/s. The second phase involved extensive flow visualization of the model for the same angle of attack range at a velocity of 10 m/s. Flow visualization using one-inch smoke tube was accomplished first in an attempt to gain an appreciation for the overall effect of various flow patterns on the aircraft dynamics.

C. EXPERIMENTAL PROCEDURE

1. Balance Calibration

Calibration of the Task balance was carried at the NASA Ames Calibration Laboratory. The necessary balance constants and individual channel accuracies were determined and are listed in Appendix C. The balance was mounted on the model support system and the entire assembly installed in the wind tunnel. The model was not mounted at this time. The balance output leads were connected and the data acquisition hardware energized. A balance channel excitation voltage of 5.00 DC volts was then applied through the signal conditioner. Variation of the excitation voltage was less than 0.003 volts. The data acquisition system was then allowed a warm-up period of one hour prior to use. A gain setting of 1000 was used as the signal amplifier was zeroed and each balance circuit was zeroed to within 200 nanovolts

29

across the wheatstone bridge circuitry. Prior to mounting the model calibrated weights were suspended from the balance and the data acquisition software run to compare balance output with the calibration specifications. The normal and side force readings were accurate to within 0.05%. The model was then mounted on the support assembly and the initial tare readings were obtained. The data acquisition system remained energized through the completion of the experimental procedures to maintain the balance circuit excitation voltages.

2. Prerun Calibration and Testing

Prior to each day's run the data acquisition system was cycled for approximately 30 minutes to allow the circuitry to settle at operating temperature. The static weight test was then repeated with the model mounted to ensure the balance circuits were still within calibration accuracy. If a discrepancy was noted, the model was removed and the balance calibration procedures repeated.

3. Data Collection

Data collection was divided into two separate stages. In the first stage force and moment data were taken. Runs between -5 and +5 degrees angle of attack at test section velocities of 10, 35 and 50 meters per second were made to determine the zero-lift angle of attack. After this determination runs at the same three velocities between -35 and +85 degrees angle of attack in increments of five degrees

were completed. Finally, repeated runs at 50 m/s were accomplished for angles of attack between 15 and 70 degrees angle of attack. The Reynolds number at 50 m/s was 3.49 x 10^5. This value is based on the mean aerodynamic chord of the model (3.88 inches).

In the second stage of the investigation, flow visualization was accomplished using the one-inch smoke tube at a velocity of 10 m/s. Cross sectional photographs of the flow over the model were taken to identify the areas most likely affected by vortex generation and separation.

D. EXPERIMENTAL CORRECTIONS

Corrections to account for model blockage were calculated from the following equations [Ref. 22]:

$$q = q_m(1+2\varepsilon)$$
$$U = U_m(1+\varepsilon)$$

where:

q = dynamic pressure (lb/ft^2

q_m = measured reference pressure (lb/ft^2)

U = horizontal velocity (ft/sec)

U_m = measured horizontal velocity (ft/sec)

ε = blockage factor

and:

$$\varepsilon = 0.25*(\text{model frontal area/test section area})$$

The model frontal area was highly angle of attack dependent.

The blockage corrections are shown in Table 2 and Figure 13. These corrections are applied in the data conversion program listed in Appendix C. The minimum and maximum values for percent blockage are based on the cross sectional areas of the model at zero and 90 degrees angle of attack, respectively. A linear interpolation between these values was then used to generate a blockage formula which was angle of attack dependent.

TABLE 2. BLOCKAGE FACTORS

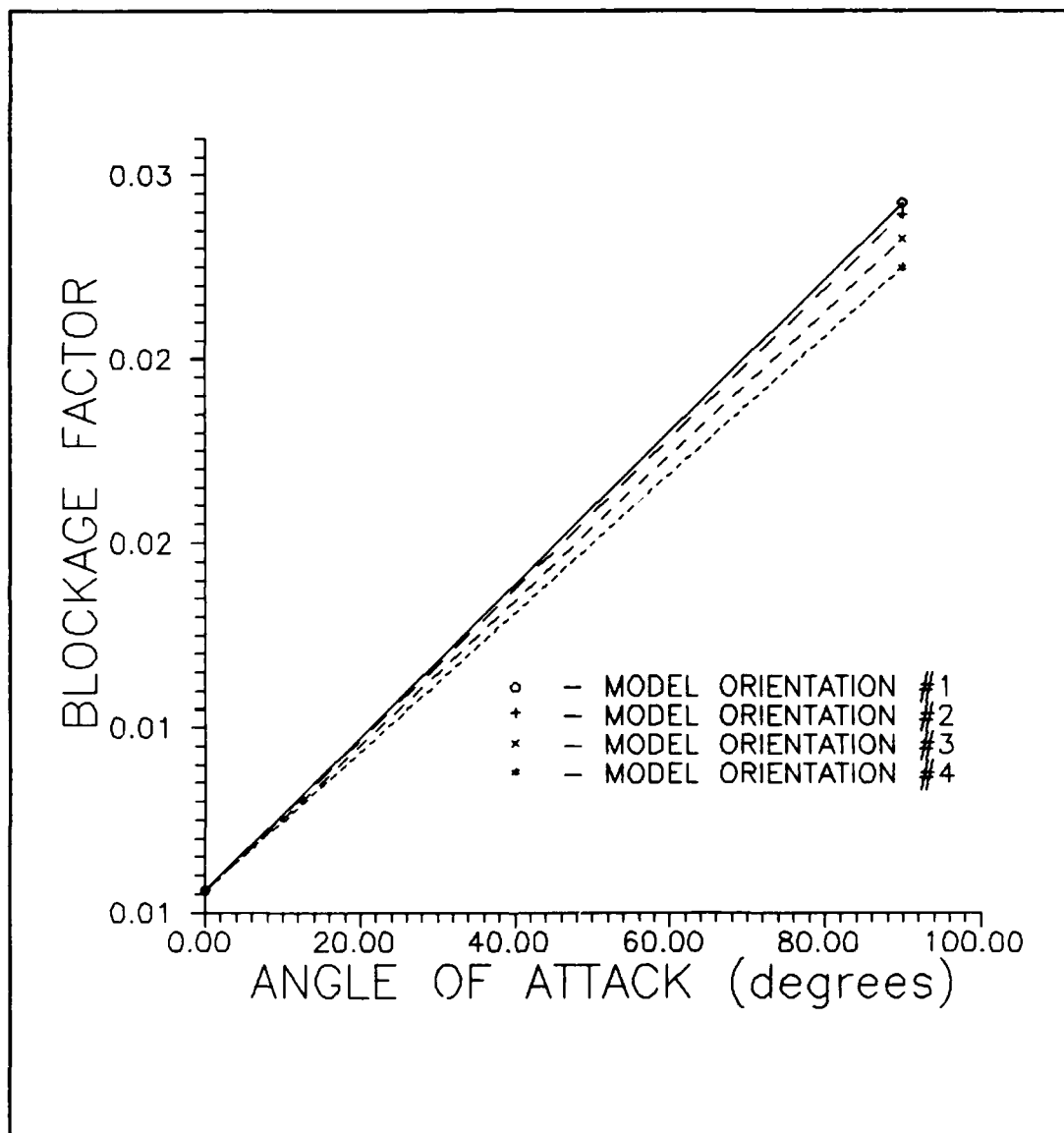| Model Orientation		Minimum Blockage (percent) PITCH = 0	Maximum Blockage (percent) PITCH = 90
1	0 < YAW < 15 ROLL = 0	3.04	10.49
2	YAW = 0 ROLL = 15	3.04	10.38
3	YAW = 0 ROLL = 30	3.04	10.10
4	YAW = 0 ROLL = 45	3.04	9.80

Figure 13. Blockage Correction Factors

III. RESULTS AND DISCUSSION

The results of this investigation are presented and discussed in two parts. First, a series of 32 photographic sequences of flow phenomena will be presented and analyzed. Second, the force and moment data collected in the investigation will be examined.

A. FLOW VISUALIZATION DATA

Flow visualization by laser sheet, though a very recent development, has already proven to be of enormous value in the detailed study of flow structure [Ref. 17]. The system installed in the Naval Postgraduate School low speed wind tunnel test facility certainly provides this capability but is not without its limitations. Problems with the flow quality in the tunnel test section and with smoke injection techniques were recognized by Chlebanowski when the flow visualization system was installed [Ref 7]. Consequently, this investigator's initial efforts were directed toward determining what improvements, if any, could be made in the basic system prior to its use in this high angle of attack research project. A summary of these efforts and the results are included in Appendix D.

In excess of 900 frames of 35mm black and white film were exposed and over nine hours of videotape recorded during the investigation. The results of the 35mm photography are

presented in a series of 32 numbered photographic sequences which are presented as Figures 14 through 130 in Appendix E. Each sequence is listed below with the corresponding figure numbers and an analysis of the observed flow phenomena. Results are presented depending on aircraft orientation in the three categories of pitch only, pitch and roll and pitch and yaw. Model attitude was varied between 0 and 90 degrees of pitch, 0 and 45 degrees of roll and 0 and 15 degrees of yaw. The majority of flow visualization photography was performed between 20 and 70 degrees of pitch and to the maximum values of roll and yaw previously specified. "Station" refers to the number of inches aft of the nose at which the laser sheet cuts the longitudinal axis. Table 3 lists some prominent stations and model features at these locations. Figure 7 is scaled for visual reference.

1. Pitch Only

Sequence Number 1, Figures 14 through 18. Figure 14 shows a pair of symmetric nose generated vortices at station 2 and 45 degrees angle of attack. Increasing the angle of attack to 50 degrees results in the asymmetric vortices shown in Figure 15. As the laser sheet scans from station 2 to station 6 the development of the asymmetric flow can be traced until both vortices have been shed from the aircraft model. This flow behavior is well-documented for slender forebodies such as the nose section of the YF-17.

TABLE 3. STATION IDENTIFICATION ON THE MODEL

Station	Description (see Figure 7)
0	Tip of nose
4	Forwardmost edge of canopy
5.25	Beginning of leading edge extensions (LEX)
10	Intersection of LEX and wing leading edge
12	Model center of pressure; balance center point
14	Intersection of vertical stabs and fuselage
14.5	Trailing edge of wings

Sequence Number 2, Figures 19 through 21. This series of three photographs taken at stations 1, 3 and 5 and 65 degrees angle of attack show the vortices rapidly becoming asymmetric and shedding from the body of the model. Figure 19 clearly shows the vortices already becoming asymmetric although the photograph was taken at station 1. Figure 20, taken at station 3 shows no evidence of vortex flow and Figure 21, at station 6 shows the expected wake-like flow.

2. Pitch and Roll

Sequence Number 3, Figures 22 through 24. This sequence shows the change in vortex symmetry at station 1 as the roll angle is increased from 15 degrees to 45 degrees with the pitch angle held constant at 65 degrees. Comparison of Figure 22 with Figure 19 shows little change in the

orientation of the two vortices other than a slight separation of the bottom vortex from the nose surface. Figure 23 shows the development of a significant separation of the bottom vortex which increases as the model is rolled to 45 degrees in Figure 24. The nose geometry of the YF-17 is a major factor in this phenomenon.

Sequence Number 4, Figures 25 through 27. The roll angle is increased from 15 degrees to 45 degrees at station 1 as in the previous sequence but at a reduced angle of attack of 55 degrees. The degree of asymmetry between the various roll angles is much less severe than at the higher angle of attack.

Sequence Number 5, Figures 28 through 31. With the laser sheet positioned at station 2 and angle of attack set at 65 degrees the effect of changing roll angle is evidenced by the asymmetry which was also evident at station 1. It is interesting to note the degree of separation between the two vortices and their position relative to one another.

Sequence Number 6, Figures 32 and 33. A comparison of nose generated vortex positions at station 6 with the model at 60 degrees angle of attack and roll angles of 0 degrees and 45 degrees respectively shows the vortex closest to the body becomes stronger and better defined with the increased roll angle. The reduced relative angle of attack of the upwind side of the model appears to promote this behavior.

37

Sequence Numbers 7 through 11, Figures 34 through 63.
This series of 30 photographs follows the development and
shedding of nose generated vortices between 45 degrees and 70
degrees angle of attack from model stations 2 through 6 at 15
degrees of roll. Comparisons between the degrees of
asymmetry, vortex shedding points, and turbulent flow
transitions are possible with a great amount of continuity.
Photographs taken at station 2 reveal the effect changing
pitch and changing yaw. Figures 34 through 39 reveal the
bottom vortex sheds sooner with increasing pitch while the
top vortex weakens but remains attached to the fuselage. At
70 degrees of pitch the flow is in transition from vortex to
wake-like. Figures 34 through 39 confirm the increase in
asymmetry with roll angle noted at station 1. Figures 40
through 45 illustrate how the vortices tend to rotate toward
the centerline which had previously separated them when they
were symmetric. Figures 44 and 45 also show the transition
of the flow from asymmetric shed vortices to wake-like. The
top vortex which barely remains attached in Figure 44 has
separated and essentially disappeared in Figure 45.
Photographs taken at station 4 are presented in Figures 46
through 51. Photographs taken at station 5, and included
herein as Figures 52 through 57, clearly demonstrate the
separation of the nose generated vortices from the body of
the model aircraft. Between 50 and 55 degrees of pitch and
the top vortex sheds and the flow rapidly becomes wake-like

38

in the vicinity of the fuselage. The vortices are still present but separated by a great distance from the model. At station 6, Figures 58 through 63 show the vortices separated from the body with completely wake-like flow occurring at approximately 50 degrees of pitch.

Sequence Number 12, Figures 64 through 69. With the laser sheet at station 4 and the roll angle set at 30 degrees the pitch angle was varied between 45 and 70 degrees angle of attack. When compared to the previous sequences which were recorded at 15 degrees of roll the degree of vortex asymmetry at first appears to be greater for the higher roll angle as the pitch angle increases. However, this trend reverses as the pitch angle passes approximately 55 degrees until there is virtually no difference in the flow patterns between the two roll angles.

Sequence Number 13, Figures 70 through 73. The laser sheet was held steady at station 7 while the model was pitched from 45 degrees to 60 degrees angle of attack at a constant roll angle of 30 degrees. The forebody vortex generated on the upwind side of the model has shifted over to the downwind side of the fuselage as expected and is easily seen in Figure 70. Increasing the angle of attack slightly to 50 degrees results in the separation of this vortex from the body. Further increases in the angle of attack reveal completely separated and turbulent flow at station 7 by 60 degrees angle of attack.

Sequence Number 14, Figures 74 through 76. With the model at 45 degrees angle of attack and the laser sheet positioned at station 8 the effect of rolling from 15 degrees to 45 degrees is dramatic. The strake generated vortex on the downwind side of the fuselage gains strength as can be seen by the tightening of the flow and improved definition of the vortex core. The reduction in relative angle of attack on the downwind strake with increasing pitch is responsible.

Sequence Number 15, Figures 77 through 79. The same phenomena present in the previous sequence is evident here at an angle of attack of 55 degrees. The difference between successive roll angles at the higher angle of attack is much more pronounced with the flow going from completely turbulent in Figure 77 to asymmetric and semi-attached at 45 degrees of roll in Figure 79.

Sequence Number 16, Figures 80 through 82. Increasing the angle of attack to 70 degrees and rolling from 15 degrees to 45 degrees reveals that reducing the effective angle of attack no longer causes the generation and strengthening of the vortices as was the case in the previous two sequences. The flow remains turbulent and wake-like at all roll angles.

Sequence Number 17, Figures 83 through 86. The disappearance of the upwind strake generated vortex and the stability of the downwind strake generated vortex are documented in this series of four photographs taken at

station 10 with the model angle of attack increasing from 25 degrees to 45 degrees and the roll angle held constant at 30 degrees. Station 10 is the point on the fuselage where the leading edge of the wing meets the leading edge of the LEX. At 25 degrees angle of attack strake generated vortices are visible on both sides of the fuselage. The left side vortex is slightly larger indicating less strength and stability. This is predictable given the higher relative angle of attack on that side. Increasing the angle of attack to 30 degrees cause the left side vortex to burst while the right side, or downwind vortex weakens slightly but remains intact. Figures 85 and 86 complete the sequence.

Sequence Number 18, Figures 87 through 89. At a constant 45 degrees angle of attack, the flow at station 10 is visible as the roll angle is increased from 15 degrees to 45 degrees. The completely turbulent flow seen in Figure 87 is altered drastically by the increasing roll angle as evidenced by the well developed vortex flow visible in Figure 89. The upwind side of the fuselage remains immersed in turbulent flow throughout.

Sequence Number 19, Figures 90 through 92. This series of photographs taken at station 10 with a roll angle of 45 degrees, shows little or no change in vortex position or strength as the angle of attack increases from 35 degrees to 45 degrees. The high roll angle keeps the downwind side

of the fuselage at a relatively low angle of attack thus minimizing the effects on that vortex in this regime.

Sequence Number 20, Figures 93 and 94. These two photographs illustrate the transition from vortex flow to turbulent flow. Figure 93 clearly shows the vortex core at station 11 on the downwind wing of the model at 40 degrees angle of attack and 30 degrees of roll. With the laser sheet at station 12, as in Figure 94, the vortex core is no longer visible and the smoke has dispersed to fill the entire illuminated region. The remains of the downwind forebody generated vortex are also visible in both photographs appearing as the large curls visible in the upper left portion of the laser sheet.

Sequence Number 21, Figures 95 through 97. The flow over the downwind wing of the model at 40 degrees, 35 degrees and 25 degrees is examined between stations 11 and 12 at a constant roll angle of 45 degrees. Figure 95, at 40 degrees, shows the existence of a single, strake generated vortex. Figure 96, at 35 degrees, reveals the presence of a small vortex located mid-span in addition to the expected strake generated vortex visible near the wing root. Figure 97, at 25 degrees clearly shows the presence of this mid-span vortex and indicates the increase in strength due to the reduced angle of attack. The second vortex was generated by the leading edge of the wing. Of secondary interest is the plume of smoke visible in Figure 97. This plume results from the

airflow through the boundary layer bleed air slots located between the LEX's and the fuselage. The slots were eliminated from the F/A-18 because of the deleterious effect they had on the strake generated vortices.

Sequence Number 22, Figures 98 through 103. At a constant 30 degrees angle of attack and roll the laser sheet was moved from station 8 to station 12. This series of photographs shows the degeneration of the downwind strake generated vortex to the point of bursting.

Sequence Number 23, Figures 104 through 108. Degeneration of the downwind strake generated vortex is examined at station 13 with the model increasing in angle of attack from 15 to 35 degrees. Roll angle remains constant at 30 degrees. As the angle of attack increases the vortex loses definition until it eventually cannot be distinguished from the turbulent flow over the remainder of the wing.

Sequence Number 24, Figure 109. This solitary figure is included because of an interesting observation in the photograph. The model is oriented at 25 degrees angle of attack and 15 degrees of roll. The LEX generated vortex visible on the upwind strake is at station 9. A second vortex, much smaller and of opposite rotational direction than the main vortex, can be seen inside the LEX vortex core. This secondary vortex appears to be generated by the sharp edge of one of the boundary layer bleed slots mentioned in a previous sequence.

3. Pitch and Yaw

Sequence Number 25, Figures 110 and 111. The difference in the formation of nose generated vortices is clear when comparing Figures 110 and 111. At a yaw angle of 5 degrees with the laser sheet at station 1 the model was pitched from 50 degrees angle of attack to 65 degrees angle of attack. The vortices in Figure 110 are nicely formed and very nearly symmetric. With the angle of attack increased to 65 degrees as in Figure 111, the vortices have already begun to go asymmetric. There was no evidence of vortex unsteadiness at the higher angle of attack.

Sequence Number 26, Figures 112 through 115. The rapid development of asymmetry and ultimate shedding of the vortex flow is detailed in this series of four photographs. The model is steady at 60 degrees angle of attack at a yaw angle of 15 degrees. The vortices are completely asymmetric at station 1 in Figure 112 although shedding has not yet occurred. By station 2, shown in Figure 113, the top vortex has been shed and the other vortex has weakened nearly to the point of separation. Figures 114 and 115 complete the flow development and provide a graphic depiction of the rapidity with which such a drastic change in the flow pattern can occur.

Sequence Number 27, Figures 116 through 119. With a yaw angle of 5 degrees and an angle of attack of 30 degrees, the bursting of the upper wing vortex is traced from station

10 to station 15. The loss of vortex coherence is clear when Figures 117 and 118 are compared. In Figure 119, the vertical tails are immersed in completely turbulent flow which has proven, in other investigations, to be a major factor in reducing the fatigue life of the tail structures.

Sequence Number 28, Figures 120 and 121. The two photographs in this sequence were taken less than two seconds apart at station 2 with the aircraft at a constant 50 degrees angle of attack and 5 degrees of yaw. The unsteadiness of the forebody generated vortices is evident when the orientation of the vortex cores are compared. Both vortices remained attached but never in the same place for very long.

Sequence Number 29, Figures 122 and 123. As in the previous sequence, the nose generated vortices visible in this pair of photographs taken only seconds apart show the great degree of unsteadiness in the flowfield. The laser sheet was positioned at station 3 with the aircraft at pitch and yaw angles of 55 degrees and 10 degrees respectively. The vortex cores are much larger than those in the previous figures due to the slightly higher yaw and angle of attack.

Sequence Number 30, Figures 124 through 126. The impact of angle of attack on the formation and structure of vortex flow is very evident in this series of three photographs. With the laser sheet at station 2 and the yaw angle set at 10 degrees the angle of attack was increased from 45 degrees to 65 degrees. Figure 124, taken at 45

degrees, shows the nose generated vortices relatively symmetric and attached. A marked degree of asymmetry in Figure 125 depicts the effect of increasing the angle of attack by 10 degrees to 55 degrees. At 65 degrees angle of attack, as in Figure 126, the vortices have completely separated yet maintain their asymmetry with respect to the fuselage of the model.

Sequence Number 31, Figures 127 and 128. Both figures are photographs taken of the model at 45 degrees angle of attack, 5 degrees of yaw and station 6. The pronounced difference is representative of the degree of unsteadiness which was present. Vortex core movement was of quite a large magnitude and extremely unpredictable.

Sequence Number 32, Figures 129 and 130. The only incidents of vortex position switching occurred with the model at a yaw angle of 5 degrees between 55 degrees and 60 degrees angle of attack. Figures 129 and 130 recorded such a switching episode at station 4 and 60 degrees angle of attack. The switching was quite random with the interval between averaging three to five seconds.

B. FORCE AND MOMENT DATA

Appendix F presents the raw force and moment data generated by the data acquisition program. The data is presented in graphic form, as Figures 131 through 142, for ease of interpretation. This raw data was processed through the coefficients translation program in Appendix C to

46

nondimensionalize the data, taking into account the test conditions and model blockage factors. The reduced data is presented in Appendix G as Figures 143 through 154. The differences between the raw data and the reduced data are minimal. The force and moment analysis that follows refers to the reduced data in Appendix G.

The normal force plots in Figures 143 and 144 show a characteristic rise with increasing angle of attack to a maximum value where the magnitude attains a near steady state even though angle of attack continues to rise. Figure 143 plots separate curves for each roll angle. The normal force coefficients are nearly equal through 30 degrees angle of attack where they start to level off and separate. At this point, the roll angle and normal force coefficient become inversely proportional with the highest roll angle experiencing the lowest normal force. This makes perfect sense in that the higher roll angle configuration presents less surface area. Leveling of the normal force curves can be correlated to the transition of the flow over the model from vortex flow to separated wake-like flow. Sequence numbers 17, 21 and 23 clearly show this degeneration of airflow over the model with increasing angle of attack. At 35 degrees angle of attack and 30 degrees of roll, Figure 108 in sequence 23 captures separated flow on the downwind wing just after vortex bursting occurred. The curve for 30 degrees of roll angle in Figure 143 reveals the normal force

47

coefficient levelling at this point. The curves corresponding to the four different yaw angles are presented in Figure 144. The plots are nearly identical due to the unchanged planform area and provide a degree of confidence in the balance readings given the time separation between data collection for each angle. The curves exhibit the same levelling tendency as the zero degree roll angle curve in Figure 143 for exactly the same reasons.

The side force coefficient plots in Figures 145 and 146 contain data which can be correlated to the observed flow phenomena present at certain angles of attack, roll and yaw as discussed in the previous section. Each curve in Figure 145 represents a different roll angle. At zero degree angle of attack and zero degree of roll angle the force coefficients for each curve intersect at zero. The side force magnitude generally increases with increasing pitch and roll to a point where the magnitude levels off except in the case of zero degrees of roll. The peak in the curve for zero degrees of roll between 45 degrees and 65 degrees angle of attack corresponds to a region of active nose vortices. The asymmetric shedding of these vortices are responsible for the variation in side force coefficient evident in the curve. Photographic sequence numbers 1 and 2 show the asymmetric shedding of vortices responsible for the region of increased side force seen in the zero degree roll curve in Figure 145. The same type of shedding vortex behavior can be seen for all

roll angles in sequences 3 through 12. However, the curves for roll angles greater than zero do not clearly define the areas of increased side force due to the shedding vortices because of the offsetting effect of the crossflow component of the freestream velocity. The shedding vortices are active but somewhat negated.

Figure 146 plots side force coefficient versus angle of attack for four different yaw angles. In the vicinity of zero degree angle of attack all curves for yaw angles greater than zero exhibit rise in magnitude in response to the crossflow component of the relative wind. All the curves show the same characteristic peak between 45 degrees and 65 degrees angle of attack, though the curves corresponding to positive yaw angles peak to a lesser degree than the curve for zero degree yaw. Maximum asymmetric vortex activity was identified in numerous photographic sequences in this angle of attack range and unquestionably accounts for the side force fluctuations present in the coefficient plots. Sequence number 30 is especially clear in its tracing of the development and eventual shedding of nose generated vortices between 45 degrees and 65 degrees angle of attack. Sequence number 28, records the unsteadiness of these vortices with the model at 50 degrees angle of attack and only 5 degrees of yaw. The curve for a yaw angle of 5 degrees indicates a certain degree of unsteadiness in this region.

Figures 147 and 148 present the rolling moment coefficients data for roll angles and yaw angles, respectively. The peak seen in Figure 147 between 30 degrees and 60 degrees angle of attack is a result of the asymmetry between the LEX generated vortices on either side of the fuselage. Sequence numbers 14 through 19 contain the supporting photographic evidence which shows that the largest magnitude of rolling moment coefficient should correspond to an angle of attack of 45 degrees and a roll angle of 45 degrees. Figures 87, 88 and 89 capture the development of a strong downwind wing vortex with increasing roll angle while the upwind wing remains immersed in separated flow. The maximum rolling moment coefficient in Figure 147 reflects this observation. The minimum rolling moment in the same angle of attack range belongs to the zero degrees roll curve. This should be expected as this is the model attitude which generates the least asymmetry between the LEX generated vortices. Figure 148 also shows a peak in the 30 degrees to 50 degrees angle of attack range. The greatest magnitude of rolling moment coefficient corresponds to a yaw angle of 15 degrees which can be expected to generate the greatest asymmetry between the LEX generated vortices in the yaw only test configuration.

Figures 149 and 150 plot the yawing moment coefficients for the various roll and yaw angles. Both graphs present extremely erratic data in different angle of attack ranges.

The data in Figure 149, showing roll angles between zero degree and 45 degrees appears to be responding mostly to the side forces generated by crossflow. The two large magnitude fluctuations seen at 70 degrees angle of attack for the zero degree roll angle and at 80 degrees angle of attack for the 45 degree roll angle do not readily correspond with any of the observed flow phenomena. In addition, the large fluctuations seen in the curves in Figure 150 between zero degree and 45 degrees angle of attack were not expected in view of the degree of unsteadiness observed in the flow in sequence numbers 29 and 31. The large yawing moments would have seemed more likely to occur near 55 degrees angle of attack where the greatest unsteadiness in the flow was visually recorded. It is suspected that the data acquisition system was too slow to accurately reflect changes in yawing moment.

IV. CONCLUSIONS AND RECOMMENDATIONS

A low speed wind tunnel investigation was made into the high angle of attack aerodynamics of a fighter aircraft model using flow visualization and balance measurements. The investigation marked the first attempt at qualitative flow analysis using the newly installed laser sheet flow visualization system to identify flow phenomena that may prove important in the design and performance of supermaneuverable aircraft. The following conclusions are drawn from the results of the experimental investigation:

1. The Naval Postgraduate School low speed wind tunnel facility laser sheet flow visualization system is a valuable research tool subject to limitations resulting from restricted visual access to the test section and moderate test section turbulence.

2. A correlation between the observed flow phenomena and force and moment measurements existed between 25 degrees and 70 degrees angle of attack.

3. The predominant aerodynamic force between 45 degrees and 65 degrees angle of attack is the asymmetric shedding of vortices generated by the slender nose and leading edge extensions (strakes) of the model. Maximum side forces are generated in this angle of attack range.

4. Below 45 degrees angle of attack, the flow characteristics are governed by complex multiple vortex interactions along the upper surface of the fuselage and wings coupled with nose generated vortices.

The following recommendations are made based on the results of this investigation:

1. Extensive wind tunnel modifications to improve visual access to the test section and reduce turbulence are required to utilize the laser sheet flow visualization system to its full potential.

2. Motorize the laser optics to render the data gathering effort less labor intensive.

3. Expand the flow visualization effort on the fighter aircraft model to include negative angles of attack to -45 degrees.

4. Perform laser Doppler velocimetry and hotwire measurements to quantify the flow phenomena identified in this investigation.

5. Incorporate the capabilities of the Department of Aeronautics and Astronautics water tunnel flow visualization system into the current high angle of attack research effort.

LIST OF REFERENCES

1. Gallaway, C. R., and Osborn, R. F., Aerodynamics Perspective of Supermaneuverability, AIAA Paper 85-4068, October 1985.

2. Hamilton, W. L., and Skow, A. M., Operational Utility Survey: Supermaneuverability, AFWAL-TR-85-3020, September 1984.

3. Murri, D. G., and Rao, D. M., Exploratory Studies of Actuated Forebody Strakes for Yaw Control at High Angles of Attack, AIAA Paper 87-2557, 1987.

4. Herbst, W. B., "Future Fighter Technologies," Journal of Aircraft, Volume 17, Number 8, pp. 561-566, August 1980.

5. Well, K. H., Faber, B., and Berger, E., "Optimization of Tactical Aircraft Maneuvers Utilizing High Angles of Attack," Journal of Guidance, Volume 5, Number 2, pp. 131-137, March-April 1982.

6. Patierno, J., "Evolution of the Hybrid Wing-YF-17/F-18 Type," Proceedings of the Evolution of Aircraft Wing Design Symposium, pp. 131-139, March 1980.

7. Chlebanowski, J. S., Jr., Flow Visualization by Laser Sheet, M. S. Thesis, Naval Postgraduate School, Monterey, California, pp. 1-23, March 1988.

8. Webster, F. R., High Angle of Attack Flight Tests of the F-15C, AFFTC-TR-83-33, Edwards Air Force Base, California, October 1983.

9. Deffenbaugh, F. D., and Koerner, W. G., "Asymmetric Vortex Wake Development on Missiles at High Angles of Attack," Journal of Spacecraft, Volume 14, Number 3, pp. 155-161, March 1977.

10. Yanta, W. J., and Wardlaw, A. B., Jr., "Flowfield About and Forces on Slender Bodies at High Angles of Attack," AIAA Journal, Volume 19, Number 3, pp. 296-302, March 1981.

11. Reding, J. P., and Ericsson, L. E., Maximum Vortex-Induced Side Forces on Slender Bodies, AIAA Paper 77-1155, 1977.

12. Chapman, G. T., and Keener, E. R., The Aerodynamics of Bodies of Revolution at Angles of Attack to 90 Degrees, AIAA Paper 79-0023, 1979.

13. Rabang, M. P., Turbulence Effects on the High Angle of Attack Aerodynamics of a Vertically Launched Missile, M. S. Thesis, Naval Postgraduate School, Monterey, California, p. 3, June 1988.

14. Rao, D. M., Moskovitz, C., and Murri, D. G., "Forebody Vortex Management for Yaw Control at High Angles of Attack," Journal of Aircraft, Volume 24, Number 4, pp. 248-254, April 1987.

15. Mueller, T. J., The Visualization of Low Speed Separated and Wake Flows, AIAA Paper 87-2422, 1986.

16. Erickson, G. E., and others, Water Facilities in Retrospect and Prospect--An Illuminating Tool for Vehicle Design, AGARD CP-413, pp.1-27.

17. Meuller, T. J., "Recent Development in Smoke Flow Visualization," Proceedings of the Third International Symposium on Flow Visualization, 1983, Yang, W. J., Editor, Flow Visualization III, pp. 30-40, Ann Arbor, Michigan, USA, Hemisphere Publishing Corporation.

18. Malcolm, G. N., and Nelson, R. C., Comparison of Water and Wind Tunnel Flow Visualization Results on a Generic Fighter Configuration at High Angles of Attack, AIAA Paper 87-2423-CP, Atmospheric Flight Mechanics Conference, Monterey, California, 1987.

19. Laboratory Manual for Low Speed Wind Tunnel Testing, Department of Aeronautics, Naval Postgraduate School, Monterey, California, pp. 1-8, October 1983.

20. Pietzman, F. W., Low Speed Wind Tunnel Investigation to Develop High Altitude Wall Correction in the Northrop 7x10 Foot Low Speed Wind Tunnel, NAL-117 and NAL-153, Northrop Corporation, p. 6, May 1978.

21. Calibration for TASK Mark 14-C Balance, Balance Calibration Laboratory, NASA-Ames Research Facility, July 1987.

22. Rae, W. H., and Pope, A., Low Speed Wind Tunnel Testing, Second Edition, John Wiley and Sons, p. 94, New York, 1984.

23. Berd, E., "Smoke Tunnel Development at VFW," Proceedings of the Second International Symposium on Flow Visualization, 1980, Merzkirch, Wolfgang, Editor, Flow Visualization II, pp. 313-319, Bochum, West Germany, Hemisphere Publishing Company.

APPENDIX A
BALANCE CALIBRATION CONSTANTS

BALANCE CALIBRATION   CAL DATE 7247 COMP DATE 7287

INV #440517

KIND FORCE   PIN NO. 3

SIZE 1.00

MAKE TASK 140   RIG NO. 2

GA	CAPACITY	MAX LOAD	JHMS	X_GAGE	CAL SHUNT	CAL ROG
N1	400.00	400.00	350.	0.1667	100.K	4625
N2	400.00	400.00	350.	0.1667	100.K	4626
A	100.00	100.00	175.		50.K	4618
S1	200.00	200.00	350.	0.1375	100.K	4623
S2	200.00	200.00	350.	0.1375	100.K	4597
RM	21.00	20.83	175.		50.K	4623

	K_POS(1)	K_POS(2)	K_NEG(1)	K_NEG(2)	MAX DEV	% ACC
N1	5.0861E-02	-5.4826E-09	5.1591E-02	1.7157E-08	0.224	0.056
N2	4.7211E-02	-1.7015E-08	4.7763E-02	8.9153E-09	0.196	0.049
A	1.4309E-02	-7.1962E-10	1.4290E-02	-1.3322E-09	0.115	0.115
S1	3.1309E-02	-3.8153E-08	3.2073E-02	-8.9316E-09	-0.263	0.132
S2	3.0366E-02	-3.8607E-08	3.1167E-02	-7.2517E-09	0.315	0.153
RM	3.0885E-03	2.5672E-09	3.0908E-03	-2.4769E-09	0.042	0.204

DEG OF FIT = 2   ACCURACY = 15

INT-DEG-OF-FIT = 2

N1/N2+ =-5.8036E-03	N1/N2- =-1.0257E-02
N1/A + = 0.0000E+00	N1/A - = 0.0000E+00
N1/S1+ =-4.1655E-03	N1/S1- = 4.5396E-03
N1/S2+ = 0.0000E+00	N1/S2- = 0.0000E+00
N1/RM+ =-5.8079E-02	N1/RM- = 4.4940E-02
N2/N1+ =-4.6218E-02	N2/N1- =-5.1778E-02
N2/A + = 2.8393E-03	N2/A - = 4.4056E-03
N2/S1+ = 8.1694E-03	N2/S1- = 9.0385E-03
N2/S2+ =-4.1463E-03	N2/S2- = 0.0000E+00
N2/RM+ =-7.7279E-02	N2/RM- = 6.1125E-02
A /N1+ =-8.6893E-04	A /N1- = 2.1217E-03

```
A /N2+ = 0.0000E+00          A /N2- =-9.15245-04
A /S1+ =-6.0359E-04          A /S1- = 0.0000E+00
A /S2+ =-7.7722E-05          A /S2- = 0.0000E+00
A /RM+ = 1.1115E-01          A /RM- = 9.7148E-02
S1/N1+ = 6.3459E-04          S1/N1- = 7.1275E-03
S1/N2+ = 0.0000E+00          S1/N2- = 0.0000E+00
S1/A + = 0.0000E+00          S1/A - = 8.9235E-03
S1/S2+ = 0.0000E+00          S1/S2- = 0.0000E+00
S1/RM+ = 1.1148E-01          S1/RM- = 5.2630E-02
S2/N1+ = 2.4237E-03          S2/N1- = 3.7176E-03
S2/N2+ = 0.0000E+00          S2/N2- = 5.2619E-03
S2/A + =-2.2455E-03          S2/A - =-7.2915E-03
S2/S1+ =-6.6785E-03          S2/S1- =-6.3560E-03
S2/RM+ = 2.6377E-01          S2/RM- = 6.2581E-02
RM/N1+ = 0.0000E+00          RM/N1- =-3.5945E-04
RM/N2+ = 1.9928E-04          RM/N2- = 0.0000E+00
RM/A + = 0.0000E+00          RM/A - = 0.0000E+00
RM/S1+ = 0.0000E+00          RM/S1- = 0.0000E+00
RM/S2+ = 2.5893E-04          RM/S2- = 0.0000E+00
N1/N2*N2+ = 7.1926E-07       N1/N2*N2- =-7.9499E-07
N1/A *A + = 0.0000E+00       N1/A *A - = 0.0000E+00
N1/S1*S1+ =-4.0352E-06       N1/S1*S1- = 1.9670E-06
N1/S2*S2+ = 0.0000E+00       N1/S2*S2- = 0.0000E+00
N1/RM*RM+ = 6.7860E-04       N1/RM*RM- = 3.2320E-04
N2/N1*N1+ = 6.8577E-07       N2/N1*N1- =-5.2897E-06
N2/A *A + = 1.7755E-05       N2/A *A - =-1.0467E-05
N2/S1*S1+ =-2.1719E-06       N2/S1*S1- = 4.8493E-07
N2/S2*S2+ =-1.8582E-06       N2/S2*S2- = 0.0000E+00
N2/RM*RM+ = 1.9294E-03       N2/RM*RM- = 1.1773E-03
A /N1*N1+ =-4.4537E-07       A /N1*N1- = 4.2547E-06
A /N2*N2+ = 0.0000E+00       A /N2*N2- =-4.5946E-06
A /S1*S1+ =-4.7936E-06       A /S1*S1- = 0.0000E+00
A /S2*S2+ = 4.1033E-06       A /S2*S2- = 0.0000E+00
A /RM*RM+ =-2.0697E-04       A /RM*RM- = 7.5001E-04
S1/N1*N1+ =-5.5350E-06       S1/N1*N1- = 1.2923E-05
S1/N2*N2+ = 0.0000E+00       S1/N2*N2- = 0.0000E+00
S1/A *A + = 0.0000E+00       S1/A *A - = 4.0345E-05
S1/S2*S2+ = 0.0000E+00       S1/S2*S2- = 0.0000E+00
S1/RM*RM+ =-2.4592E-03       S1/RM*RM- = 9.3969E-04
S2/N1*N1+ =-1.7099E-06       S2/N1*N1- = 5.2110E-07
S2/N2*N2+ = 0.0000E+00       S2/N2*N2- = 8.6265E-06
S2/A *A + =-1.2072E-05       S2/A *A - =-3.7054E-05
S2/S1*S1+ = 2.7825E-06       S2/S1*S1- =-9.9830E-06
S2/RM*RM+ =-6.2217E-03       S2/RM*RM- =-8.0007E-04
RM/N1*N1+ = 0.0000E+00       RM/N1*N1- =-1.5497E-07
RM/N2*N2+ =-1.1512E-07       RM/N2*N2- = 0.0000E+00
RM/A *A + = 0.0000E+00       RM/A *A - = 0.0000E+00
RM/S1*S1+ = 0.0000E+00       RM/S1*S1- = 0.0000E+00
RM/S2*S2+ = 5.1560E-08       RM/S2*S2- = 0.0000E+00
```

```
2900 'Program to scan with the DMM and RELAY.MUX.01
2910 'This program was writen by T.SESTAK and modified by
2920 'D. LEEDY for use with the VLSAM model.
2930 '
2940 'This section after the SHELL program directs reading
2950 'the voltages from the balance, computes forces measured
2960 'by the strain guages, then stores the values in two 2965
'arrays,
2970 'one for the TARE one for FORCE.  This data file can then

2980 'be used for graphs or other displays.  Each test run
2990 'will generate a windtun.dat file which should be copied
3000 'under another name before the next test run so that it
3010 'will not be overwritten.
3020 '
3030     'dimension arrays
3040 DIM READING[7],FORCE[140,8],TARE[8],TREAD[7,10]
3050 COLOR 14,1,1
3060 CLS
3070 '
3080 AOA=0
3090 VALUE=5
3100 LOCATE 12,28
3110 PRINT"SETTING UP DATA FILES"
3120 '
3130     'The program will write the data to several files.
3140 STATEFILE$ = "C:\PCIB\WIND.HPC"        'stored in PCIB
subdirectory
3150 DATAFILE$ = "C:WINDTUN.DAT"            'stored on disc C
3160 DISKFILE$ = "A:WINDTUN.DAT"            'stored on disc A
3170 BALANFILE$ = "C:\MODEL\BALANCE.DAT     'stored on disc C
3180 '
3190 RELAY.SETTLING.TIME = .8               '800 ms
3200 LOCATE 16,35:PRINT"D O N E"
3210 CALL DELAY(VALUE)
3220 '
3230 CLS:LOCATE 12,28:PRINT"INITIALIZING INSTRUMENTS"
3240 CALL INITIALIZE.SYSTEM(STATEFILE$)
3250 IF PCIB.ERR <> 0 THEN ERROR PCIB.BASERR
3260 CALL ENABLE.SYSTEM
3270 IF PCIB.ERR <> 0 THEN ERROR PCIB.BASERR
3280 LOCATE 16,35:PRINT"D O N E"
3290 CALL DELAY(VALUE)
```

```
3300 '
3310 'This part of the program is to preserve the data if
3320 'if the program is aborted in mid run.  Parity errors
3330 'in the Hewlett Packard PC Instruments setup caused by
3340 'electrical noise and undervoltage at NPS requires
3350 'this.  A voltage regulated, uninteruptible power source
3360 'would ameliorate this problem. Just in case- this little

3370 'sequence allows reentry into the program and the data
3380 'arrays with minimal inconvenience.
3390 '
3400 CLS:LOCATE 12,20:INPUT"WERE YOU INTERRUPTED (Y OR N)";A$
3410 IF A$="Y" GOTO 3570
3420 '
3430 'The next three variables are counters in the arrays
3440 'FORCE and TARE
3450 '
3460 TRIAL = 0
3470 TRY = 0
3480 '
3490 'open the datafile so each scan can be recorded
3500 '
3510 OPEN DATAFILE$ FOR OUTPUT AS #1
3520 CLOSE #1
3530 OPEN BALANFILE$ FOR OUTPUT AS #3
3540 CLOSE #3
3550 GOTO 3700
3560 '
3570 OPEN DATAFILE$ FOR INPUT AS #1
3580 INPUT#1,TARE(1),TARE(2),TARE(3),TARE(4),TARE(5),
3585 TARE(6),TARE(7),TARE(8)
3590 FOR X = 1 TO 140
3600 INPUT
#1,FORCE(X,1),FORCE(X,2),FORCE(X,3),FORCE(X,4),FORCE(X,5),
3605 FORCE(X,6),FORCE(X,7),FORCE(X,8)
3610 NEXT X
3620 CLOSE #1
3630 '
3640 GOTO 3700
3650 'A$ is used as a marker for interrupted run sequences
3660 'in the program, it is set to <>"Y" so the
3670 'uninterrupted  sequences  are  used  unless  otherwise
directed
3680 '
3690 A$="N"
3700 KEY OFF
3710 '
3720 'prompt to begin each scan or quit program if desired
3730 '
3740 CLS:LOCATE 12,10
```

```
3750 INPUT "TO START SCAN ENTER ANY KEY EXCEPT Q, Q TO
QUIT";ANSWER$
3760 IF ANSWER$ = "Q" THEN GOTO 6630
3770 '
3780 'THIS ENTERS THE AOA FOR EACH TRIAL AND DISPLAYS IT IN
THE PRINTOUT
3790 '
3800 CLS:LOCATE 12,10
3810 PRINT "THE CURRENT ANGLE OF ATTACK IS ";AOA
3820 '
3830 '
3840 LOCATE 15,10:PRINT "INPUT THE ANGLE OF ATTACK (AOA) FOR
THE NEXT TRIAL"
3850 INPUT AOA          'READING(1)
3860 GOTO 3870
3870 '
3880 READING(1)=AOA
3890 '
3900 'This variable is a marker in the iteration loop
3910 'interaction equations for convergence.
3920 '
3930 CYCLE = 0
3940 '
3950 'This loop scans the pitch angle and 6 balance channels
3960 'and stores the values in the array READING
3970 'Each channel is read ten times and averaged.
3980 'The user may reject the current readings and input a new
set.
3990 '
4000 CLS
4010 PRINT"******************** DIRECT BALANCE READINGS
*********************
4020 PRINT"                    CHECK OF SYSTEM OPERATION
4030 PRINT
                  " IN VOLTS     N1        N2        S1
    S2        A      R "
4040 PRINT
                  " ********     ******    ******    ******
    ******    ******    ******"
4050 '
4060 'This file is for storing the direct voltage readings and
averages.
4070 'The data file is continually appended.
4080 'The data is for further analysis of the direct voltage
readings.
4090 OPEN BALANFILE$ FOR APPEND AS #3
4100 '
4110 FOR CNT = 1 TO 10
4120 FOR CHANNEL = 2 TO 7
4130    CALL OUTPUT(RELAY.MUX.01, CHANNEL)
4140            IF PCIB.ERR <> 0 THEN ERROR PCIB.BASERR
```

```
4150      CALL DELAY(RELAY.SETTLING.TIME)
4160              IF PCIB.ERR <> 0 THEN ERROR PCIB.BASERR
4170      CALL MEASURE(DMM.01, READING[CHANNEL])
4180              IF PCIB.ERR <> 0 THEN ERROR PCIB.BASERR
4190 TREAD(CHANNEL,CNT) = READING(CHANNEL)
4200 NEXT CHANNEL
4210 PRINT USING
          "            +.###### +.###### +.#####
+ . # # # # # #            + . # # # # # #
+.#####";READING(2),READING(3),READING(4),READING(5),READIN
G(6),READING(7)
4220 PRINT #3, USING
          "      +###.#      +.######    +.#####
+ . # # # # # #     + . # # # # # #      + . # # # # #
+.#####";READING(1),READING(2),READING(3),READING(4),READIN
G(5),READING(6),READING(7)
4230 NEXT CNT
4240 '
4250 '   CALL SUBROUTINE TO AVERAGE READINGS
4260 GOSUB 6690
4270 '
4280 PRINT"- - - - - - - - - - - - - - - - - - - - - - - - -
- - - - - - - - - -"
4290 PRINT USING
          "MEAN VALUE +.###### +.###### +.#####
+ . # # # # # #            + . # # # # # #
+.#####";READING(2),READING(3),READING(4),READING(5),READIN
G(6),READING(7)
4300 PRINT #3, USING
          "      +###.#    +.######    +.#####
+ . # # # # # #     + . # # # # # #      + . # # # # #
+.#####";READING(1),READING(2),READING(3),READING(4),READIN
G(5),READING(6),READING(7)
4310 CLOSE #3
4320 PRINT" ":BEEP
4330 PRINT"<CR> TO CONTINUE, "1" TO GET NEW READINGS"
4340 INPUT XYZ
4350 IF XYZ=1 GOTO 3940
4360 '
4370 'These equations take voltage readings from the balance,
4380 'converts them to counts, then applys the primary force
4390 'equations to the results.  These values are applied to
4400 'the balance interaction equations. Each channel has
4410 'separate equations for positive and negative readings
and
4420 'may have a "+" or "-" reading on any test run so the
4430 'rather involved logic path below is my solution to the
4440 'problem.  For more information consult Calibration
laboratory
4450 'guidelines at NASA Ames Research Facility for TASK
balances
```

```
4460 '
4470 '************** CONVERT SIGNAL TO FORCES ***************
4480 '*****************************************************
4490 '
4500 'Direct balance readings are multiplied by a scale factor

4510 '5000000 then divided by the balance exitation voltage
to
4520 'get a readiing in COUNTS. The program will send each
reading
4530 'to the appropriate equation and convert to force or
moment
4540 'then return to send the next reading for calculation
4550 'The data acquisition system for using this program used
an
4560 'amplifier with 1000 gain. The scale factor is divided
by 1000.
4570 '
4580 VEX=5                          'Excitation Voltage
4590 N1=READING(2)*5000!/VEX
4600 N2=READING(3)*5000!/VEX
4610 S1=READING(4)*5000!/VEX
4620 S2=READING(5)*5000!/VEX
4630 A=READING(6)*5000!/VEX
4640 R=READING(7)*416.67#/VEX
4650 '
4660 'send each reading to the appropriate equation
4670 '
4680 IF READING(2)>0 THEN GOTO 4770 ELSE GOTO 4920
4690 IF READING(3)>0 THEN GOTO 4790 ELSE GOTO 4940
4700 IF READING(4)>0 THEN GOTO 4830 ELSE GOTO 4980
4710 IF READING(5)>0 THEN GOTO 4850 ELSE GOTO 5000
4720 IF READING(6)>0 THEN GOTO 4810 ELSE GOTO 4960
4730 IF READING(7)>0 THEN GOTO 4870 ELSE GOTO 5020
4740 '
4750 '************** POSITIVE FORMULAS *************
4760 '
4770 EN1 = .050861*N1 - 5.4826E-09*(N1*N1)
4780 GOTO 4690
4790 EN2 = .047211*N2 - 1.7015E-08*(N2*N2)
4800 GOTO 4700
4810 EA = .014309*A - 7.1962E-10*(A*A)
4820 GOTO 4730
4830 ES1 = .031309*S1 - 3.8153E-08*(S1*S1)
4840 GOTO 4710
4850 ES2 = .030366*S2 - 3.8607E-08*(S2*S2)
4860 GOTO 4720
4870 ER = .0030885*R + 2.5672E-09*(R*R)
4880 GOTO 5030
4890 '
4900 '************** NEGATIVE FORMULAS *************
```

```
4910 '
4920 EN1 = .051591*N1 + 1.7157E-08*(N1*N1)
4930 GOTO 4690
4940 EN2=.047763*N2+8.915299E-09*(N2*N2)
4950 GOTO 4700
4960 EA = .01429*A - 1.3322E-09*(A*A)
4970 GOTO 4730
4980 ES1 = .032073*S1 - 8.931601E-09*(S1*S1)
4990 GOTO 4710
5000 ES2 = .031167*S2 - 7.2517E-09*(S2*S2)
5010 GOTO 4720
5020 ER = .0030908*R - 2.4769E-09*(R*R)
5030 '
5040 '
5050 'a heading for the iteration values
5060 '
5070 PRINT"
          "
5080 PRINT"******************** FORCE INTERACTION ITERATIONS
*****************
5090 PRINT"                              CHECK FOR CONVERGENCE
5100 PRINT
                   " CYCLE   AOA      N1        N2        S1
     S2       A       R "
5110 PRINT
                   "  #     DEG    POUNDS    POUNDS    POUNDS
 POUNDS   POUNDS   FT-LBS"
5120 PRINT
                   " *****   ***   ******    ******    ******
 ******   ******   ******"
5130 '
5140 'The loop that controls the balance interaction
5150 'equations and allows a visual convergence check
5160 '
5170 FOR I = 1 TO 10
5180 IF READING(2)>0 THEN GOTO 5270 ELSE GOTO 5470
5190 IF READING(3)>0 THEN GOTO 5300 ELSE GOTO 5500
5200 IF READING(4)>0 THEN GOTO 5360 ELSE GOTO 5560
5210 IF READING(5)>0 THEN GOTO 5390 ELSE GOTO 5590
5220 IF READING(6)>0 THEN GOTO 5330 ELSE GOTO 5530
5230 IF READING(7)>0 THEN GOTO 5420 ELSE GOTO 5620
5240 '
5250 '**************POSITIVE FORMULAS**************
5260 '
5270 XN1=
EN1+.0058036*N2+.0041655*S1+.058079*R-7.1926E-07*(N2*N2)+4.0
352E-06*(S1*S1)-.0006786*(R*R)
5280 GOTO 5190
5290 '
5300 XN2=
```

```
EN2+.046218*N1-.0028393*A-.0081694*S1+.0041463*S2+.077279*R-
6.8577E-07*(N1*N1)-1.7755E-05*(A*A)+2.1719E-06*(S1*S1)+1.858
2E-06*(S2*S2)-.0019294*(R*R)
5310 GOTO 5200
5320 '
5330 XA=
EA+8.6893E-04*N1+6.0359E-04*S1+7.7722E-05*S2-.11115*R+4.4537
E-07*(N1*N1)+4.7936E-06*(S1*S1)-4.1033E-06*(S2*S2)+2.0697E-0
4*(R*R)
5340 GOTO 5230
5350 '
5360 XS1 =
ES1-6.3459E-04*N1-.11148*R+5.535E-06*(N1*N1)+.0024592*(R*R)
5370 GOTO 5210
5380 '
5390 XS2=
ES2-.0024237*N1+.0022455*A+.0066785*S1-.26377*R+1.7099E-06*(
N1*N1)+1.2072E-05*(A*A)-2.7825E-06*(S1*S1)+.0062217*(R*R)
5400 GOTO 5220
5410 '
5420 XR=
ER-1.9928E-04*N2-2.5893E-04*S2+1.1512E-07*(N2*N2)-5.156E-08*
(S2*S2)
5430 GOTO 5630
5440 '
5450 '************** NEGATIVE FORMULAS ************
5460 '
5470 XN1=
EN1+.010257*N2-.0045396*S1-.04494*R+7.9499E-07*(N2*N2)-1.967
E-06*(S1*S1)-.0003232*(R*R)
5480 GOTO 5190
5490 '
5500 XN2=
EN2+.051778*N1-.0044056*A-9.038499E-03*S1-.061125*R+5.2897E-
06*(N1*N1)+1.0467E-05*(A*A)-4.8493E-07*(S1*S1)-.0011773*(R*R)
5510 GOTO 5200
5520 '
5530 XA=
EA-.0021217*N1+9.1524E-04*N2-.097148*R-4.2547E-06*(N1*N1)+4.
5846E-06*(N2*N2)-7.5001E-04*(R*R)
5540 GOTO 5230
5550 '
5560 XS1=
ES1-.0071275*N1-.0089235*A-.05268*R-1.2923E-05*(N1*N1)-4.034
5E-05*(A*A)-9.3969E-04*(R*R)
5570 GOTO 5210
5580 '
5590 XS2=
ES2-.0037176*N1-.0052619*N2+.0072915*A+.006856*S1-.062581*R-
5.211E-07*(N1*N1)-8.6265E-06*(N2*N2)+3.7054E-05*(A*A)+9.9830
01E-06*(S1*S1)+8.0007E-04*(R*R)
```

65

```
5600 GOTO 5220
5610 '
5620 XR= ER+3.5945E-04*N1+1.5497E-07*(N1*N1)
5630 '
5640 'Shift all the new variables back to the old name
5650 'for the next iteration
5660 N1=XN1
5670 N2=XN2
5680 A=XA
5690 S1=XS1
5700 S2=XS2
5710 R=XR
5720 '
5730 'A marker for the interations
5740 CYCLE = CYCLE + 1
5750 'print the iterations to watch for convergence
5760 '
5770 PRINT USING
                "   ##    +##.#  +###.##  +###.##  +###.##
+###.##  +###.##  +###.##";CYCLE,AOA,N1,N2,S1,S2,A,R
5780 NEXT I
5790 '
5800 INPUT "IF CONVERGENCE IS ADEQUATE ENTER Y, IF ANOTHER RUN
IS DESIRED ENTER N";ANSWR$
5810 IF ANSWR$ = "N" THEN GOTO 5060
5820 '
5830 NORMAL = N1 + N2
5840 SIDE = S1 + S2
5850 AXIAL = A
5860 PITCH = (N1-N2) * .0854
5870 ROLL = (S1-S2) * .0698
5880 YAW = R*12
589RINT
                " *****  ****  ********  ********  ********
 ********  ********  ********"
2600 FOR X = 1 TO 140
2610 IF COEF(X,3)=0! THEN GOTO 2640
2620  LPRINT USING" ###    +###.#      +##.####      +##.####
+##.####          +##.####          +##.####
+##.####";COEF(X,1),COEF(X,2),COEF(X,3),COEF(X,4),COEF(X,5),
COEF(X,6),COEF(X,7),COEF(X,8)
2630 NEXT X
2640 '
2650 INPUT"DO YOU WANT TO EXIT THE PROGRAM";AANS$
2660 IF AANS$<>"Y" THEN GOTO 1060
2670 END
^Z
```

APPENDIX C
COEFFICIENTS TRANSLATION PROGRAM

```
1000 '  PROGRAM BY M.P. RABANG AND MODIFIED BY D.H. LEEDY TO
READ FORCE AND MOMENT VALUES FROM A DATA FILE CREATED BY THE
DATA ACQUISITION PROGRAM.
1020 '
1030 COLOR 10,4,1
1040 '
1050 DIM TARE[8], FORCE[140,8], COEF[140,9]
1060 '
1070 CLS
1080 LOCATE 5
1090 INPUT"ENTER THE NAME OF THE INPUT FILE";INFILE$
1100 INPUT"ENTER THE NAME OF THE OUTPUT FILE";OUTFILE$
1110 INPUT"ENTER THE MINIMUM TEMPERATURE (F)";TMIN
1120 INPUT"ENTER THE MAXIMUM TEMPERATURE (F)";TMAX
1130  INPUT"ENTER THE  MODEL  ORIENTATION,  A=PY,  B=15,  C=30,
D=45";BOD$
1140 IF BOD$="A" THEN BODY=1: GOTO 1250
1150 IF BOD$="B" THEN BODY=2: GOTO 1250
1160 IF BOD$="C" THEN BODY=3: GOTO 1250
1170 IF BOD$="D" THEN BODY=4: GOTO 1250
1180 GOTO 1130
1250 INPUT"ENTER THE WIND TUNNEL VELOCITY (cm H20)";PH20
1260 INPUT"DO YOU WANT TO VIEW OUTPUT";PANS$
1270 INPUT"DO YOU WANT A HARDCOPY";ANS$
1280 '
1290 '  OPEN THE DATA FILE SO EACH SCAN IS RECORDED
1300 TRANSFILE$="C:\MISSILE\TRANS.DAT"
1310 OPEN OUTFILE$ FOR OUTPUT AS #2
1320 CLOSE #2
1330 '
1340 '  READ THE FORCE VALUES FROM THE DATA FILE
1350 OPEN INFILE$ FOR INPUT AS #1
1360 INPUT#1,TARE(1),TARE(2),TARE(3),TARE(4),TARE(5),
1365 TARE(6),TARE(7),TARE(8)
1370 FOR X = 1 TO 140
1380
INPUT#1,FORCE(X,1),FORCE(X,2),FORCE(X,3),FORCE(X,4),FORCE(X,5)
1385 FORCE(X,6),FORCE(X,7),FORCE(X,8)
1390 IF FORCE(X,1)=0! THEN GOTO 1410
1400 NEXT X
1410 CLOSE #1
1420 IF PANS$<>"Y" THEN GOTO 1610
1430 '
```

```
1440 '   DISPLAY FORCE VALUES
1450 COLOR 14,1,1
1460 CLS
1470 PRINT"FILE NAME: ";INFILE$
1480 PRINT" "
1490 PRINT"* * * * * * * * * * * * * * FORCE READINGS * * *
* * * * * * * * * * * * * *
1500 PRINT" "
1510 PRINT
                   " TRIAL    AOA      SIDE         NORMAL
AXIAL       PITCH      ROLL      YAW"
1520 PRINT
                   "   #       DEG     POUNDS        POUNDS
POUNDS     FT-LBS      FT-LBS      FT-LBS"
1530 PRINT
                   " *****    *****   ********    ********
********   ********   ********   ********"
1540 '
1550 FOR J = 1 TO 140
1560 IF FORCE(J,1)=0 THEN GOTO 1590
1570 PRINT USING"  ### +###.#   +##.####   +##.####   +##.####
   + # # . # # # #            + # # . # # # #
+##.####";FORCE(J,1),FORCE(J,2),FORCE(J,3),FORCE(J,4),FORCE(
J,5),FORCE(J,6),FORCE(J,7),FORCE(J,8)
1580 NEXT J
1590 '
1600 INPUT"ENTER <CR> TO CONTINUE";INPT$
1610 '
1620 '   BEGIN COEFFICIENTS CALCULATION
1630 A=0.020
1640 MU=3.719E-07
1650 TAV=(TMIN+TMAX)/2!
1660 RHO=2116.22/(1545*(459.7+TAV))
1670 IF SCR>0 GOTO 1740
1680 VE=(2!*2.046*PH20)/(.93*RHO)
1690 VEL=SQR(VE)
1700 RED=(RHO*VEL*(3.88/12))/MU
1710 Q=(RHO*VEL*VEL)/2!
1720 GOTO 1800
1730 '
1790 '   WRITE THE COEFFICIENTS TO THE OUTPUT FILE
1800 OPEN OUTFILE$ FOR OUTPUT AS #2
1810 OPEN TRANSFILE$ FOR APPEND AS #3
1820 WRITE #3, OUTFILE$
1830 FOR X = 1 TO 140
1840 FOR Y = 3 TO 8
1850 IF FORCE(X,1)=0 THEN GOTO 2040
1860 '   ROUTINE TO CORRECT THE DYNAMIC PRESSURE FOR BLOCKAGE
1870 '    AND BODY TYPE
1880 COEF(X,1)=FORCE(X,1)
1890 COEF(X,2)=FORCE(X,2)
```

```
1900 ALPHA = FORCE(X,2)
1910 IF FORCE(X,2) < 0 THEN ALPHA = ABS(FORCE(X,2))
1920 IF FORCE(X,2) > 90 THEN ALPHA = 180-FORCE(X,2)
1930 IF BODY=1 THEN EPS=.0002070*ALPHA+.007594
1940 IF BODY=2 THEN EPS=.0002038*ALPHA+.007594
1950 IF BODY=3 THEN EPS=.0001962*ALPHA+.007594
1955 IF BODY=4 THEN EPS=.0001878*ALPHA+.007594
1960 D = A*Q*(1+(2*EPS))
1970 COEF(X,Y) = FORCE(X,Y)/D
1980 COEF(X,9)=COEF(X,4)/COEF(X,3)
1990 NEXT Y
2000 IF FORCE(X,1)=0 THEN GOTO 2040
2010
WRITE#2,COEF(X,1),COEF(X,2),COEF(X,3),COEF(X,4),COEF(X,9),
2015 COEF(X,5),COEF(X,6),COEF(X,7),COEF(X,8)
2020
WRITE#3,COEF(X,1),COEF(X,2),COEF(X,3),COEF(X,4),COEF(X,9),
2025 COEF(X,5),COEF(X,6),COEF(X,7),COEF(X,8)
2030 NEXT X
2040 CLOSE #2
2050 CLOSE #3
2060 IF PANS$<>"Y" THEN GOTO 2300
2070 '
2080 '   DISPLAY ROUTINE
2090 COLOR 10,4,1
2100 CLS
2110 PRINT"FILE NAME: ";OUTFILE$
2120 PRINT" "
2130 PRINT"AVERAGE TEMPERATURE (F)              ";TAV
2140 PRINT"WIND TUNNNEL VELOCITY (FT/SEC)       ";VEL
2150 PRINT"WIND TUNNNEL VELOCITY (cmH2O)        ";PH2O
2160 PRINT"AIR DENSITY (LBM/FT3)                ";RHO
2170 PRINT"REYNOLDS NUMBER                      ";RED
2180 PRINT"DYNAMIC PRESSURE (LB/FT2)            ";Q
2190 PRINT" "
2200 PRINT"* * * * * * * * * * * * * FORCE COEFFICIENTS *
* * * * * * * * * * * * * *
2210 PRINT" "
2220 PRINT
                  " TRIAL    AOA      SIDE         NORMAL
AXIAL      PITCH      ROLL       YAW"
2230 PRINT
                  " *****    *****    ********     ********
*******   ********   ********   ********"
2240 FOR X = 1 TO 140
2250 IF COEF(X,3)=0 THEN GOTO 2280
2260 PRINT USING" ###  +###.#   +##.####   +##.####   +##.####
   + # # . # # # #                  + # # . # # # #
+##.####";COEF(X,1),COEF(X,2),COEF(X,3),COEF(X,4),COEF(X,5),
COEF(X,6),COEF(X,7),COEF(X,8)
2270 NEXT X
```

69

```
2280 '
2290 PRINT" "
2300 IF ANS$<>"Y" THEN GOTO 2640
2310 '   HARDCOPY ROUTINE
2320 LPRINT"INPUT FILENAME: ";INFILE$
2330 LPRINT"OUTPUT FILENAME: ";OUTFILE$
2340 LPRINT" "
2350 LPRINT"INITIAL TEMPERATURE (F)            ";TMIN
2360 LPRINT"FINAL TEMPERATURE (F)              ";TMAX
2370 LPRINT"AVERAGE TEMPERATURE (F)            ";TAV
2380 LPRINT"WIND TUNNEL VELOCITY (FT/SEC)      ";VEL
2390 LPRINT"WIND TUNNEL VELOCITY (cmH2O)       ";PH2O
2400 LPRINT"AIR DENSITY (LBM/FT3)              ";RHO
2410 LPRINT"REYNOLDS NUMBER                    ";RED
2420 LPRINT"DYNAMIC PRESSURE (LB/FT2)          ";Q
2430 LPRINT" "
2440 LPRINT" "
2450 LPRINT"* * * * * * * * * * * * * FORCE READINGS * * *
* * * * * * * * * * * * * *
2460 LPRINT" "
2470 LPRINT
                   " TRIAL    AOA      SIDE          NORMAL
AXIAL       PITCH      ROLL      YAW"
2480 LPRINT
                   "   #      DEG     POUNDS        POUNDS
POUNDS      FT-LBS     FT-LBS     FT-LBS"
2490 LPRINT
                   " *****    *****    *******      *******
*******   *******    *******    *******"
2500 FOR J = 1 TO 140
2510 IF FORCE(J,1)=0 THEN GOTO 2540
2520 LPRINT USING"  ###    +###.#      +##.####    +##.####
+##.####           +##.####            +##.####
+##.####";FORCE(J,1),FORCE(J,2),FORCE(J,3),FORCE(J,4),FORCE(
J,5),FORCE(J,6),FORCE(J,7),FORCE(J,8)
2530 NEXT J
2540 LPRINT" "
2550 LPRINT" "
2560 LPRINT"* * * * * * * * * * * * * FORCE COEFFICIENTS *
* * * * * * * * * * * * * *
2570 LPRINT" "
2580 LPRINT
                   " TRIAL    AOA      SIDE          NORMAL
AXIAL       PITCH      ROLL      YAW"
2590 LPRINT
                   " *****    ****     *******      *******
*******   *******    *******    *******"
2600 FOR X = 1 TO 140
2610 IF COEF(X,3)=0! THEN GOTO 2640
2620 LPRINT USING"  ###    +###.#      +##.####    +##.####
+##.####           +##.####            +##.####
```

```
+##.####";COEF(X,1),COEF(X,2),COEF(X,3),COEF(X,4),COEF(X,5),
COEF(X,6),COEF(X,7),COEF(X,8)
2630 NEXT X
2640 '
2650 INPUT"DO YOU WANT TO EXIT THE PROGRAM";AANS$
2660 IF AANS$<>"Y" THEN GOTO 1060
2670 END
^Z
```

APPENDIX D
FLOW VISUALIZATION SYSTEMS OPERATIONS

The low speed wind tunnel at the Naval Postgraduate School was installed in the mid 1950's. Though a good, basic design, the tunnel was not designed for flow visualization. The main problem in flow visualization is the establishment of a laminar flowfield in the test section. This is complicated by the necessity to inject smoke by some means. Recent developments in West Germany have demonstrated that the production of sharp smoke filaments depends on two critical factors.

First, a perfectly laminar flow is an absolute necessity. This was accomplished at VFW by the use of very fine mesh damping screens, a large settling chamber and high contraction ratios in the final contraction cone. In all, the VFW tunnel produces extremely low turbulence by using an open, flow-through type tunnel with three 2-D contraction cones and 12 anti-turbulence damping screens. A similar tunnel is operated by the University of Notre Dame which also uses 12 anti-turbulence damping screens and a contraction ration of 24:1 in the final section. The Naval Postgraduate School tunnel has only one contraction cone and two anti-turbulence screens prior to the test section. In addition, the contraction cone and screens are immediately following a 90-degree bend in the tunnel where the flow has just exited a

series of turning vanes. A laminar flow pattern, necessary to keeping the smoke filaments intact, simply cannot be achieved with this apparatus.

Second, the flow into the test section cannot be disturbed by the smoke injection device itself. This is usually accomplished by placing the smoke rake or tube in the contraction cone where the pressure gradient is conducive to keeping the filament intact. This is only possible if the turbulence in the cone is low enough to prevent disruption of the filament. [Ref. 23]

Early in this investigation, numerous methods for injecting smoke into the test section were evaluated. The original system featured a blower which pumped smoke through a 1.25 inch diameter rigid plastic hose to a five-filament smoke rake [Ref. 7]. This system, though adequate for demonstrating the functioning of the laser sheet flow visualization system, was not suitable for use in this experimental investigation. The blower section was not airtight and the motor was too weak to push smoke in any significant quantity through the attached tubing. Numerous leaks reduced the amount of smoke injected through the rake and rapidly filled the tunnel with unwanted smoke. The blower system and 1.25 inch tubing were replaced by a three-inch flexible hose. The length of tubing through which the smoke had to travel was reduced and all connections were made airtight. This modification provided a more efficient means

73

of routing the smoke to the selected injection device and eliminated the need for the blower assembly.

A new smoke rake was developed incorporating 21 tubes spaced one and one-half inches apart. The airfoil encasing the rake is a hollow aluminum shell that was, in fact, an old flap from an unknown aircraft. The airfoil is symmetrical with a maximum thickness of 1.6 inches and a chord of 15 inches. The rake tubes extend 14 inches aft of the trailing edge of the airfoil. The rake was extremely heavy but incorporated some features that were improvements over the original five-tube rake used when the system was installed. The hollow airfoil allowed space for the smoke to accumulate providing an even and more dense distribution. In addition, the rake was designed to allow replacement of the smoke tube section without creating a whole new airfoil. The smoke accumulation chamber is thus generic requiring only the manufacture of a new trailing edge section.

Though this system provided a thicker and wider sheet of smoke to the test section the problem of smoke filament diffusion still remained. As it developed, the use of a smoke rake for the study of a model aircraft at high angles of attack proved unsuitable and therefore the new rake was not used in this investigation. A smoke-wire injection system was also tried which allowed for much cleaner, less diffused smoke filaments to reach the model because of the much closer positioning possibile. This method was also not

used because the non-laminar, vortex flows that dominate at high angles of attack were not adequately highlighted by this method.

Extensive effort was put forth into the development of a method to inject a single, thick tube of smoke into the test section which would provide a satisfactory means of high angle of attack flow visualization. The system ultimately adopted consisted of a three-inch flexible hose feeding from the Rosco smoke machine to a small football-shaped settling chamber which featured a three-inch long, honeycombed flow straightener section prior to a 10:1 contraction ratio section. An eight-foot section of one-inch diameter aluminum tubing exited the contraction section providing the outlet for the smoke. The contraction section of the smoke device was mounted on an adjustable height support stand and positioned in the contraction cone of the tunnel. The exit tube extended into the test section and was supported by an adjustable height rail system just prior to the test section. To minimize the effects of the tube intrusion into the test section the tube was highly polished and the exit orifice was honed razor sharp to prevent turbulence from flow over the edge caused by pipe thickness. The combination of the flow straightener, contraction cone and long tube provided for some acceleration of a one-inch diameter tube of smooth smoke over the model.

Recording the flow over the model also proved to have limitations. The equipment discussed previously was more than adequate for the recording of flow phenomena. The problems resulted from restricted visible access to the tunnel test section through the three available viewing windows. For angles of attack between 45 and 90 degrees direct photography on a line perpendicular to the flow cross section was possible. From 25 to 45 degrees the view was offset by some degree and pure photography of the flow cross section while looking down the longitudinal axis of the model was not possible. Below 25 degrees angle of attack adequate photographic coverage of flow cross sections was not possible from outside the tunnel.

Figure 14. Station 2 Pitch=45°, Roll=0°,Yaw=0°

Figure 15. Station 2 Pitch=50°, Roll=0°, Yaw=0°

Figure 16. Station 3 Pitch=50°, Roll=0°, Yaw=0°

78
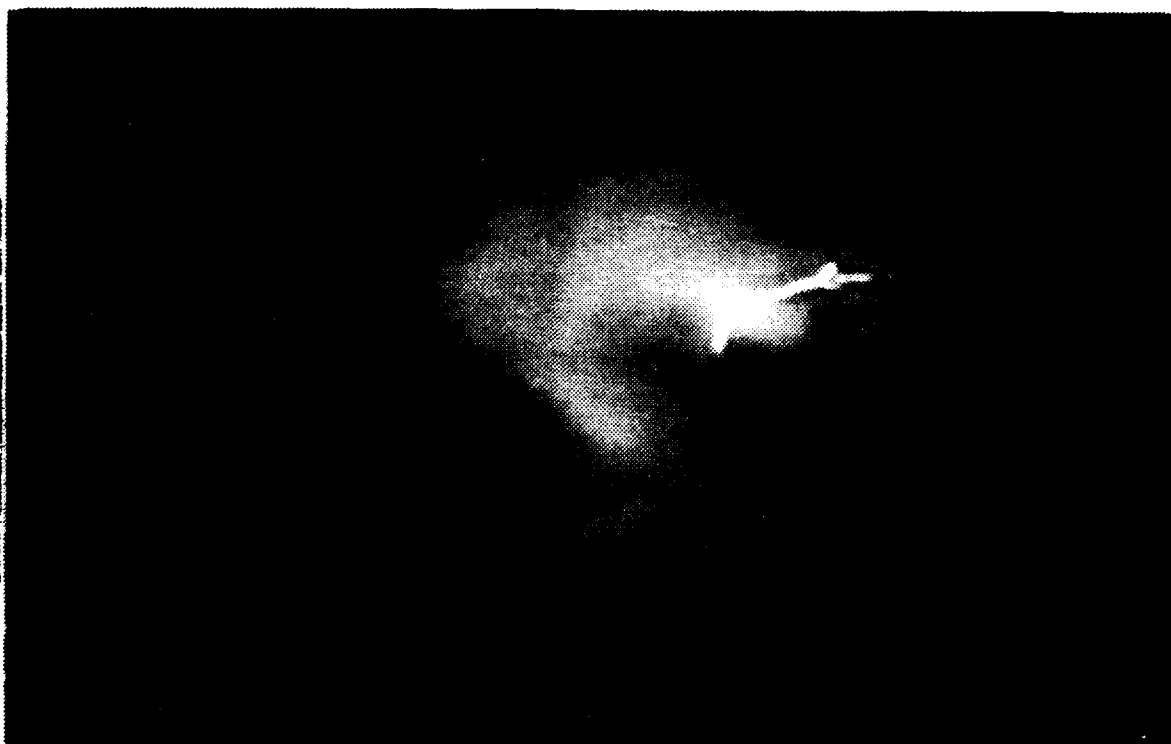
Figure 17. Station 5 Pitch=50°, Roll=0°, Yaw=0°

Figure 18. Station 6 Pitch=50°, Roll=0°, Yaw=0°

**Figure 19.** Station 1 Pitch=65°, Roll=0°, Yaw=0°

Figure 20. Station 3 Pitch=65°, Roll=0°, Yaw=0°

Figure 21. Station 6 Pitch=65°, Roll=0°, Yaw=0°

Figure 22. Station 1 Pitch=65°, Roll=15°, Yaw=0°

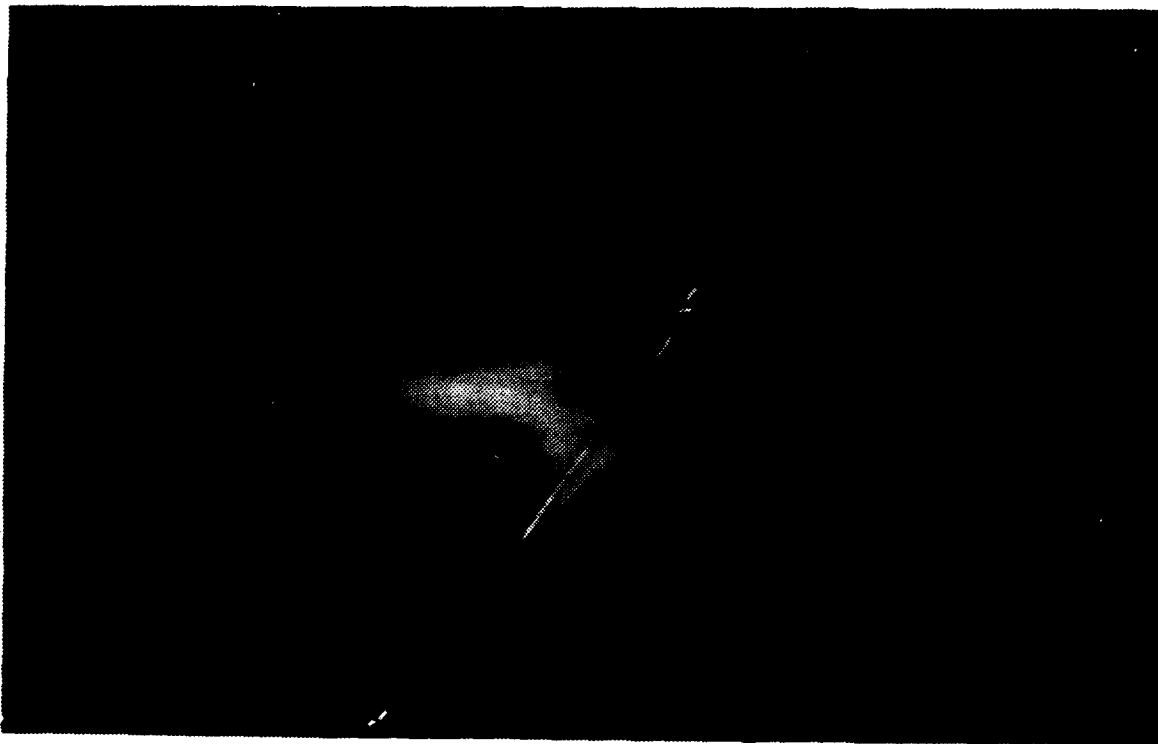**Figure 23.** Station 1 Pitch=65°, Roll=30°, Yaw=0°

Figure 24. Station 1 Pitch=65°, Roll=45°, Yaw=0°

Figure 25. Station 1 Pitch=55°, Roll=15°, Yaw=0°

Figure 26. Station 1 Pitch=55°, Roll=30°, Yaw=0°

83
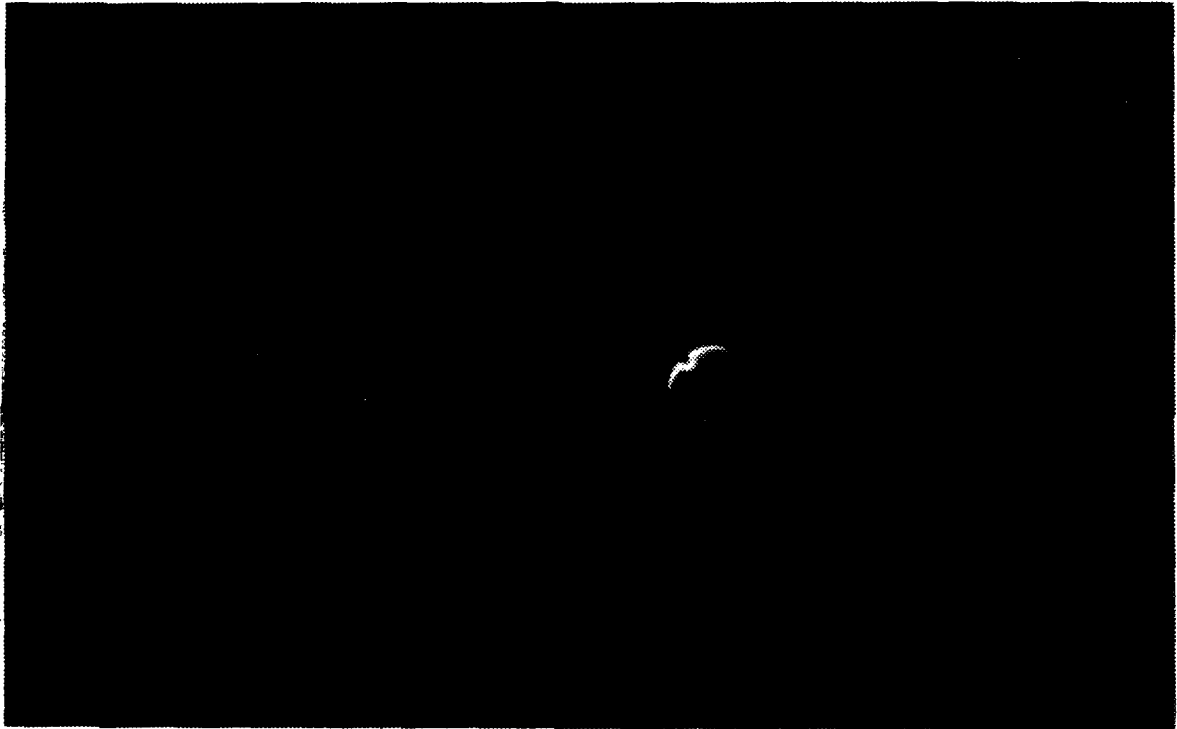
Figure 27. Station 1 Pitch=55°, Roll=45°, Yaw=0°

Figure 28. Station 2 Pitch=65°, Roll=0°, Yaw=0°

84

Figure 29.   Station 2   Pitch=65°, Roll=15°, Yaw=0°

Figure 30.   Station 2   Pitch=65°, Roll=30°, Yaw=0°
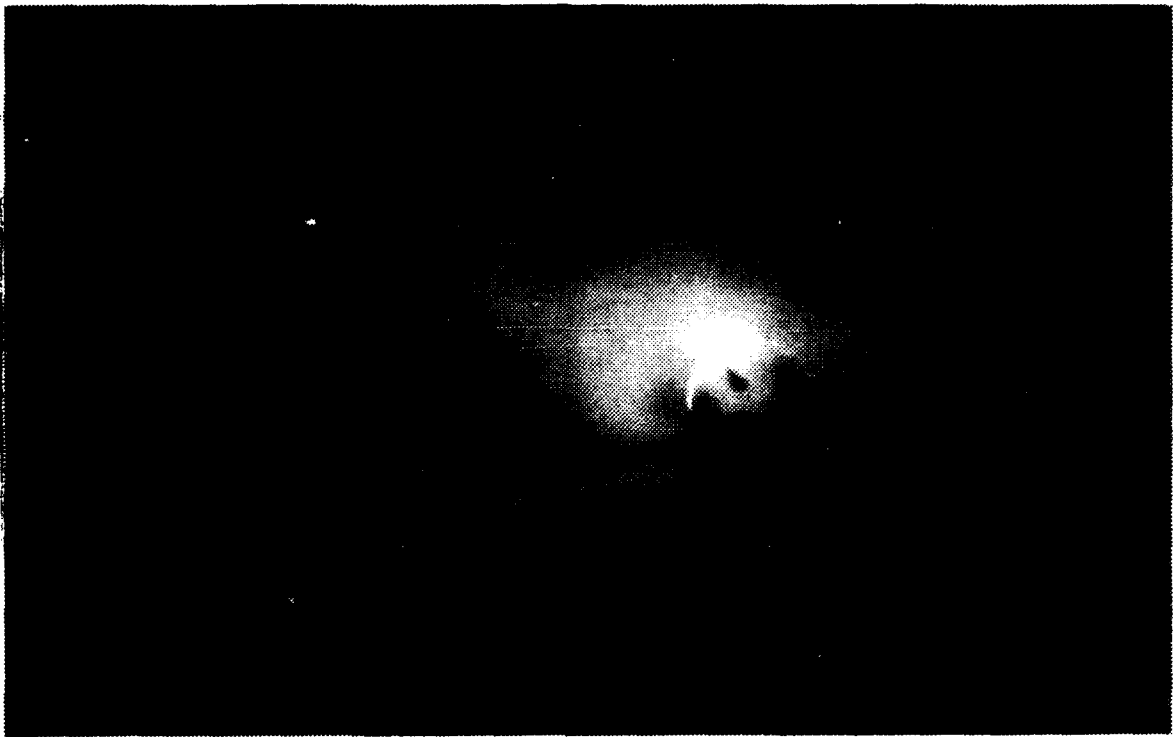
Figure 31. Station 2 Pitch=65°, Roll=45°, Yaw=0°
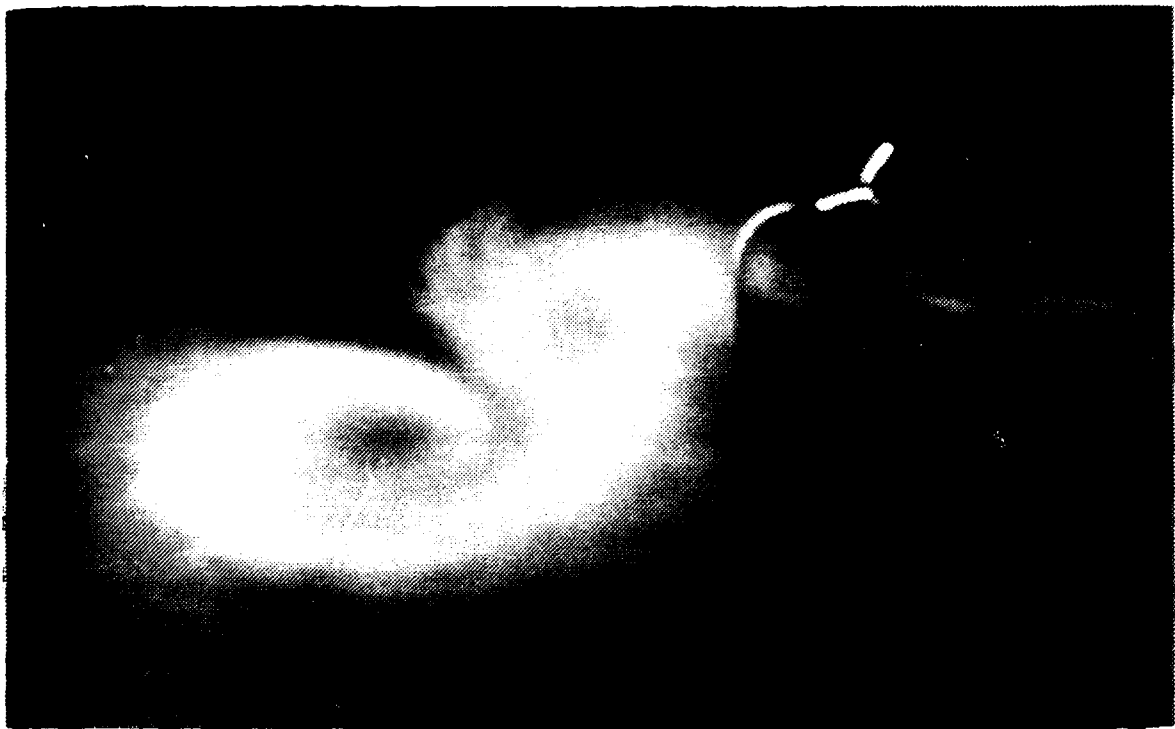
Figure 32. Station 6 Pitch=50°, Roll=0°, Yaw=0°

Figure 33. Station 6 Pitch=50°, Roll=30°, Yaw=0°

**Figure 34.** Station 2 Pitch=45°, Roll=15°, Yaw=0°

Figure 35. Station 2 Pitch=50°, Roll=15°, Yaw=0°
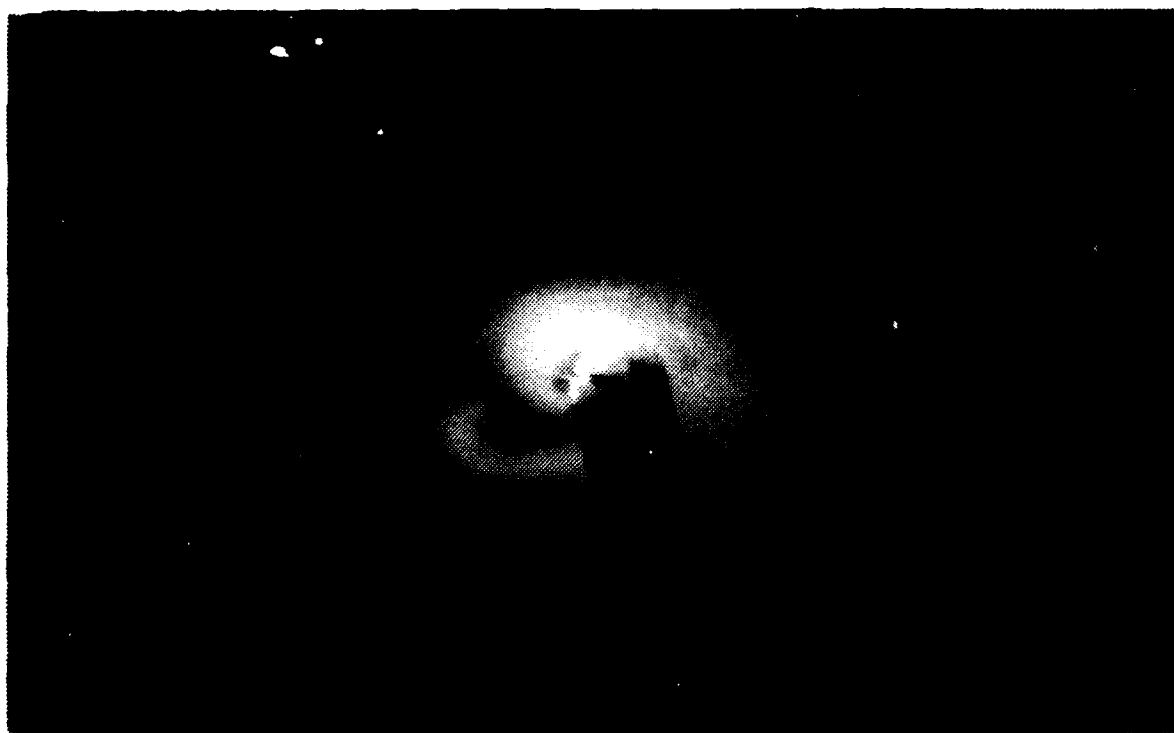
Figure 36. Station 2 Pitch=55°, Roll=15°, Yaw=0°

88
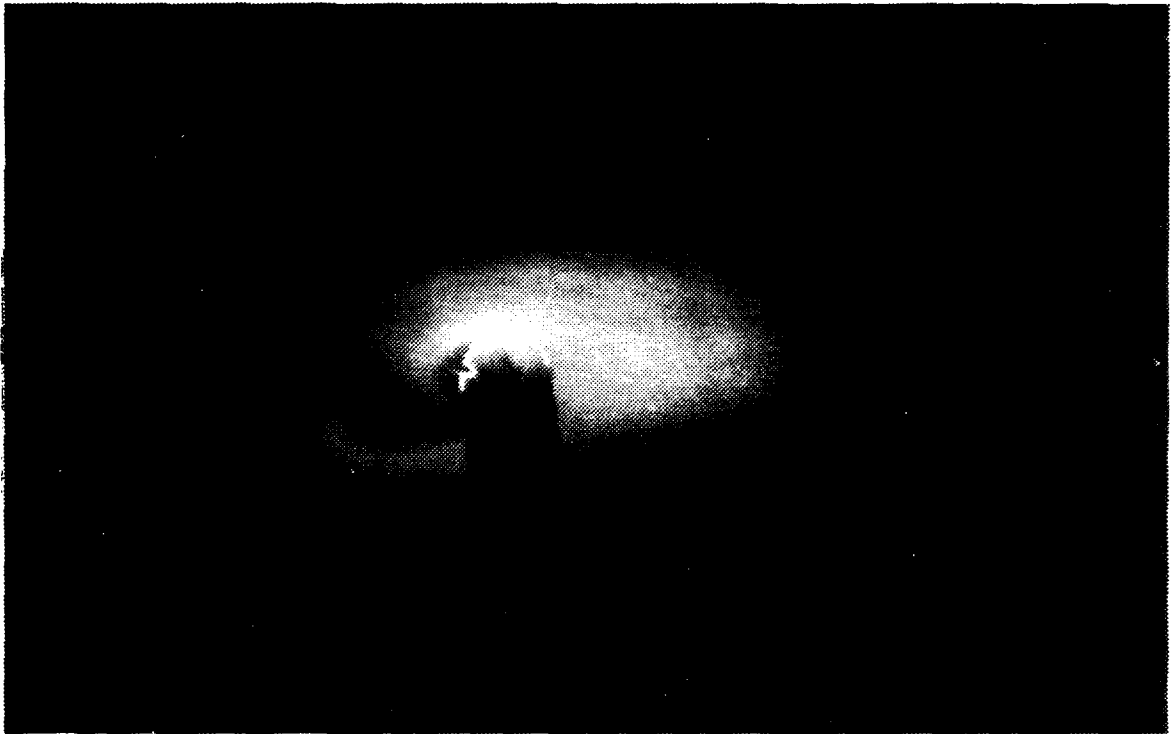
Figure 37. Station 2 Pitch=60°, Roll=15°, Yaw=0°

Figure 38. Station 2 Pitch=65°, Roll=15°, Yaw=0°

Figure 39. Station 2 Pitch=70°, Roll=15°, Yaw=0°

Figure 40. Station 3 Pitch=45°, Roll=15°, Yaw=0°

90

Figure 41. Station 3 Pitch=50°, Roll=15°, Yaw=0°

Figure 42. Station 3 Pitch=55°, Roll=15°, Yaw=0°

Figure 43. Station 3 Pitch=60°, Roll=15°, Yaw=0°

Figure 44. Station 3 Pitch=65°, Roll=15°, Yaw=0°

Figure 45. Station 3   Pitch=70°, Roll=15°, Yaw=0°
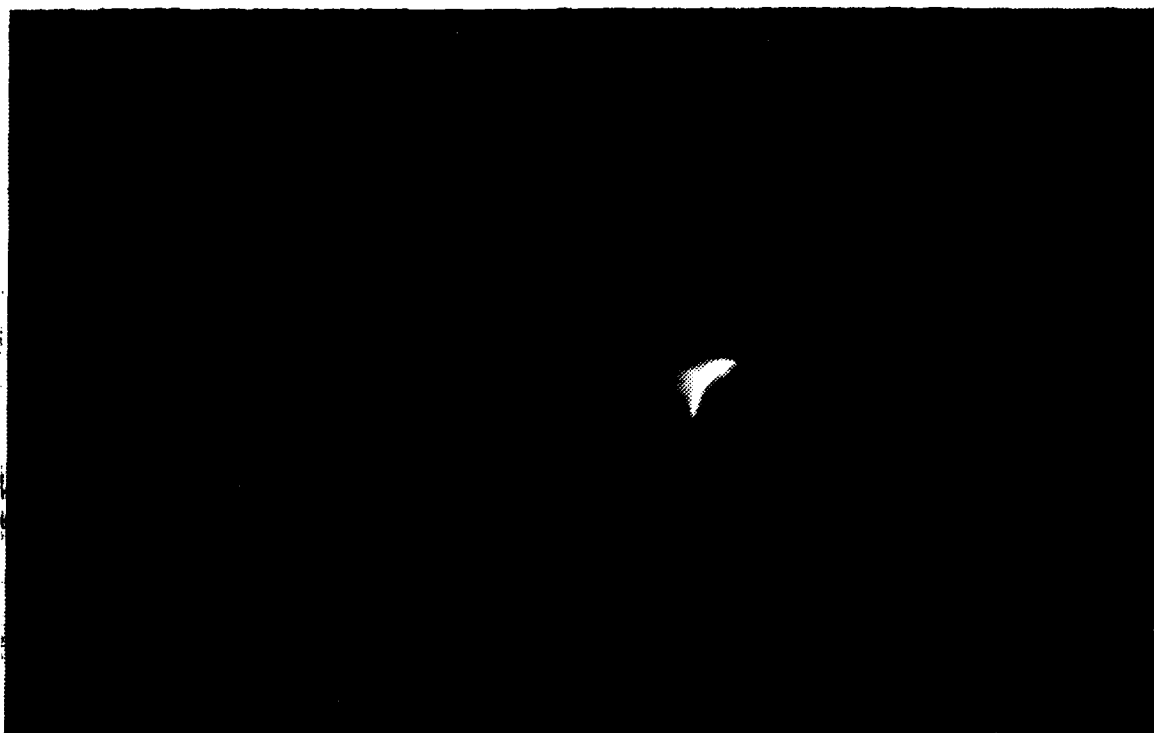
Figure 46. Station 4   Pitch=45°, Roll=15°, Yaw=0°

Figure 47. Station 4 Pitch=50°, Roll=15°, Yaw=0°

Figure 48. Station 4 Pitch=55°, Roll=15°, Yaw=0°

Figure 49. Station 4 Pitch=60°, Roll=15°, Yaw=0°

Figure 50. Station 4 Pitch=65°, Roll=15°, Yaw=0°

95

Figure 51. Station 4 Pitch=70°, Roll=15°, Yaw=0°

Figure 52. Station 5 Pitch=45°, Roll=15°, Yaw=0°

96

Figure 53. Station 5 Pitch=50°, Roll=15°, Yaw=0°
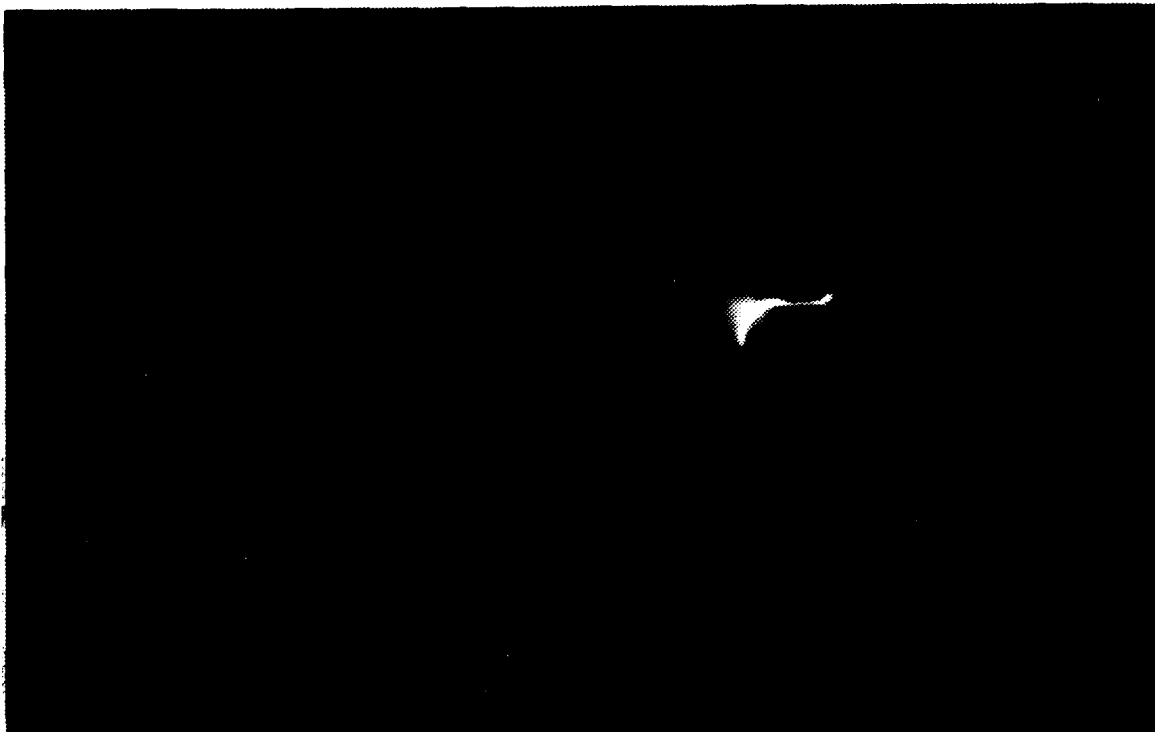
Figure 54. Station 5 Pitch=55°, Roll=15°, Yaw=0°

97

Figure 55. Station 5 Pitch=60°, Roll=15°, Yaw=0°

Figure 56. Station 5 Pitch=65°, Roll=15°, Yaw=0°

Figure 57. Station 5 Pitch=70°, Roll=15°, Yaw=0°
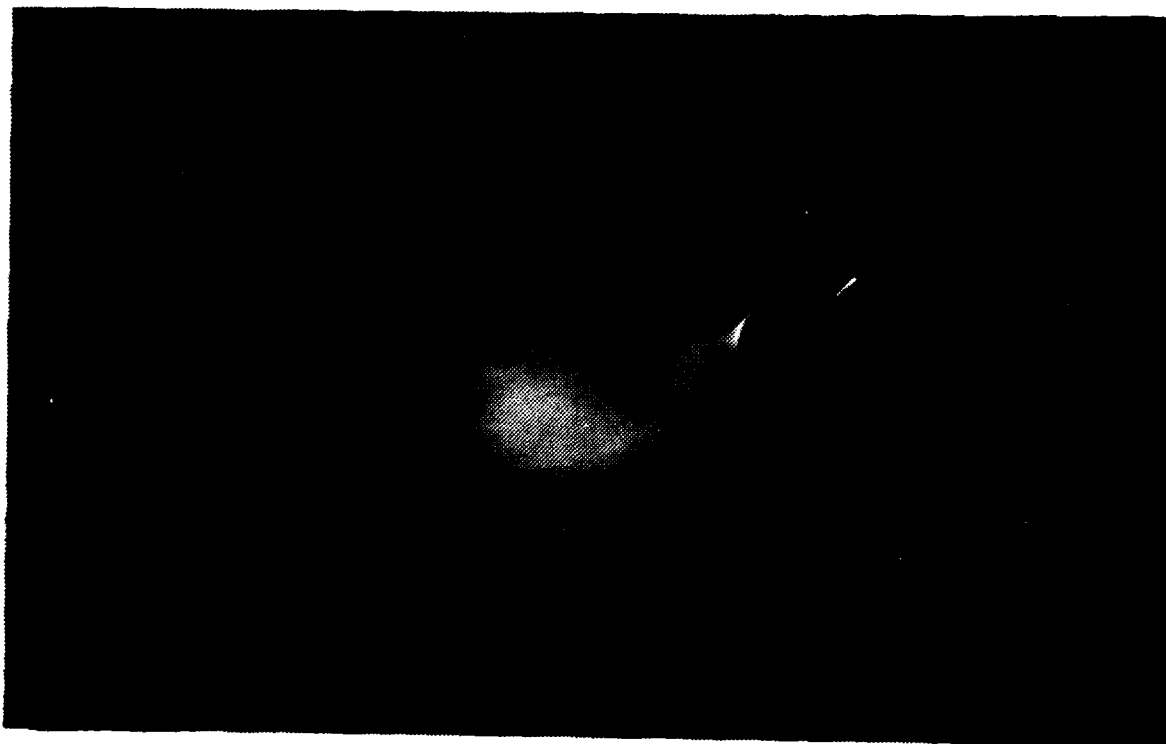
Figure 58. Station 6 Pitch=45°, Roll=15°, Yaw=0°

Figure 59. Station 6 Pitch=50°, Roll=15°, Yaw=0°

Figure 60. Station 6 Pitch=55°, Roll=15°, Yaw=0°

Figure 61. Station 6 Pitch=60°, Roll=15°, Yaw=0°

Figure 62. Station 6 Pitch=65°, Roll=15°, Yaw=0°

101
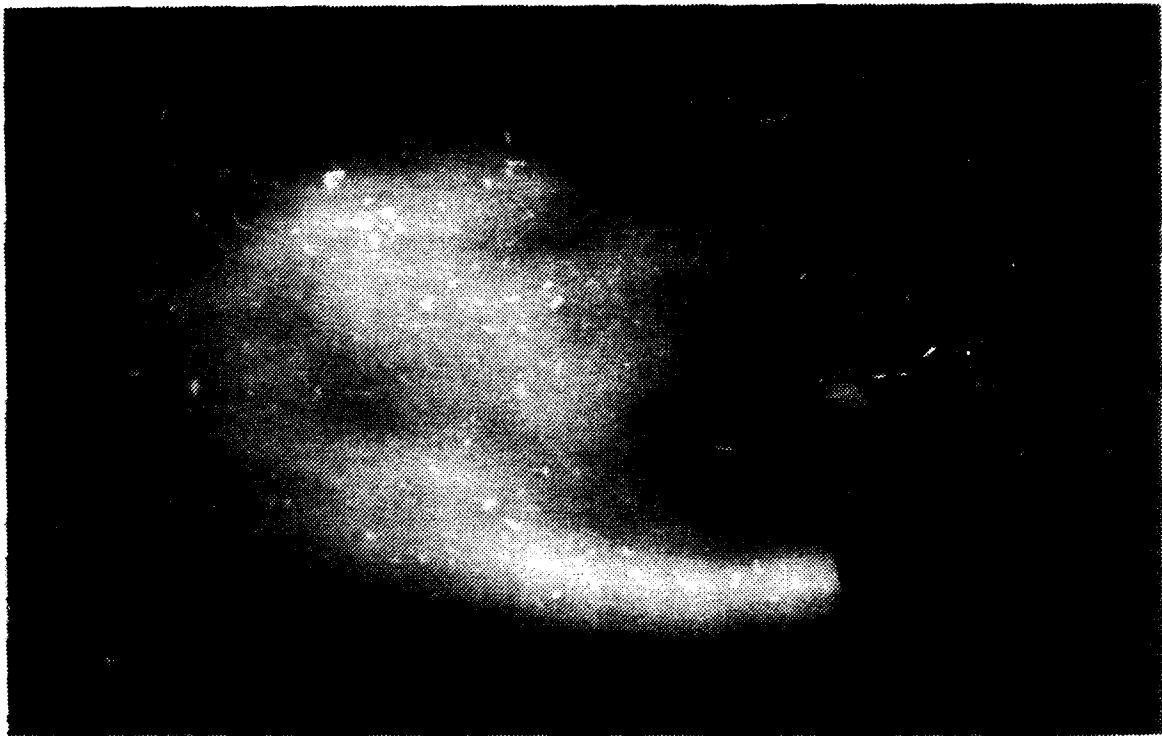
**Figure 63.** Station 6 Pitch=70°, Roll=15°, Yaw=0°

Figure 64. Station 4 Pitch=45°, Roll=30°, Yaw=0°

Figure 65.   Station 4   Pitch=50°, Roll=30°, Yaw=0°

Figure 66.   Station 4   Pitch=55°, Roll=30°, Yaw=0°

Figure 67. Station 4 Pitch≈60°, Roll=30°, Yaw=0°

Figure 68. Station 4 Pitch≈65°, Roll=30°, Yaw=0°

104

**Figure 69.** Station 4 Pitch=70°, Roll=30°, Yaw=0°

Figure 70. Station 7 Pitch=45°, Roll=30°, Yaw=0°
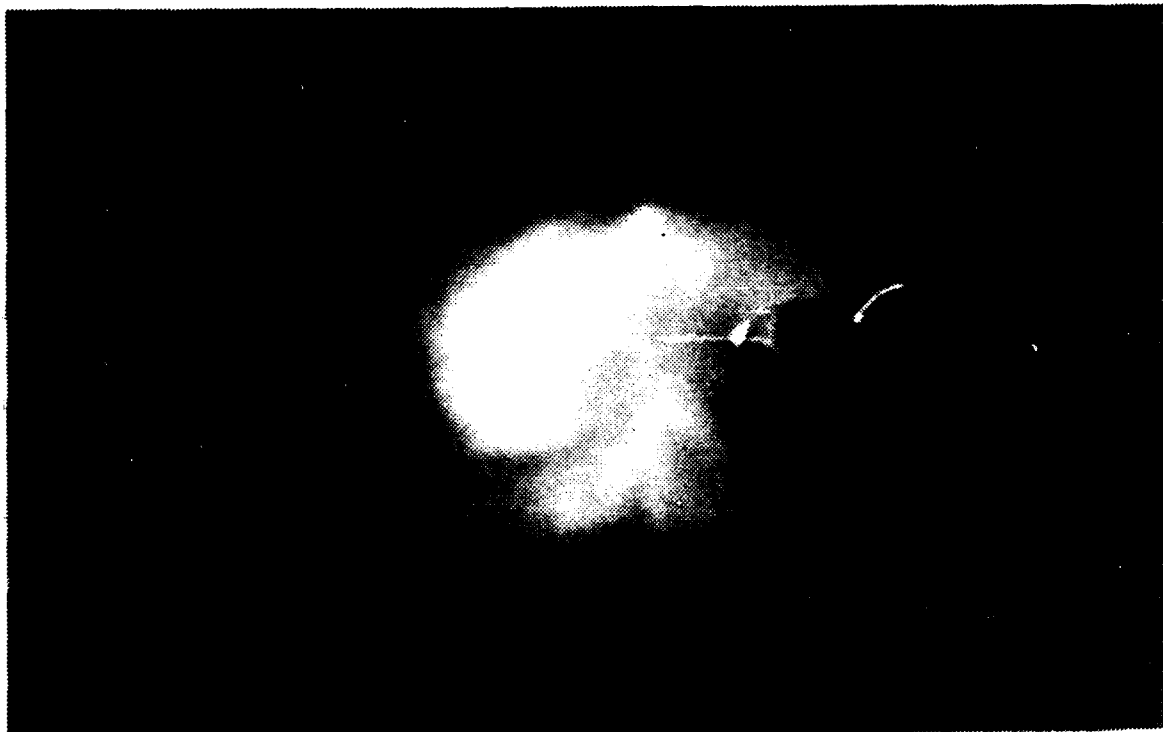
Figure 71. Station 7 Pitch=50°, Roll=30°, Yaw=0°
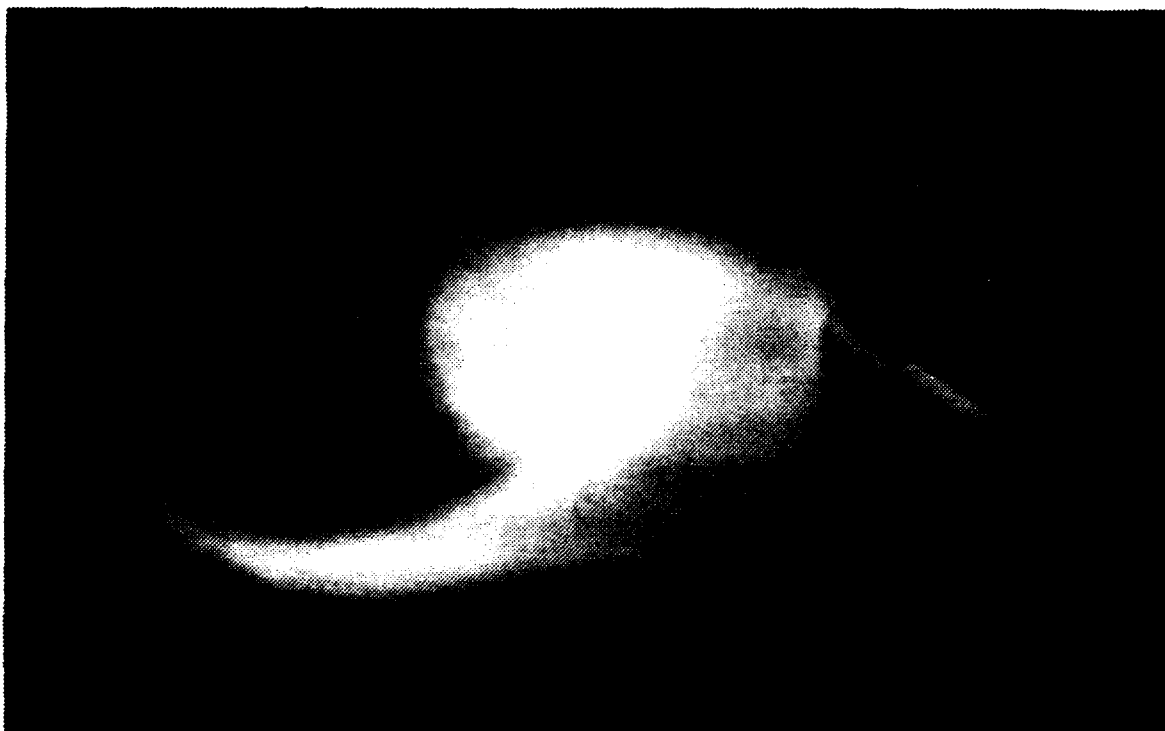

Figure 72. Station 7 Pitch=55°, Roll=30°, Yaw=0°

Figure 73. Station 7 Pitch≈60°, Roll=30°, Yaw=0°
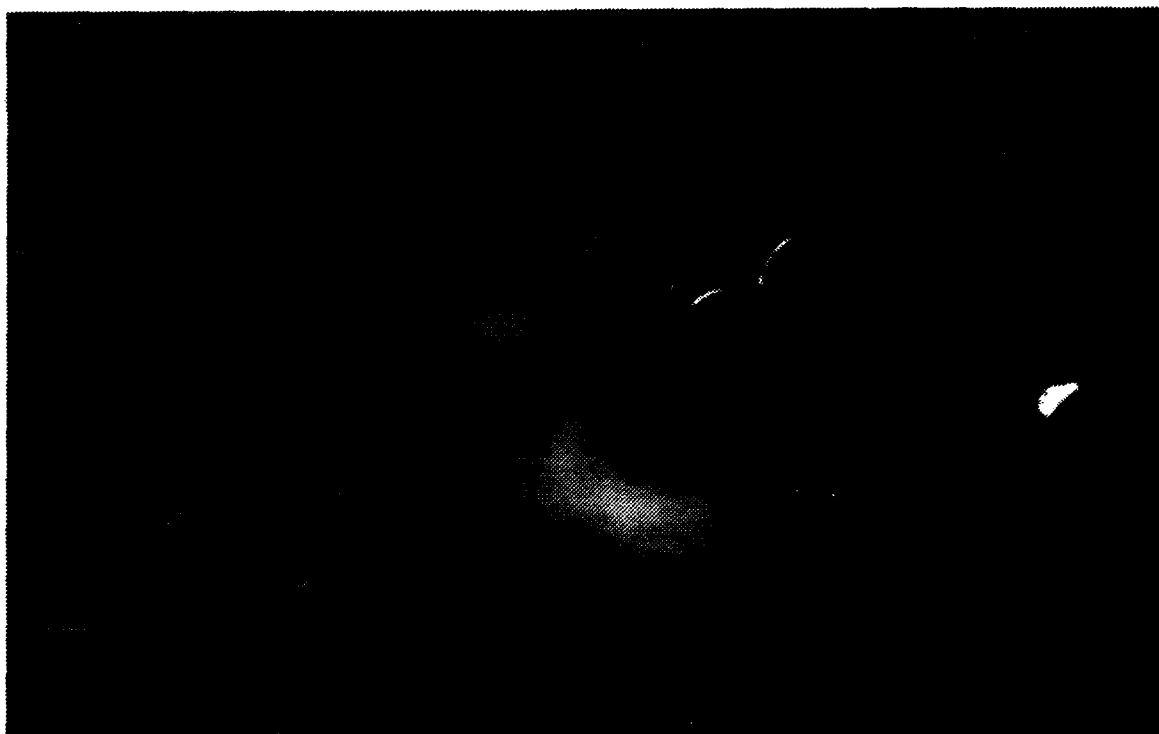
Figure 74. Station 8 Pitch=45°, Roll=15°, Yaw=0°

Figure 75. Station 8 Pitch=45°, Roll=30°, Yaw=0°

Figure 76. Station 8 Pitch=45°, Roll=45°, Yaw=0°
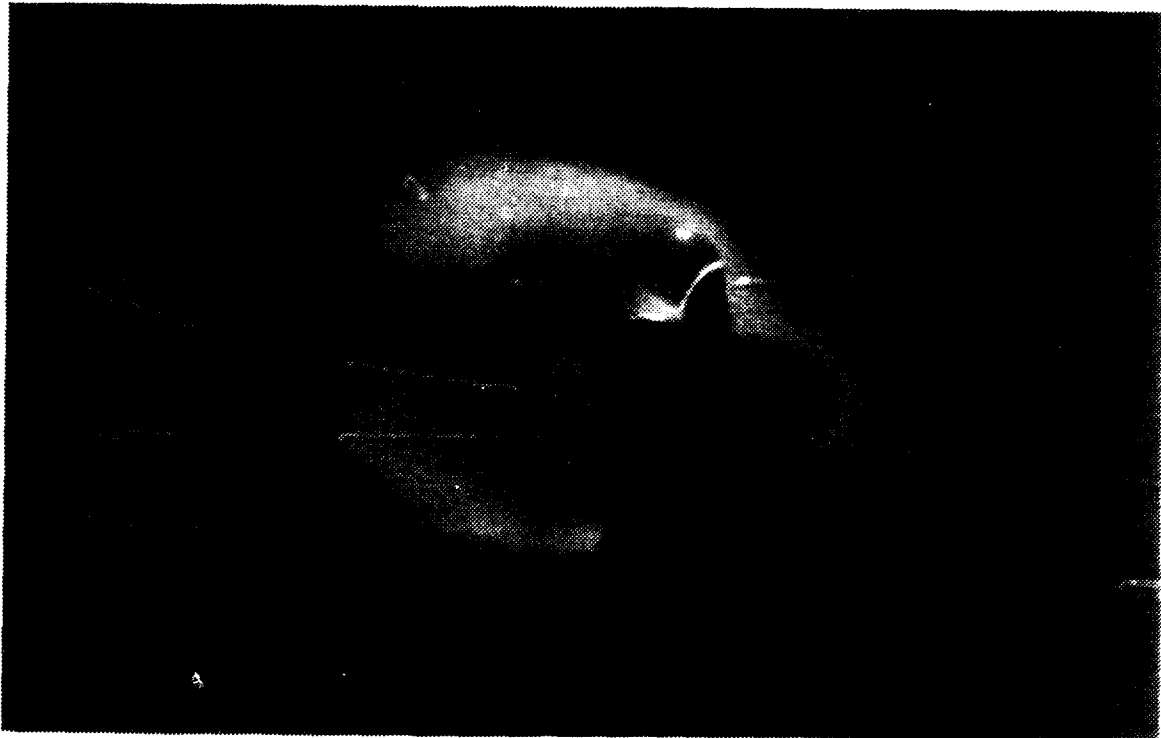
Figure 77. Station 8 Pitch=55°, Roll=15°, Yaw=0°
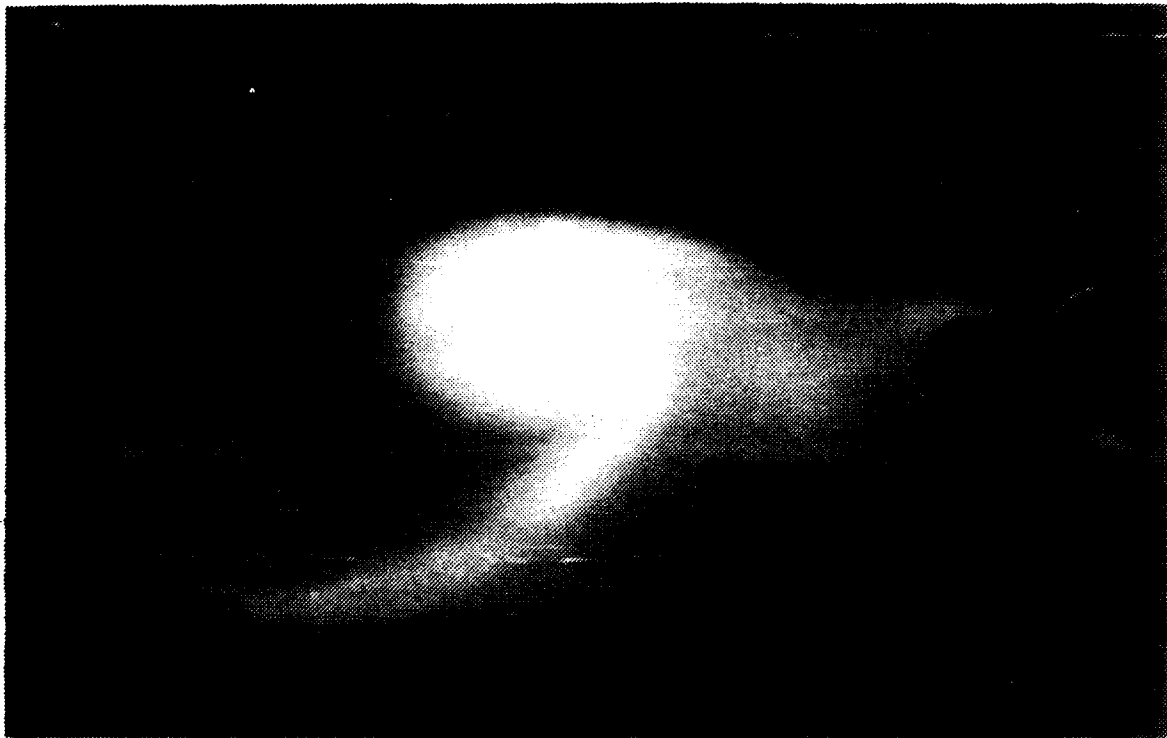
Figure 78. Station 8 Pitch=55°, Roll=30°, Yaw=0°

Figure 79. Station 8 Pitch=55°, Roll=45°, Yaw=0°

Figure 80. Station 8 Pitch=70°, Roll=15°, Yaw=0°
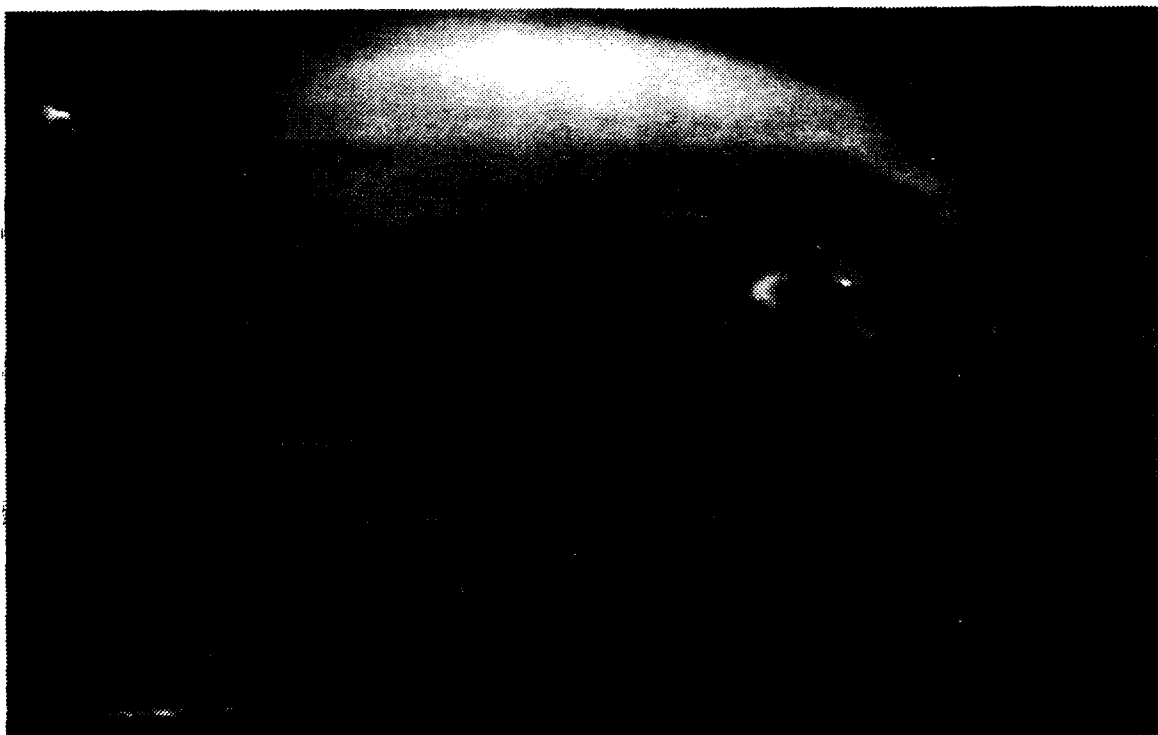
Figure 81.   Station 8   Pitch=70°, Roll=30°, Yaw=0°

Figure 82.   Station 8   Pitch=70°, Roll=45°, Yaw=0°
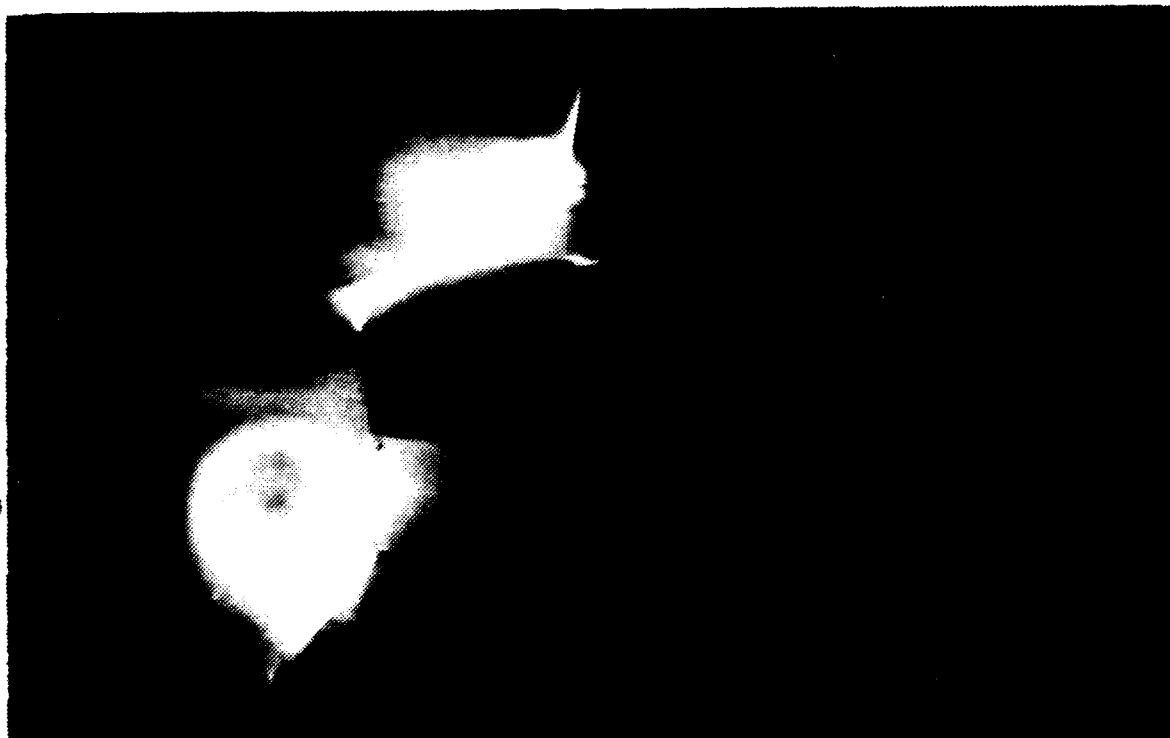
Figure 83. Station 10 Pitch=25°, Roll=30°, Yaw=0°

Figure 84. Station 10 Pitch=30°, Roll=30°, Yaw=0°

Figure 85. Station 10 Pitch=35°, Roll=30°, Yaw=0°
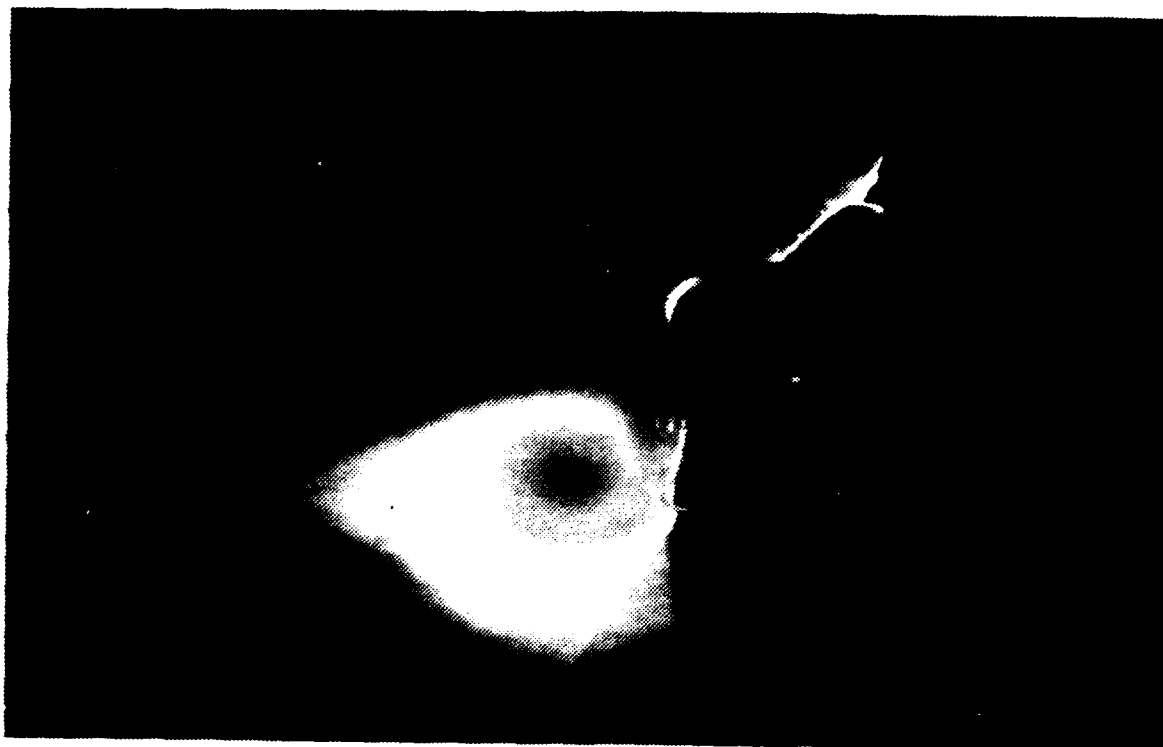
Figure 86. Station 10 Pitch=40°, Roll=30°, Yaw=0°

113

Figure 87.   Station 10   Pitch=45°, Roll=15°, Yaw=0°

Figure 88.   Station 10   Pitch=45°, Roll=30°, Yaw=0°

114
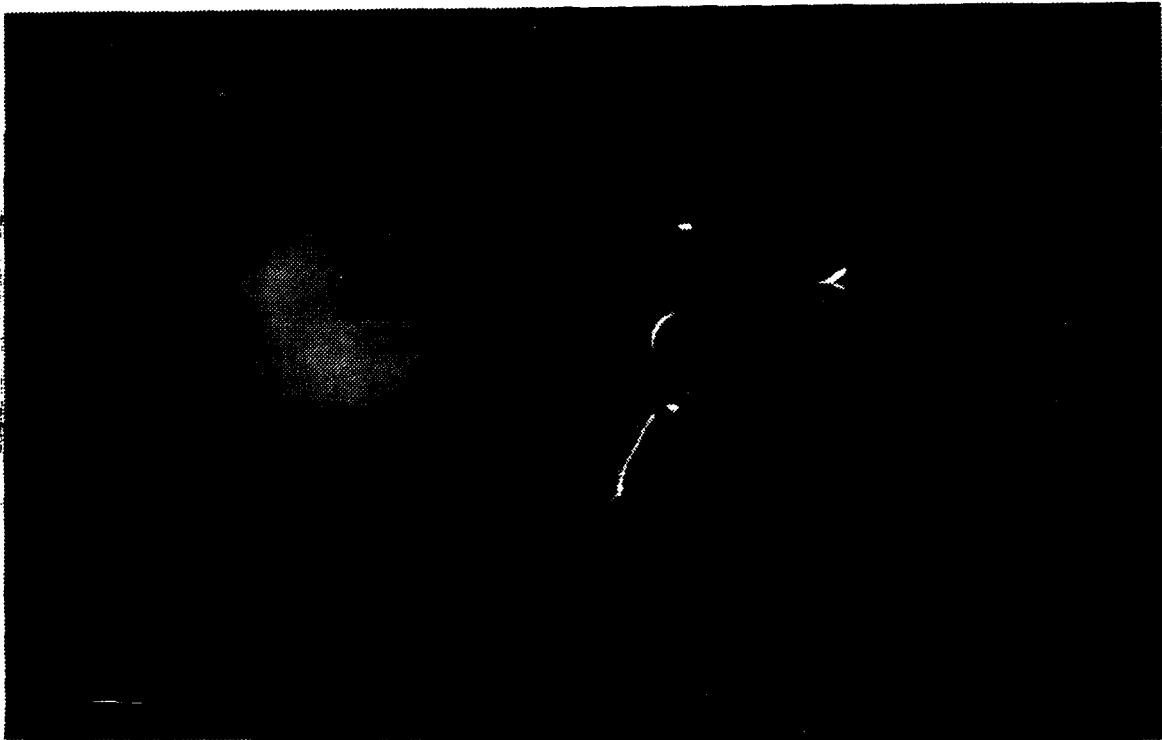
Figure 89. Station 10   Pitch=45°, Roll=45°, Yaw=0°

Figure 90. Station 10   Pitch=35°, Roll=45°, Yaw=0°

Figure 91. Station 10 Pitch=40°, Roll=45°, Yaw=0°

Figure 92. Station 10 Pitch=45°, Roll=45°, Yaw=0°

Figure 93. Station 11 Pitch=40°, Roll=30°, Yaw=0°

Figure 94. Station 12 Pitch=40°, Roll=30°, Yaw=0°

Figure 95. Station 12 Pitch=40°, Roll=45°, Yaw=0°

Figure 96. Station 11 Pitch=35°, Roll=45°, Yaw=0°

Figure 97. Station 11 Pitch=25°, Roll=45°, Yaw=0°

Figure 98. Station 8 Pitch=30°, Roll=30°, Yaw=0°

119

Figure 99. Station 9   Pitch=30°, Roll=30°, Yaw=0°

Figure 100. Station 10   Pitch=30°, Roll=30°, Yaw=0°

Figure 101. Station 11 Pitch=30°, Roll=30°, Yaw=0°

Figure 102. Station 11 Pitch=30°, Roll=30°, Yaw=0°

121

Figure 103. Station 12   Pitch=30°, Roll=30°, Yaw=0°

Figure 104. Station 13   Pitch=15°, Roll=30°, Yaw=0°
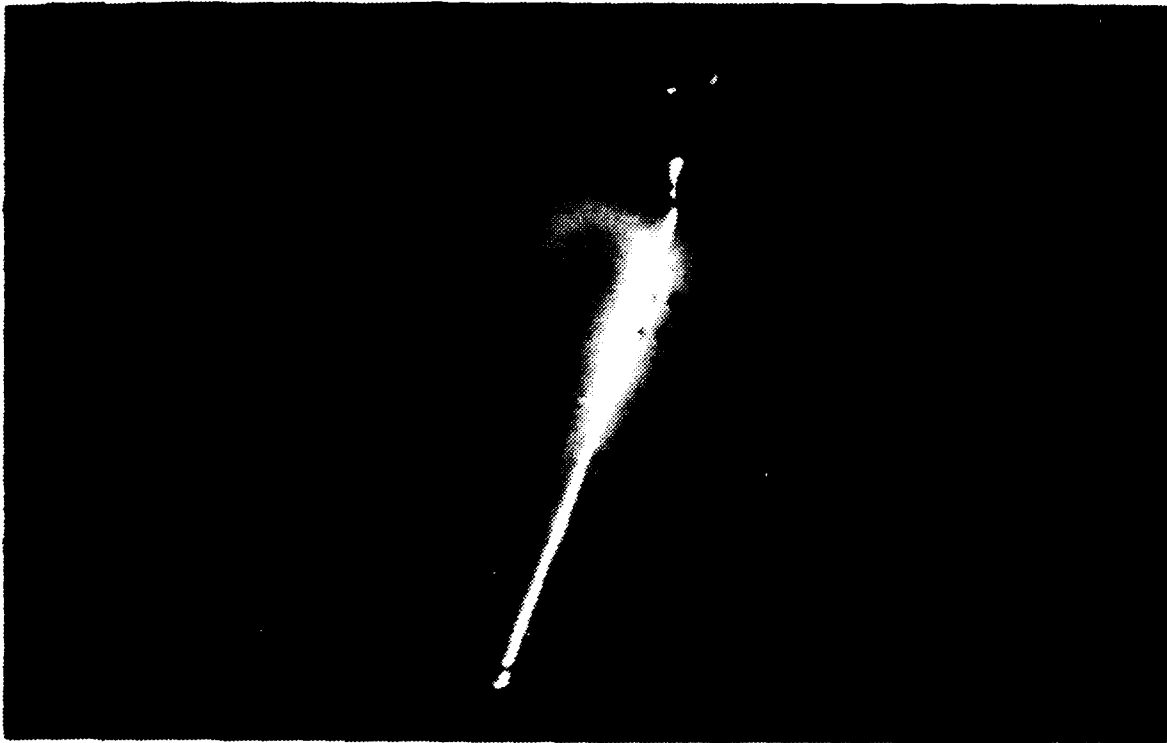
Figure 105. Station 13 Pitch=20°, Roll=30°, Yaw=0°

Figure 106. Station 13 Pitch=25°, Roll=30°, Yaw=0°

123

Figure 107. Station 13 Pitch=30°, Roll=30°, Yaw=0°

Figure 108. Station 13 Pitch=35°, Roll=30°, Yaw=0°

124

Figure 109. Station 9 Pitch=25°, Roll=15°, Yaw=0°
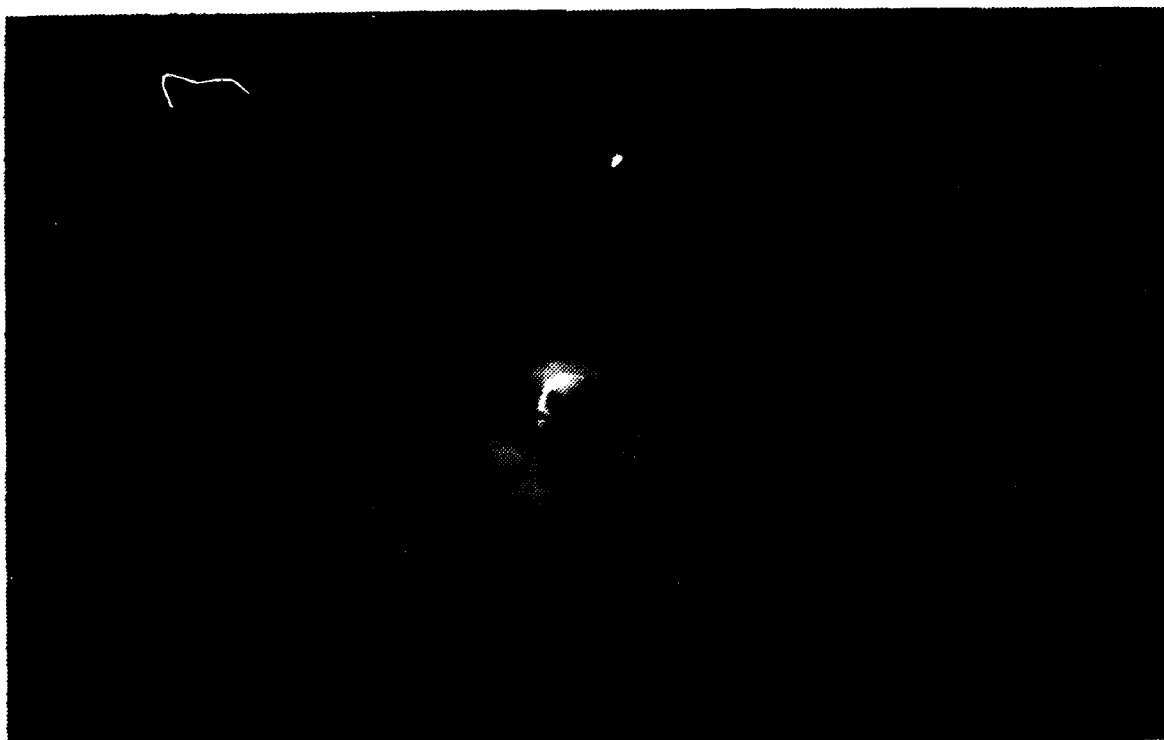
Figure 110. Station 1 Pitch=50°, Roll=0°, Yaw=5°

Figure 111. Station 1   Pitch=65°, Roll=0°, Yaw=5°
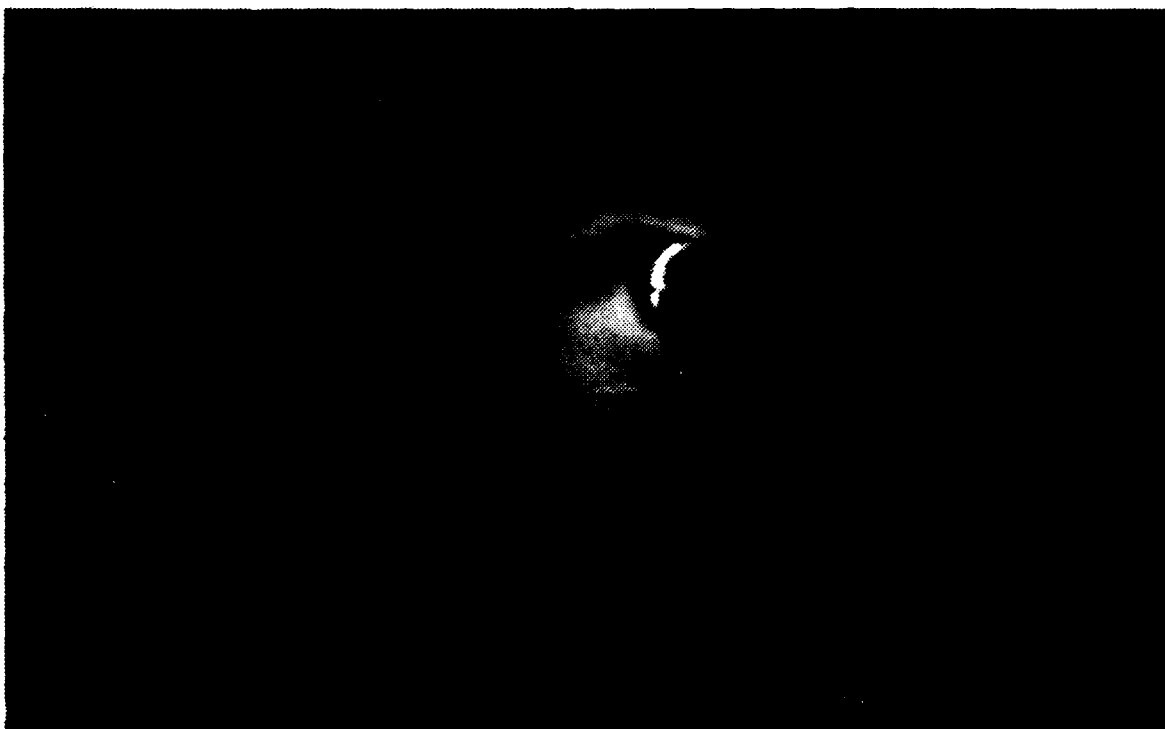
Figure 112. Station 1   Pitch=60°, Roll=0°, Yaw=15°

Figure 113.   Station 2   Pitch=60°, Roll=0°, Yaw=15°

Figure 114.   Station 3   Pitch=60°, Roll=0°, Yaw=15°
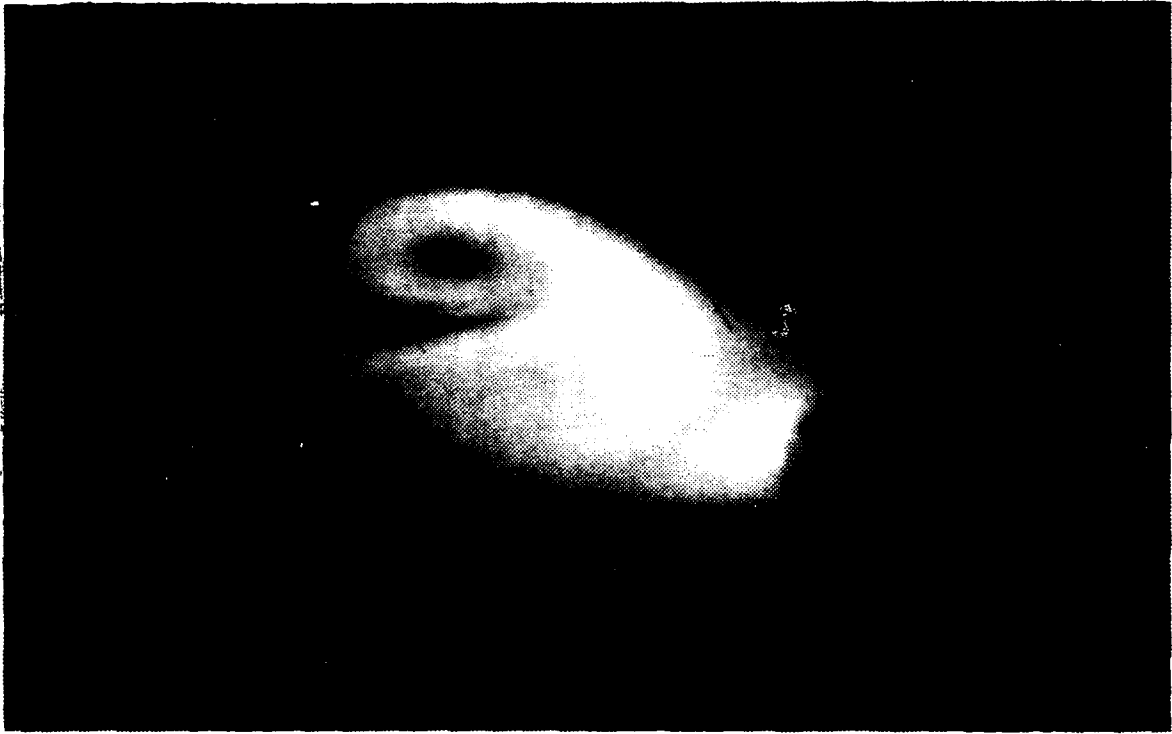
Figure 115. Station 4 Pitch=60°, Roll=0°, Yaw=15°

Figure 116. Station 10 Pitch=25°, Roll=0°, Yaw=5°
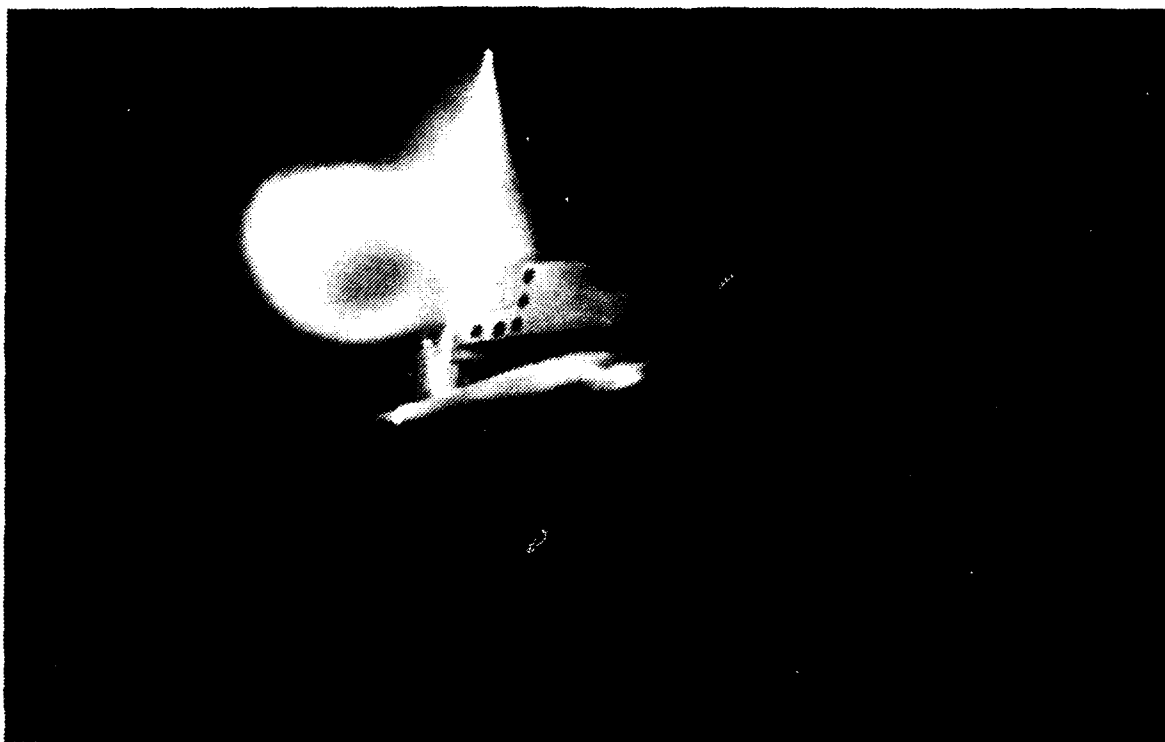
Figure 117. Station 11 Pitch=25°, Roll=0°, Yaw=5°
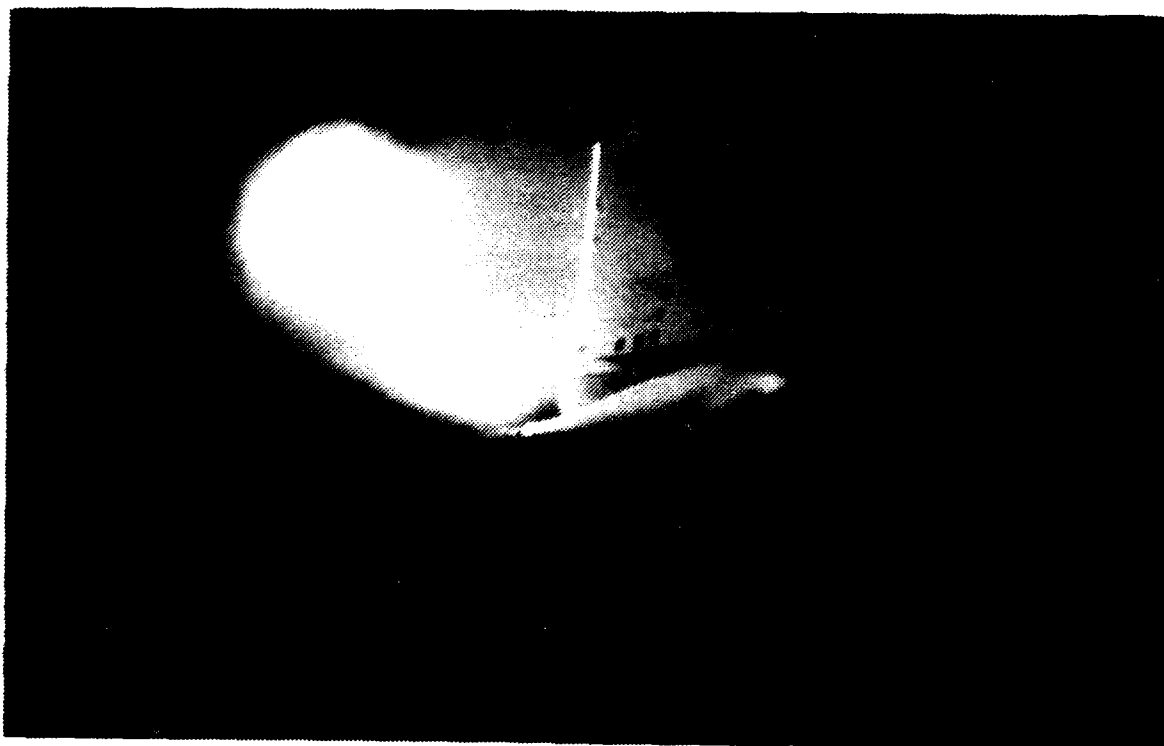
Figure 118. Station 13 Pitch=25°, Roll=0°, Yaw=5°

Figure 119. Station 15 Pitch=25°, Roll=0°, Yaw=5°

Figure 120. Station 2 Pitch=50°, Roll=0°, Yaw=5°

Figure 121. Station 2 Pitch=50°, Roll=0°, Yaw=5°
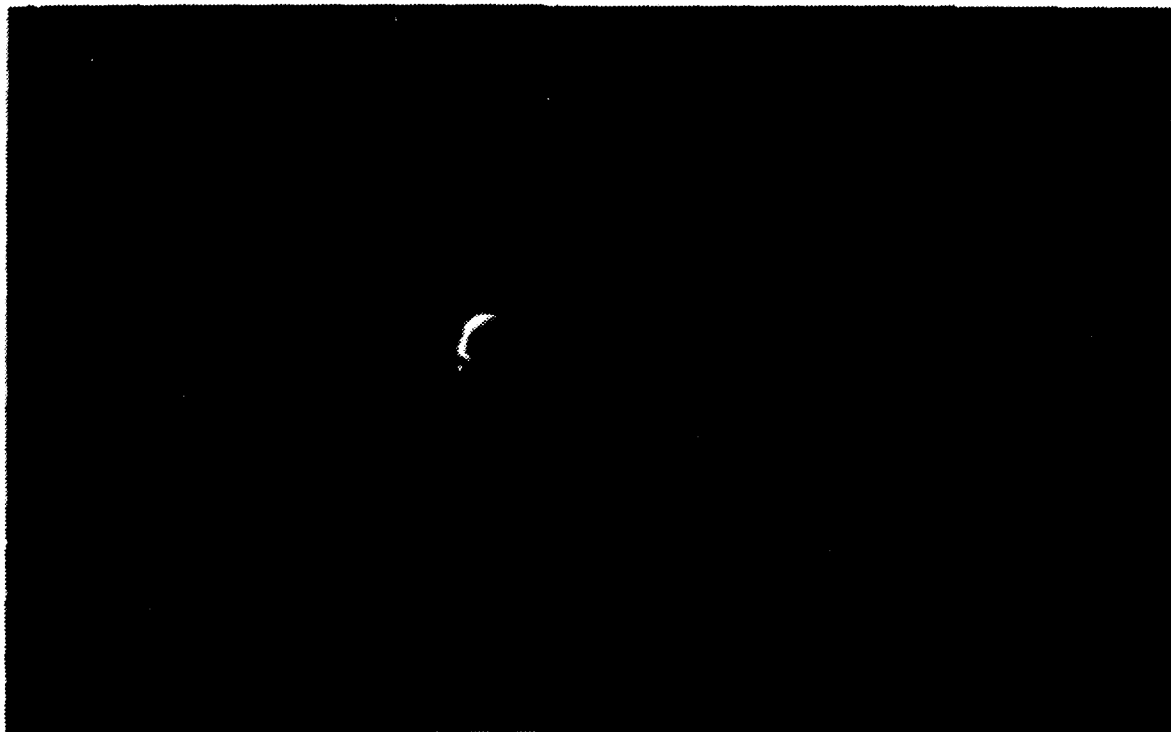
Figure 122. Station 1 Pitch=55°, Roll=0°, Yaw=10°

131
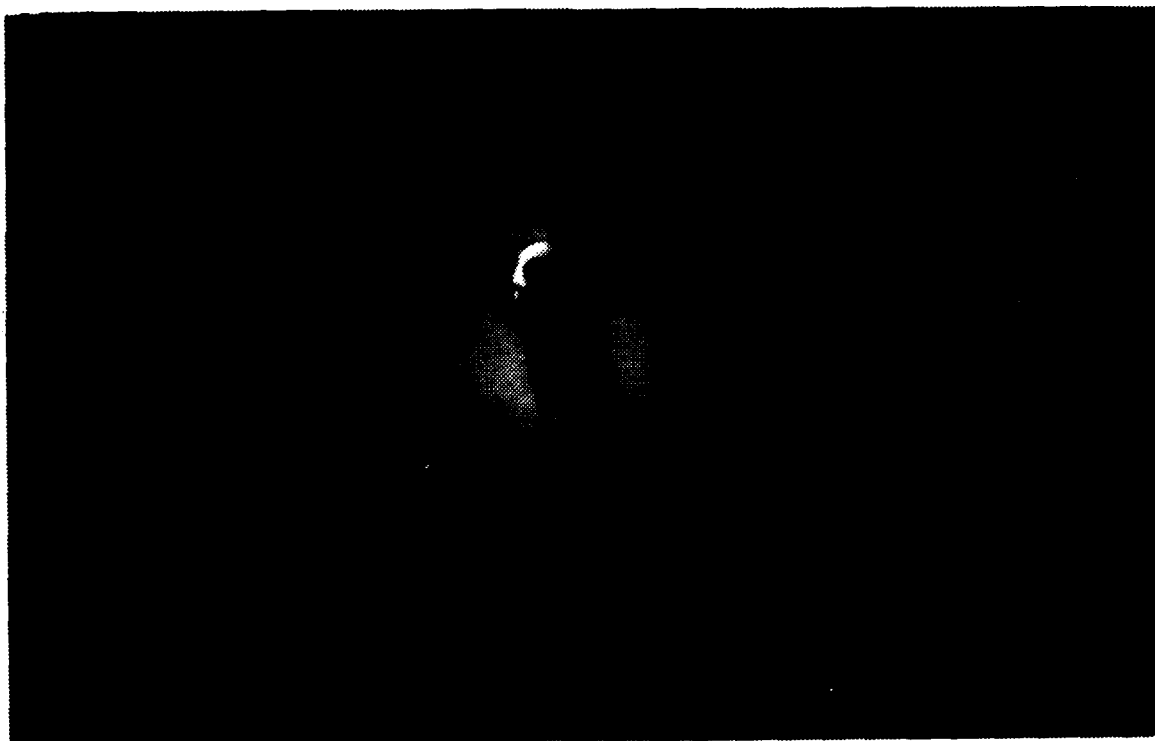
Figure 123. Station 1   Pitch=55°, Roll=0°, Yaw=10°

Figure 124. Station 2   Pitch=45°, Roll=0°, Yaw=10°
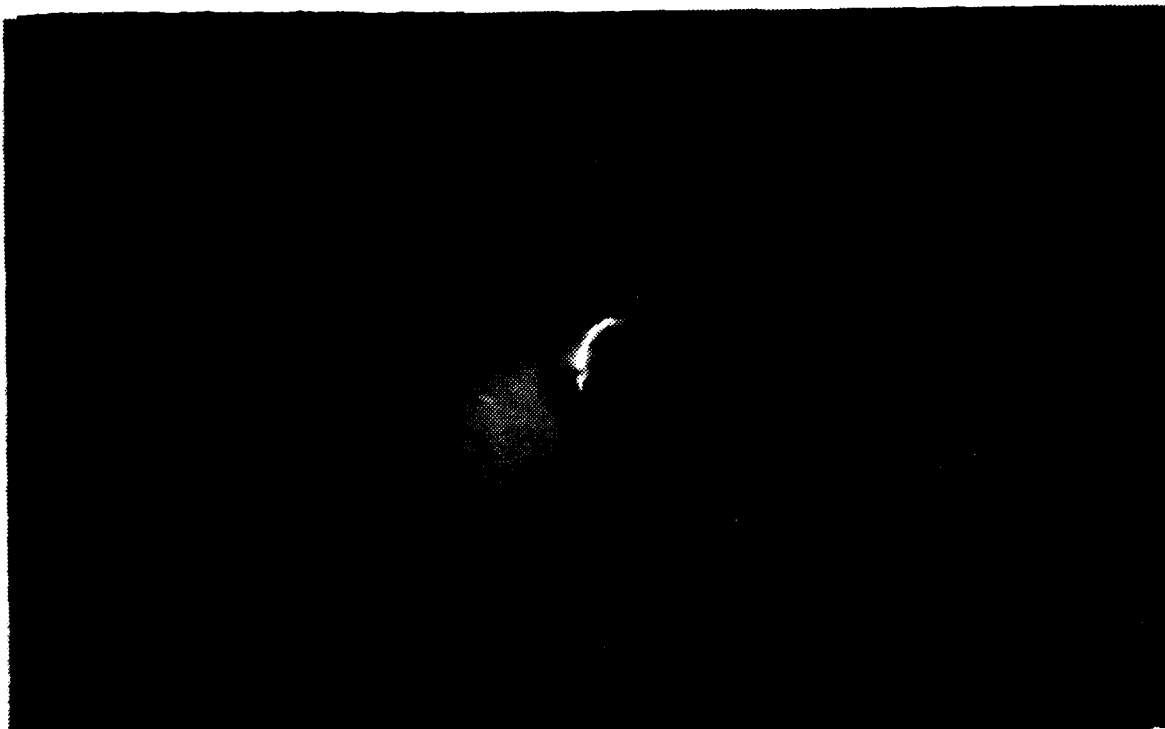
Figure 125. Station 2 Pitch=55°, Roll=0°, Yaw=10°
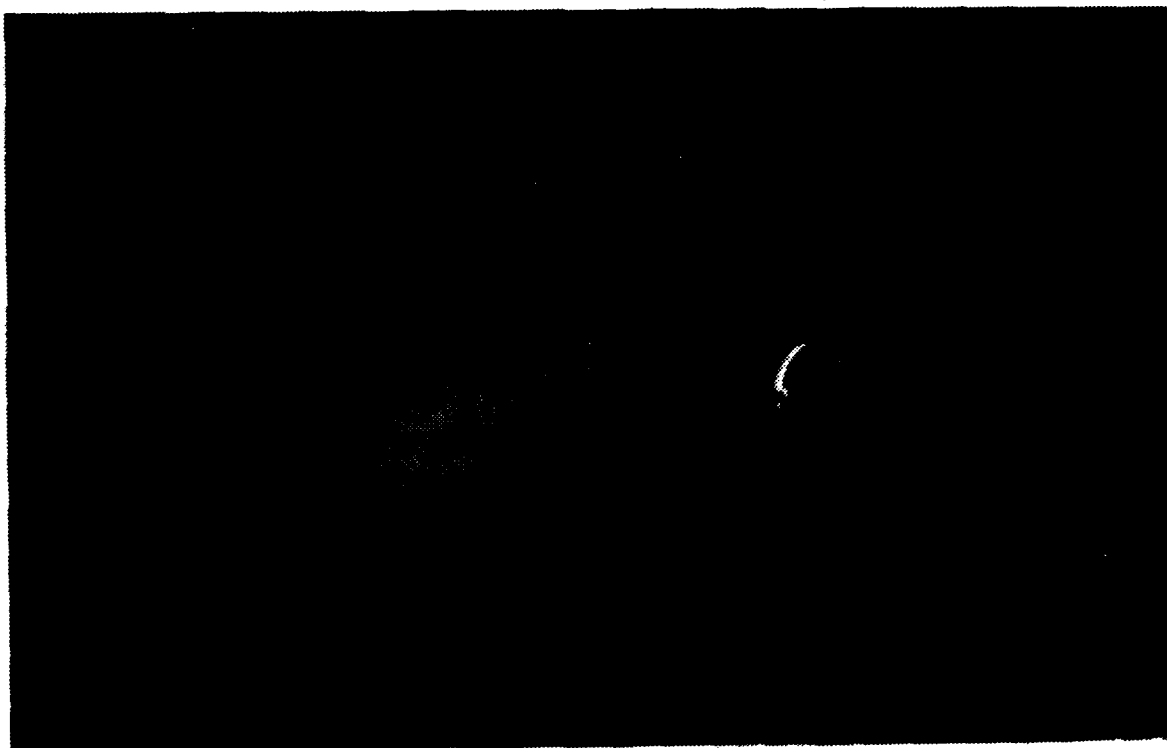
Figure 126. Station 2 Pitch=65°, Roll=0°, Yaw=10°

133

Figure 127. Station 6 Pitch=45°, Roll=0°, Yaw=5°

Figure 128. Station 6 Pitch=45°, Roll=0°, Yaw=5°

Figure 129. Station 4 Pitch=60°, Roll=0°, Yaw=5°

Figure 130. Station 4 Pitch=60°, Roll=0°, Yaw=5°

135
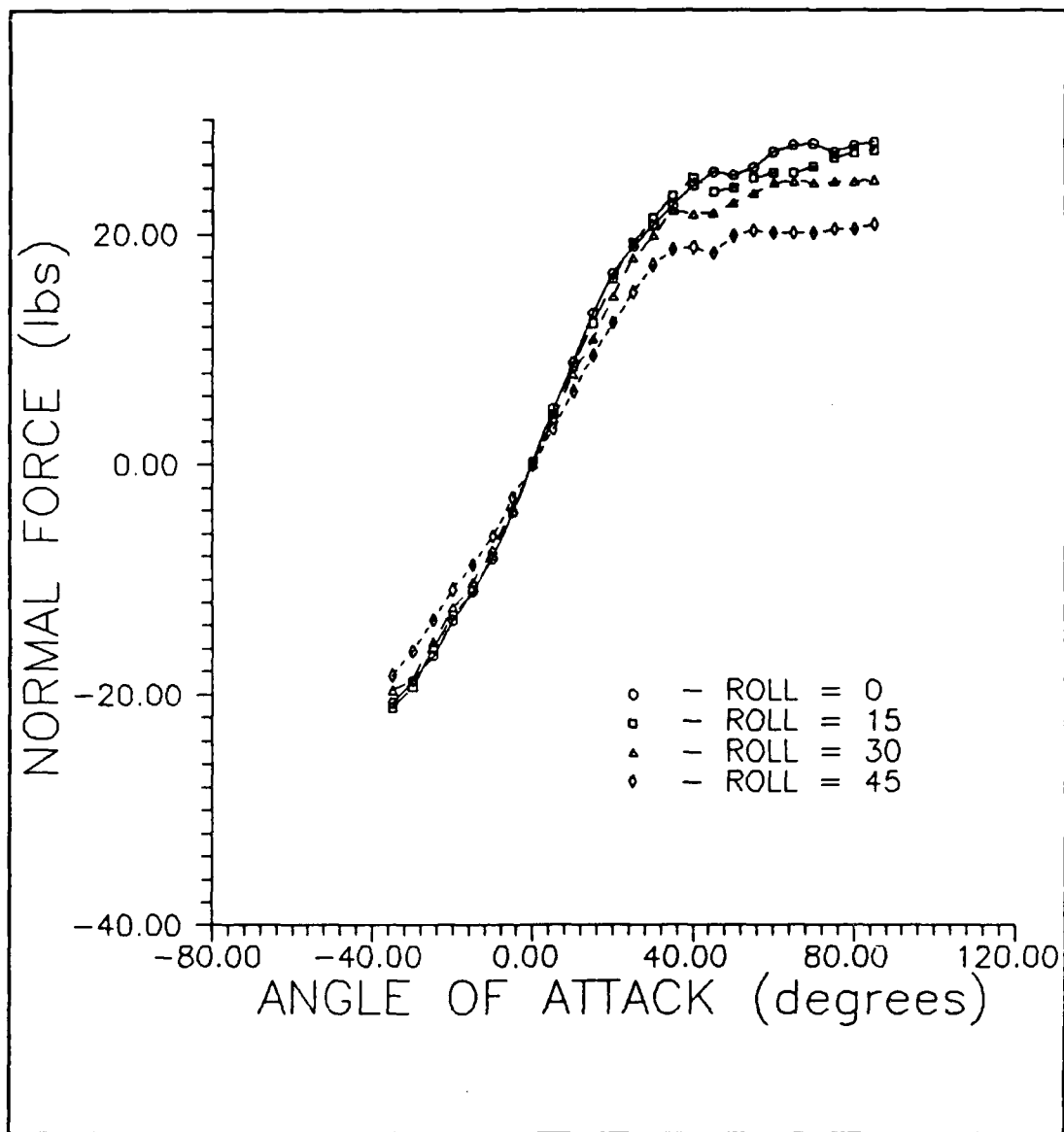
Figure 131. Normal Force (Roll)
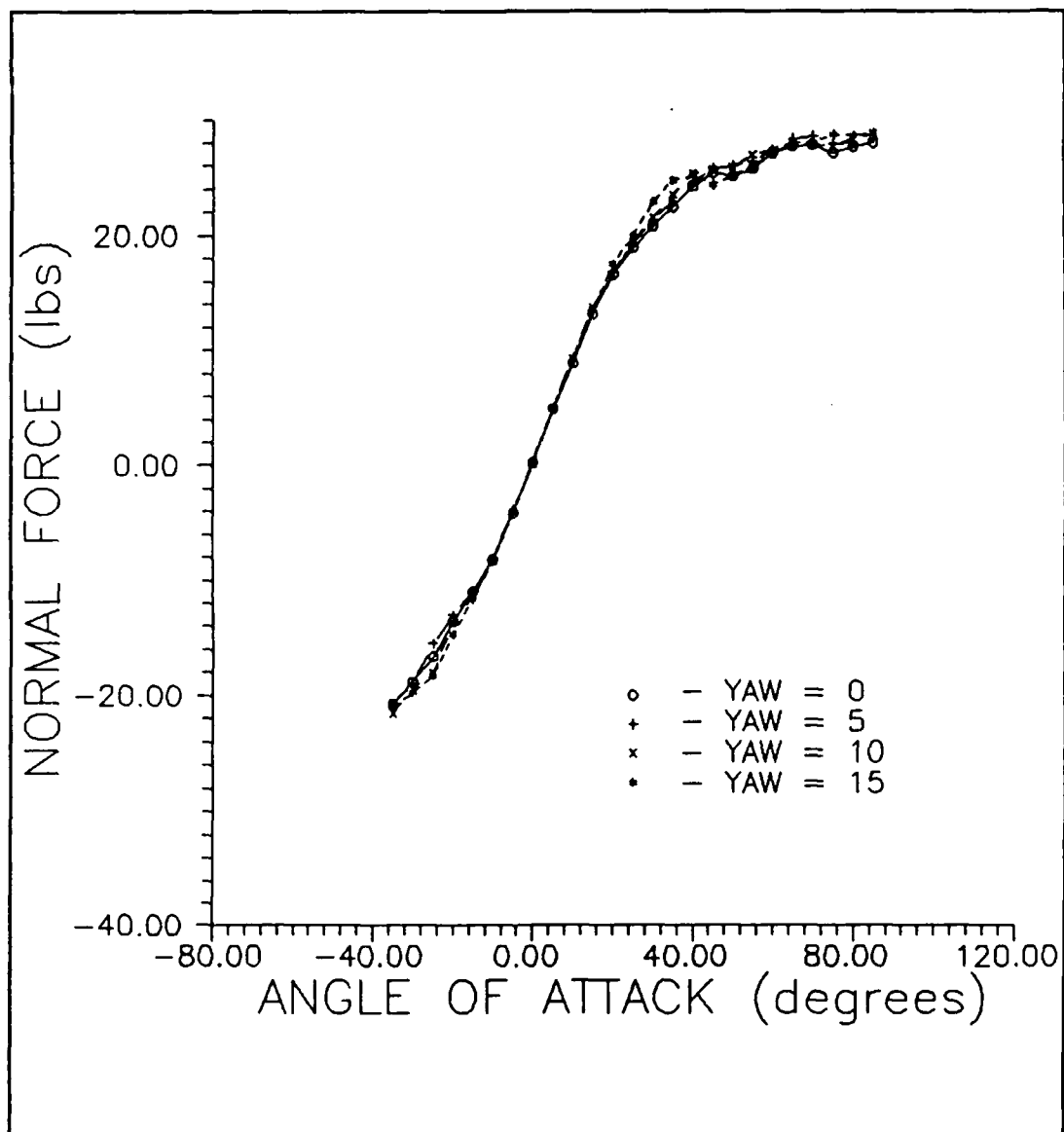
Figure 132. Normal Force (Yaw)

137
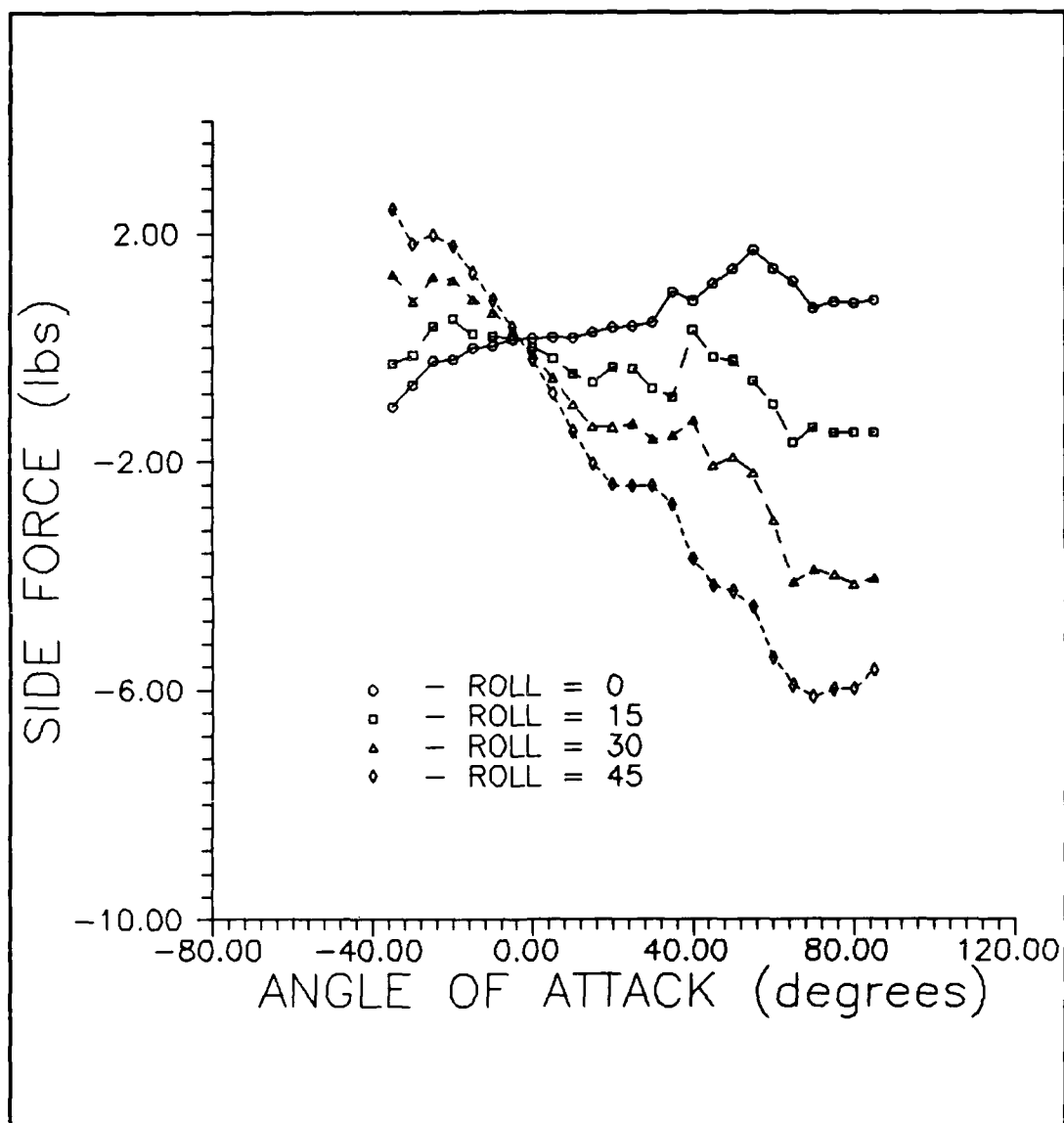
Figure 133. Side Force (Roll)

138
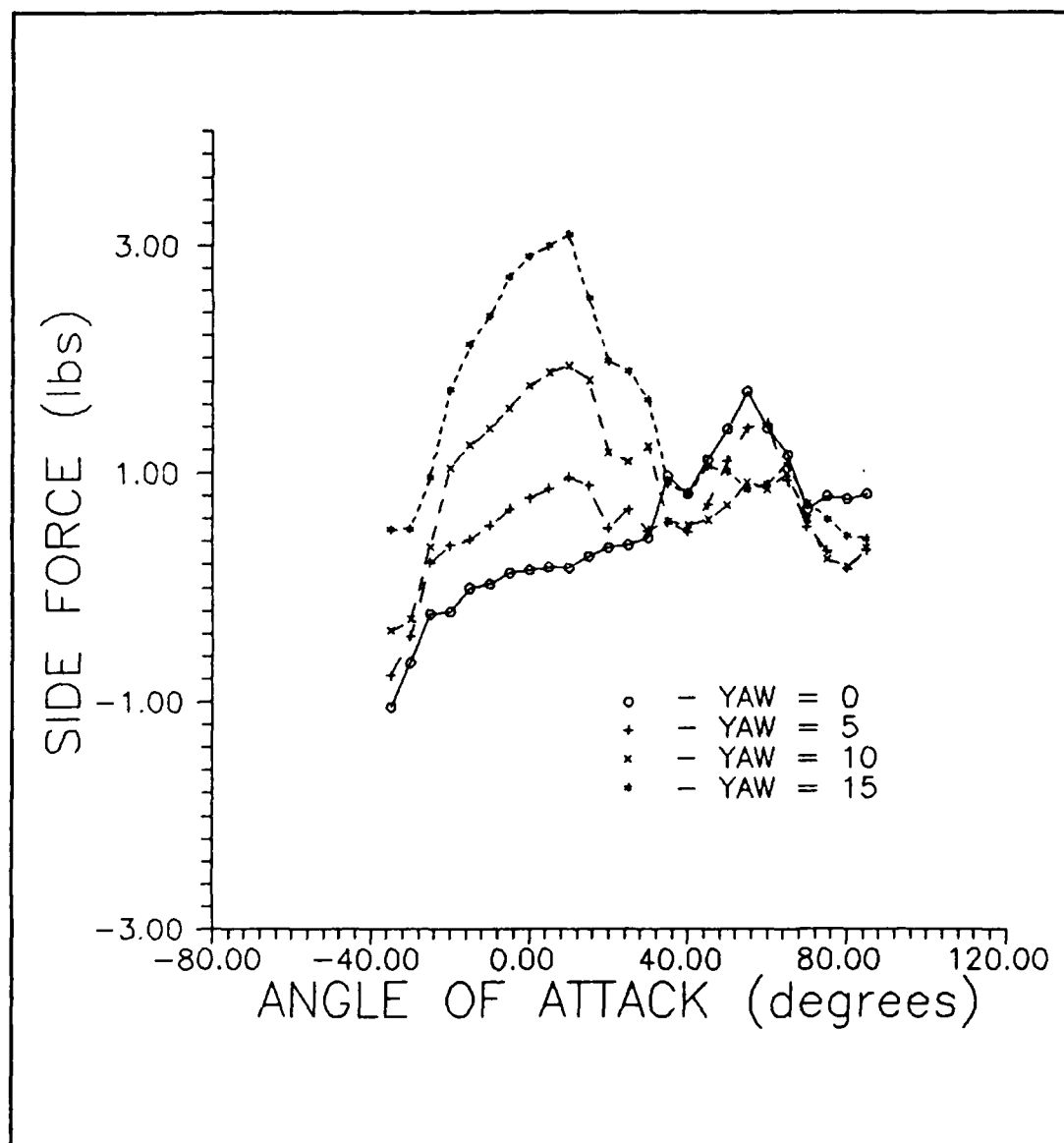
Figure 134. Side Force (Yaw)

139
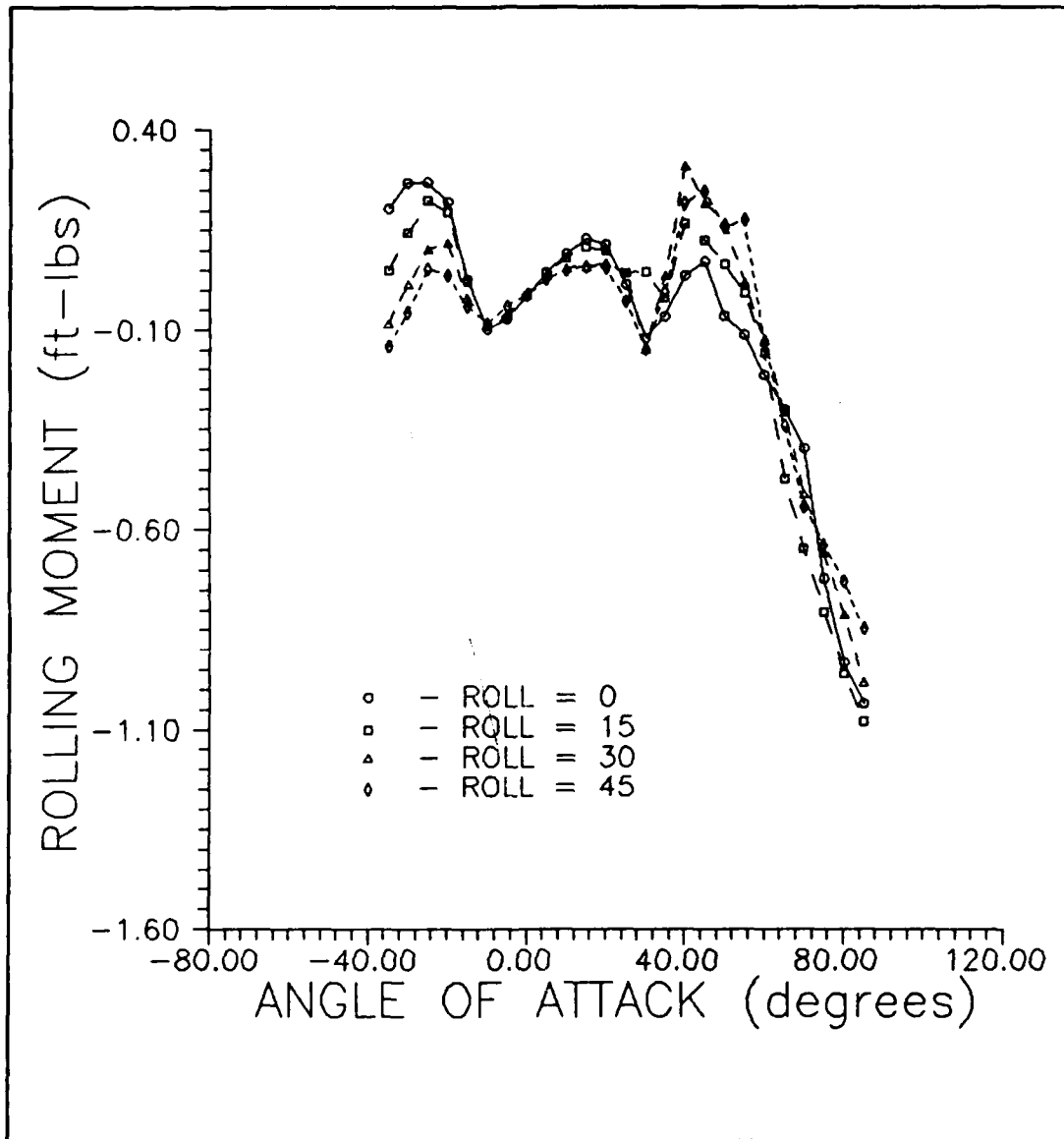
Figure 135. Rolling Moment (Roll)

140
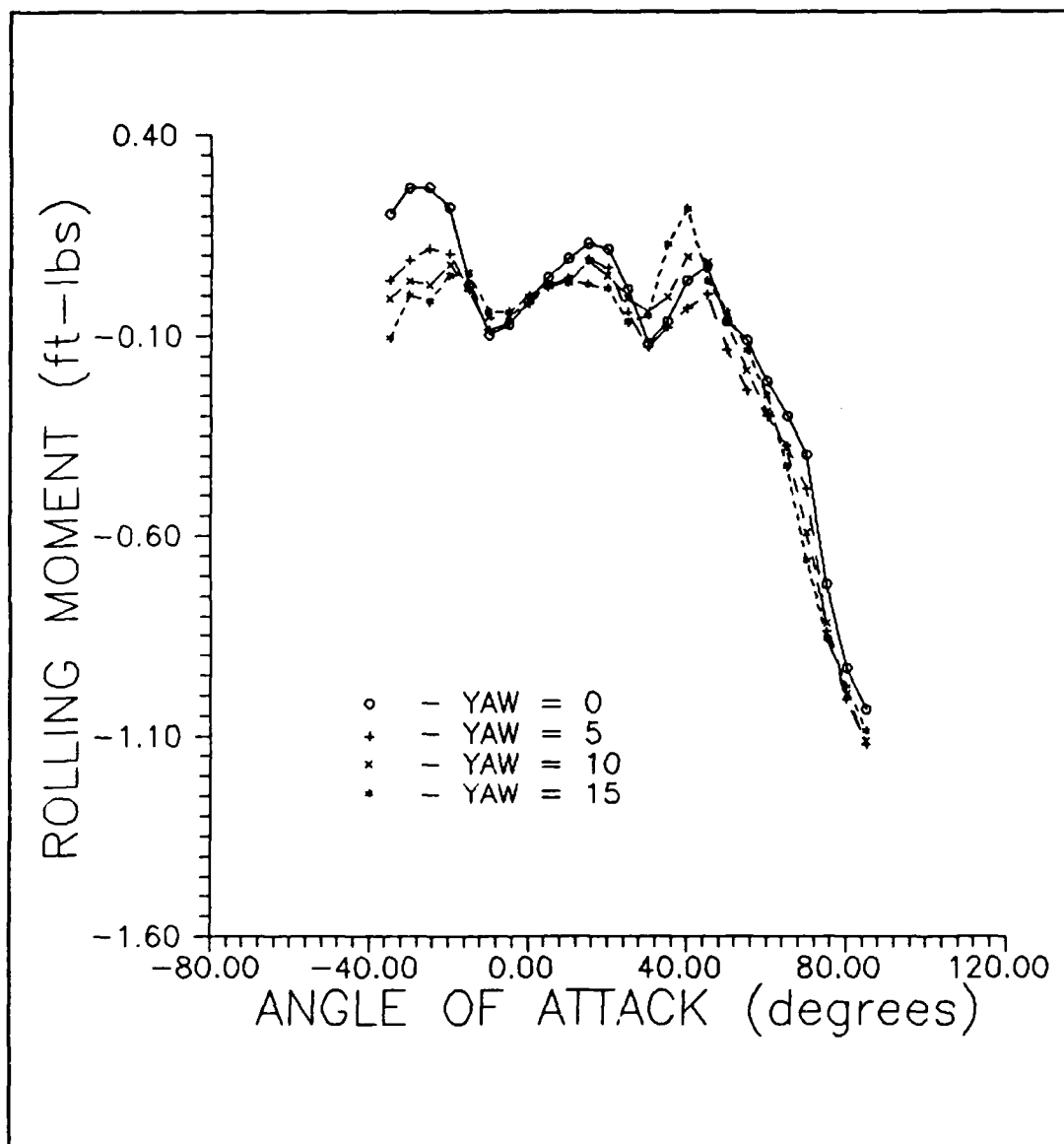
Figure 136. Rolling Moment (Yaw)
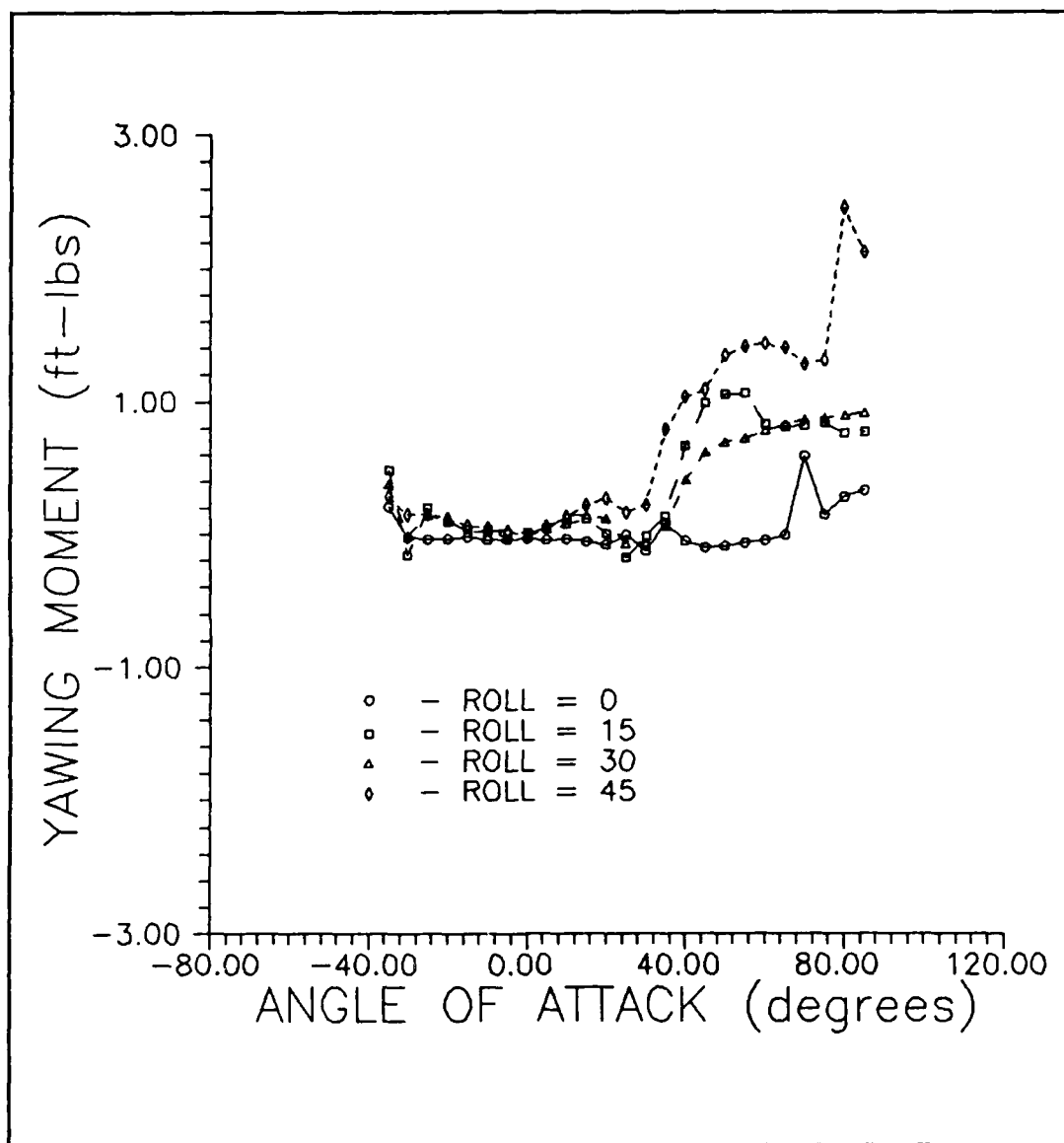
Figure 137. Yawing Moment (Roll)

142
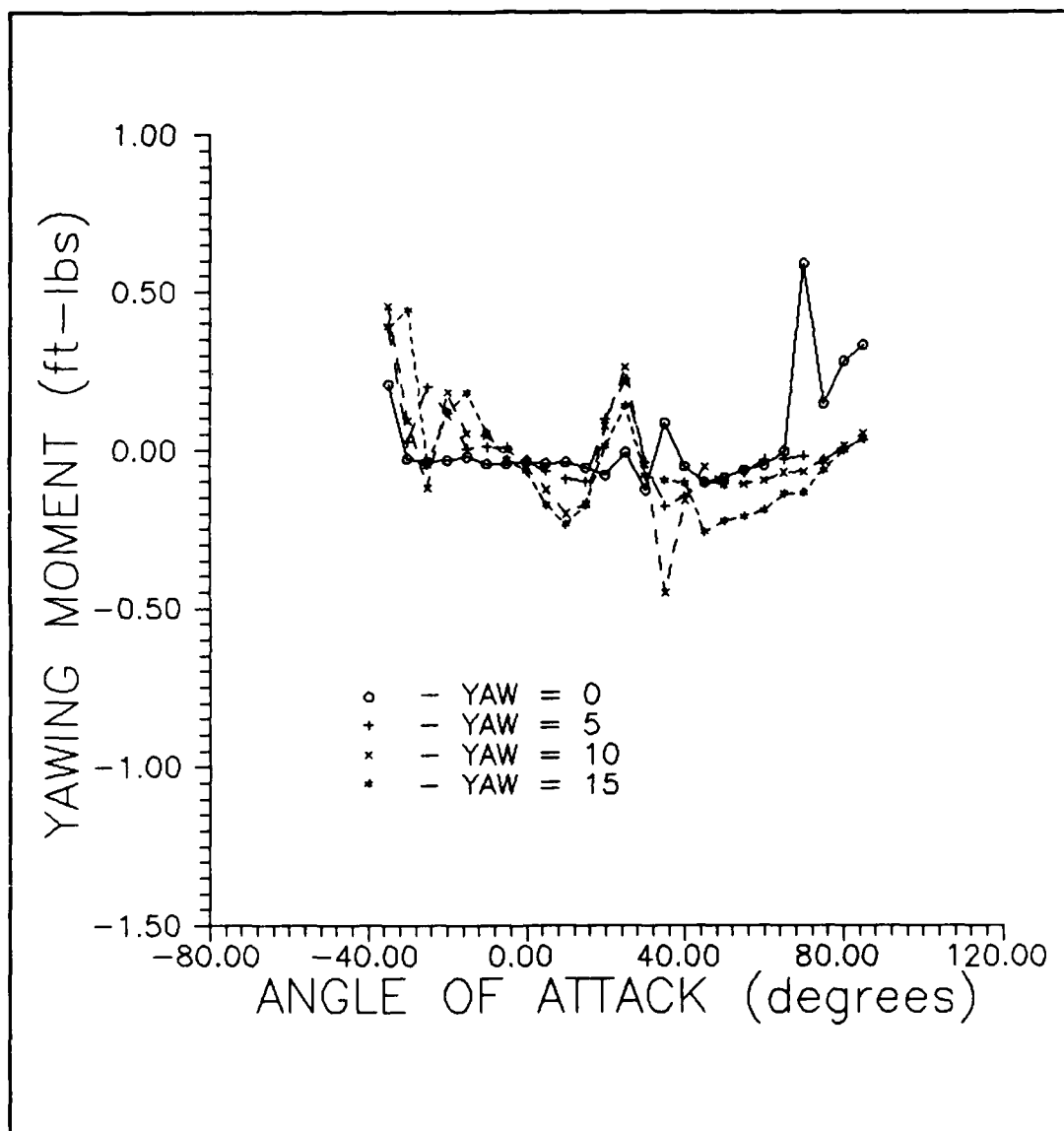
Figure 138. Yawing Moment (Yaw)

143
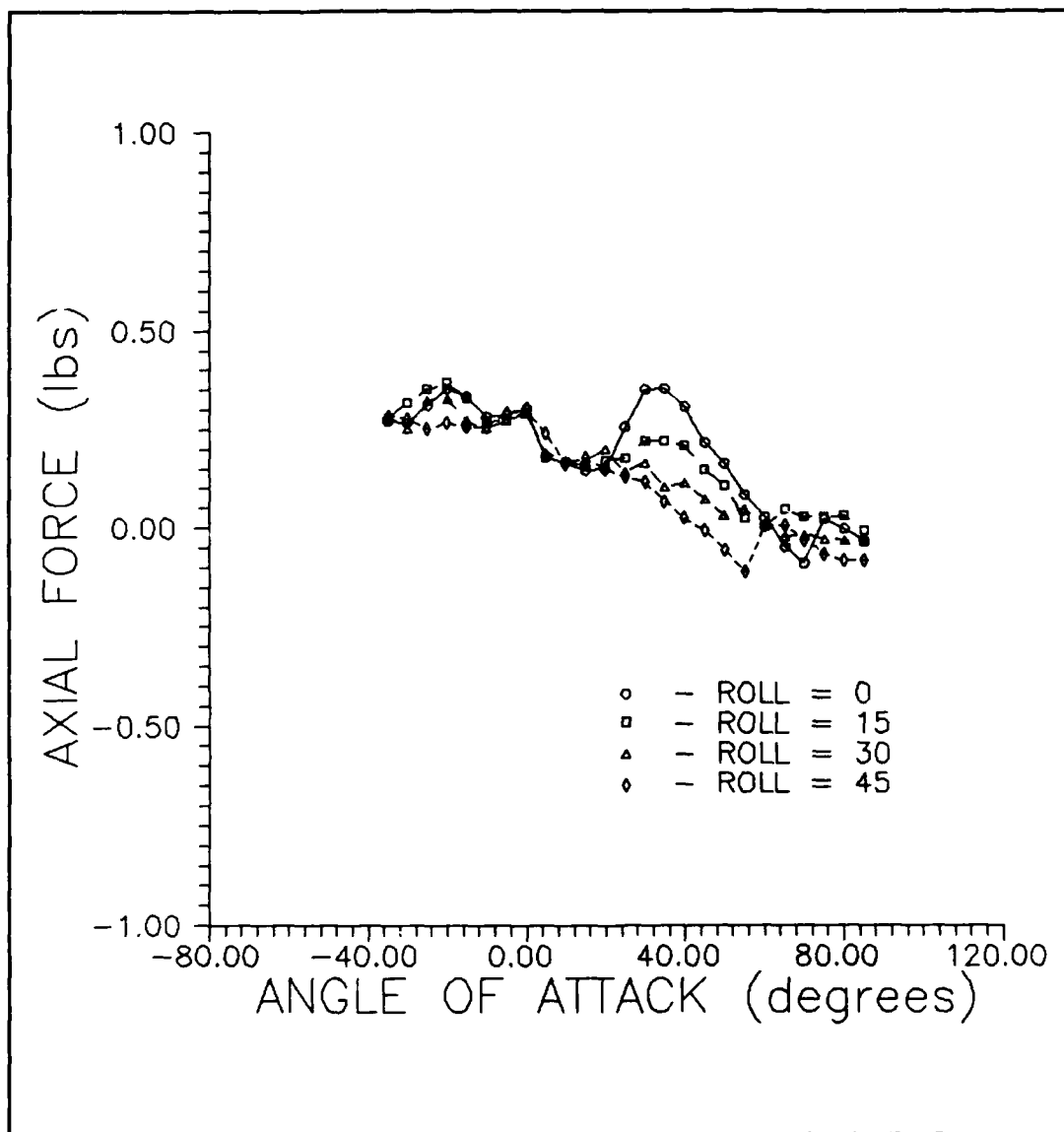
Figure 139. Axial Force (Roll)

144
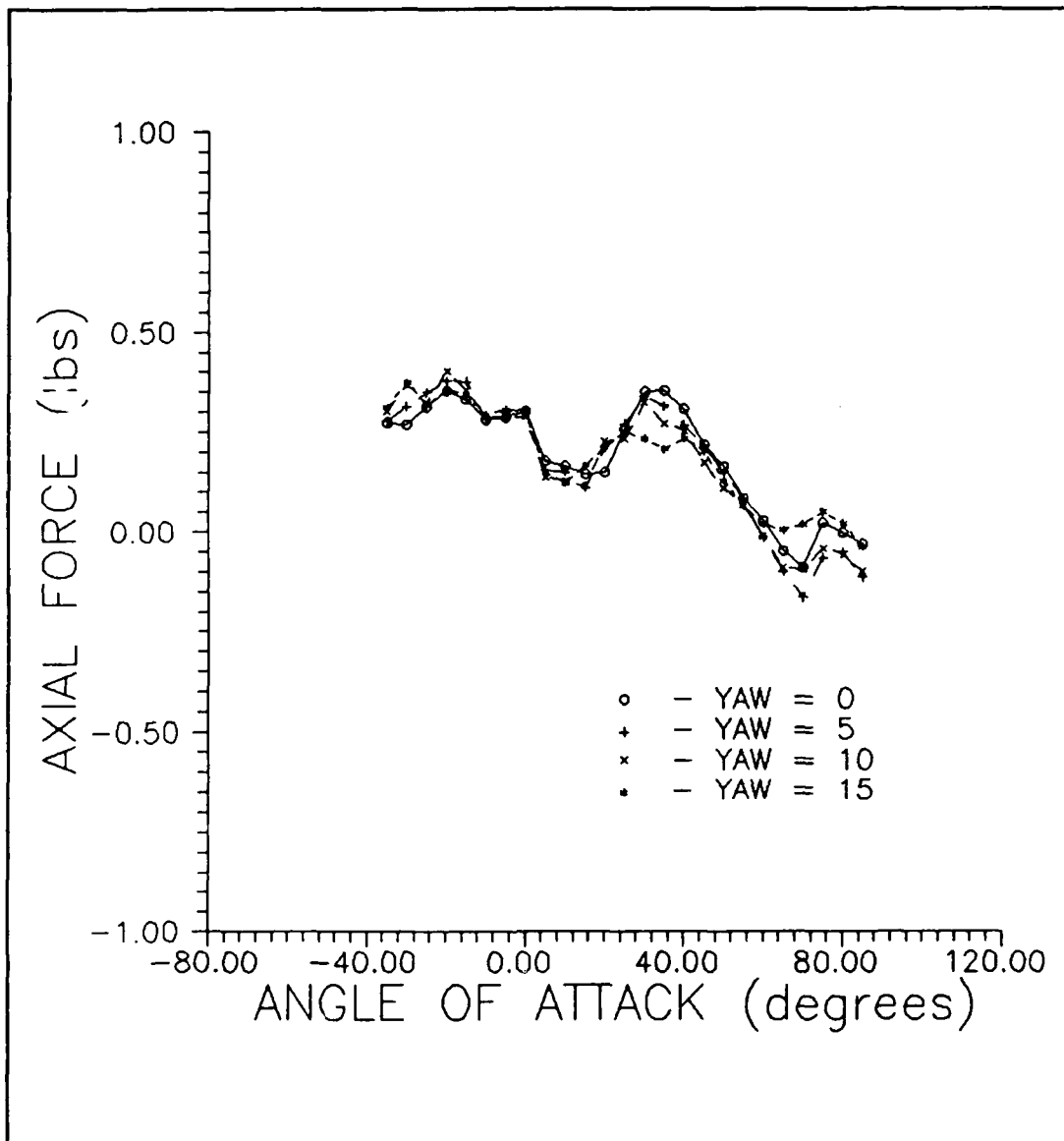
Figure 140. Axial Force (Yaw)

145
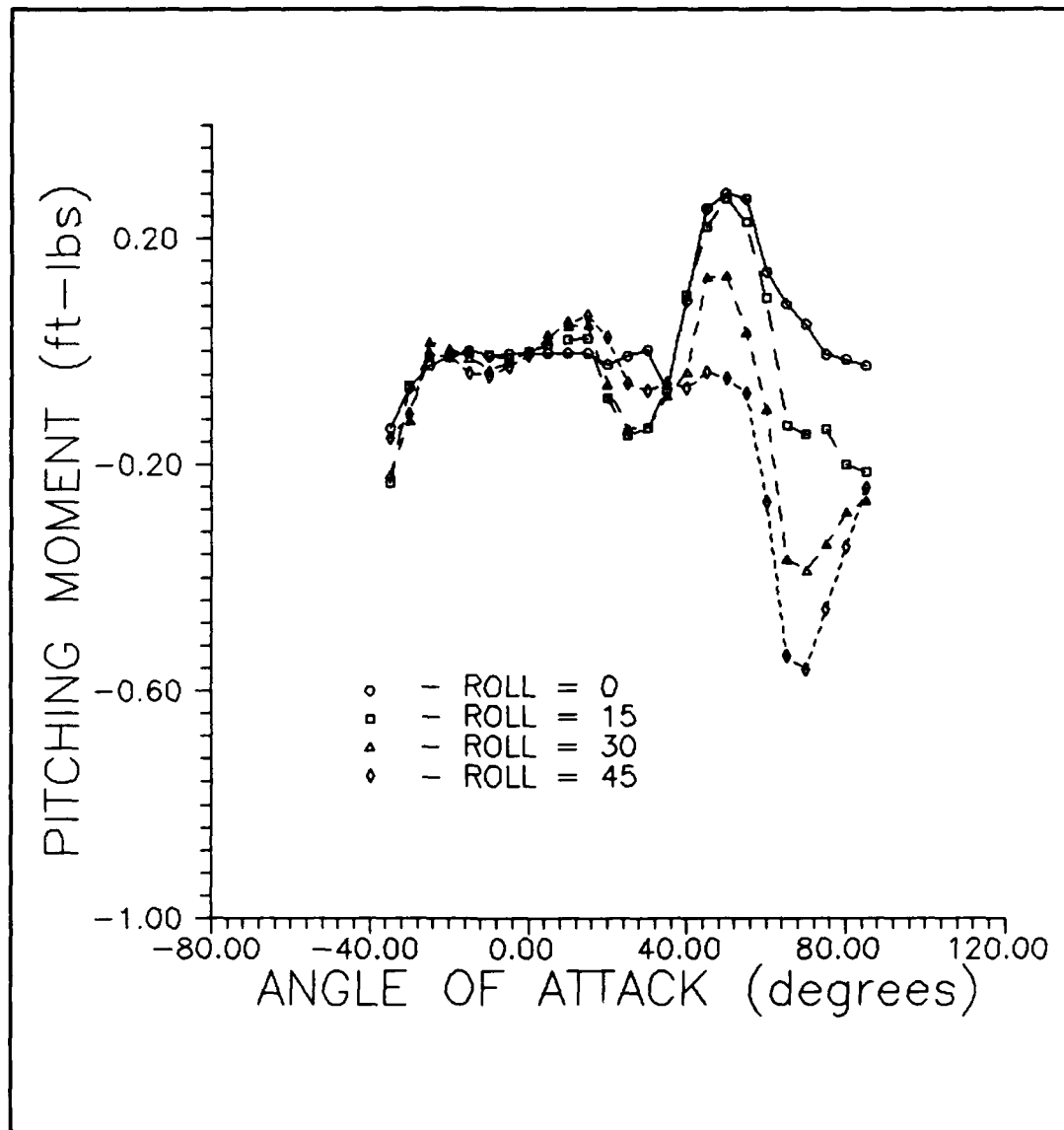
Figure 141. Pitching Moment (Roll)

146
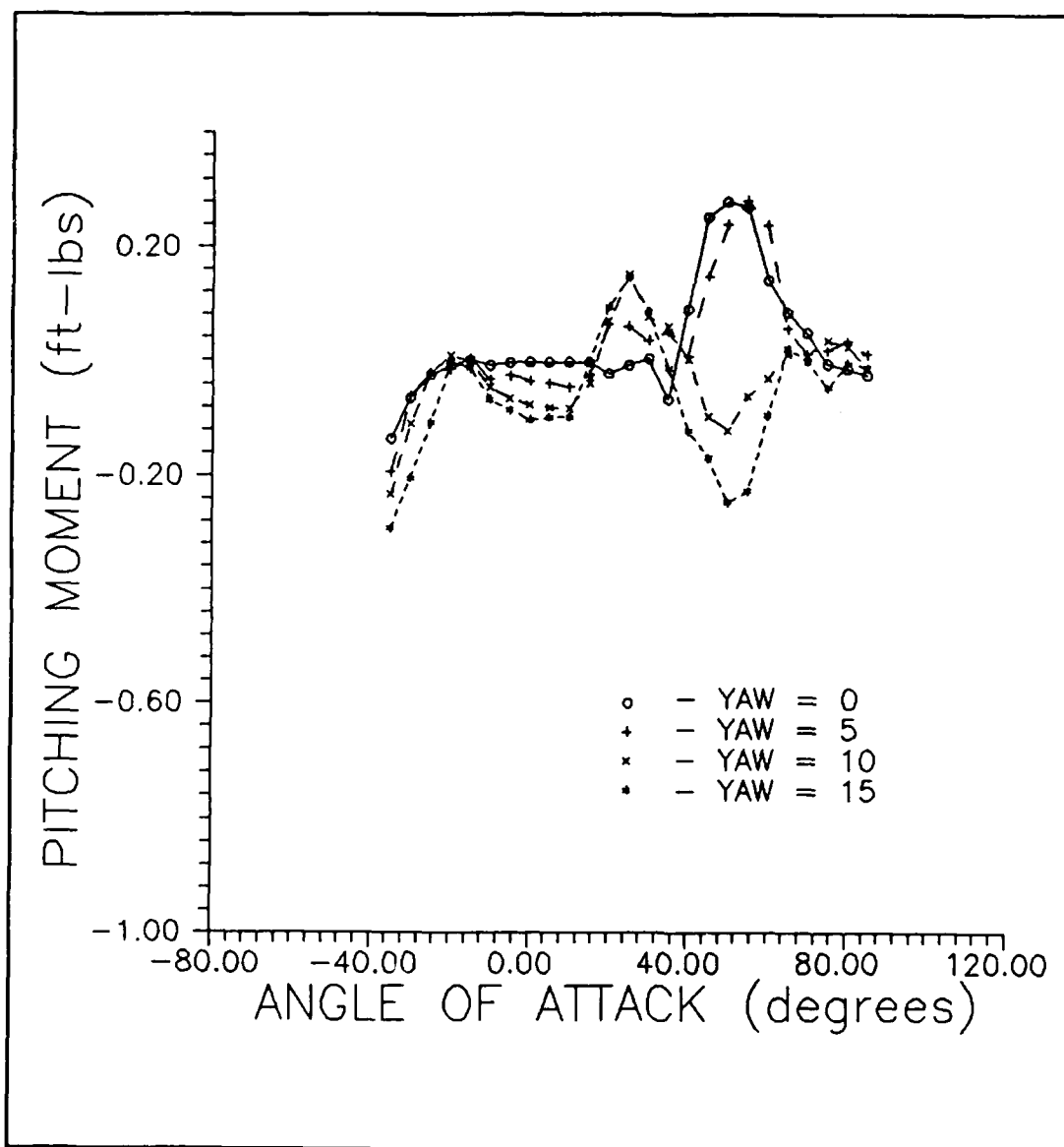
Figure 142. Pitching Moment (Yaw)

147

APPENDIX G
FORCE AND MOMENT COEFFICIENT DATA
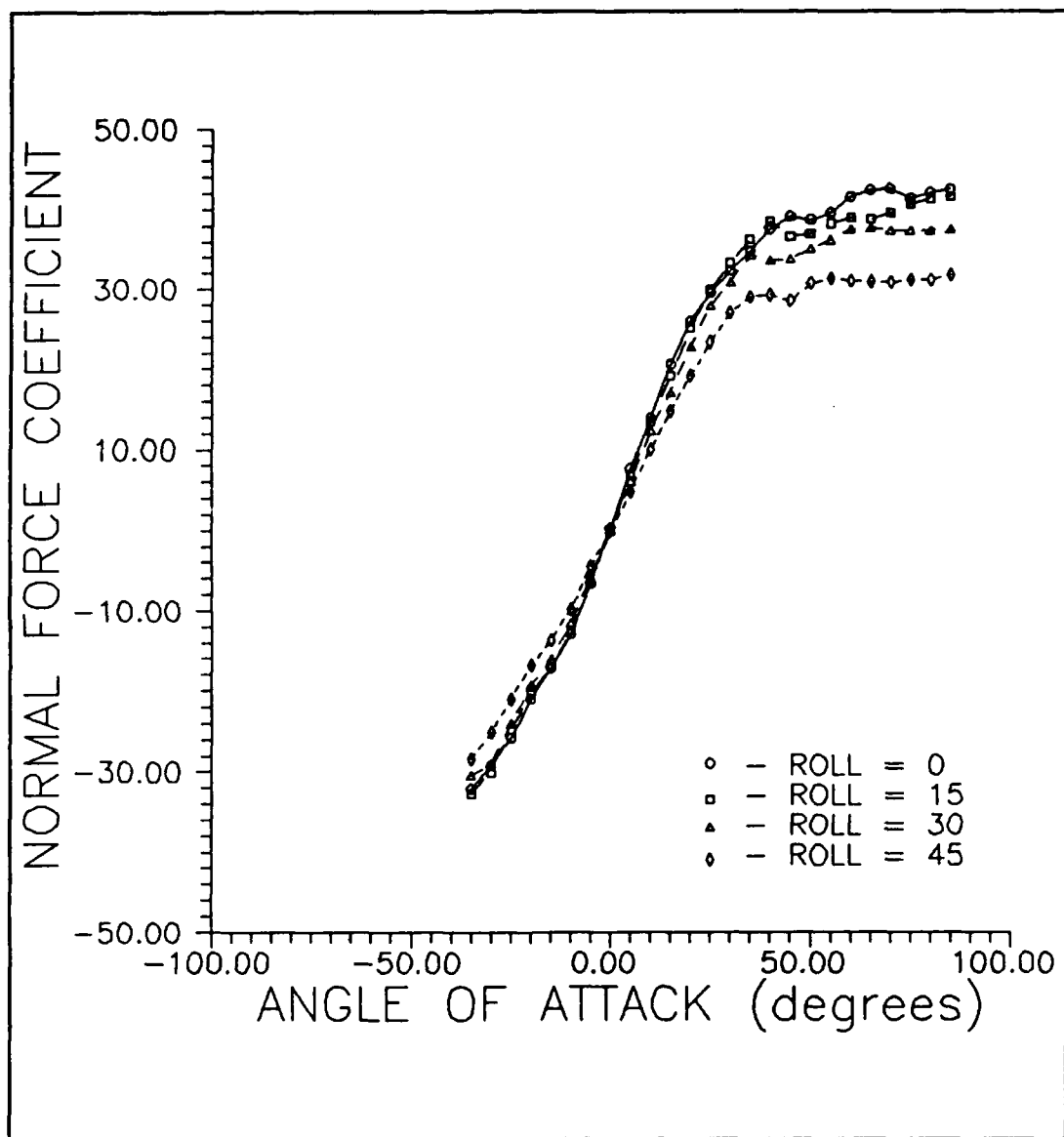
Figure 143. Normal Force Coefficient (Roll)

148
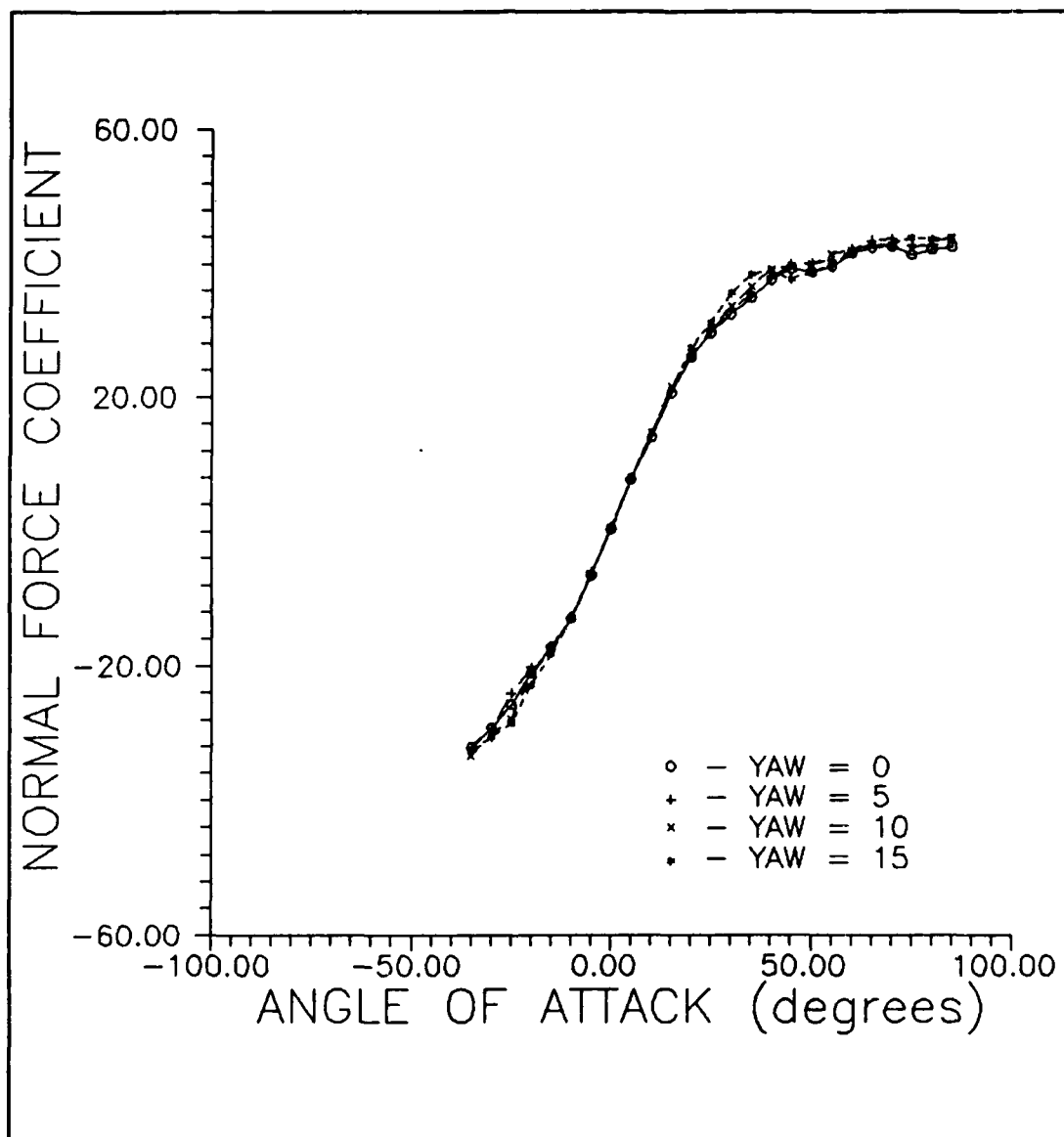
Figure 144. Normal Force Coefficient (Yaw)

149
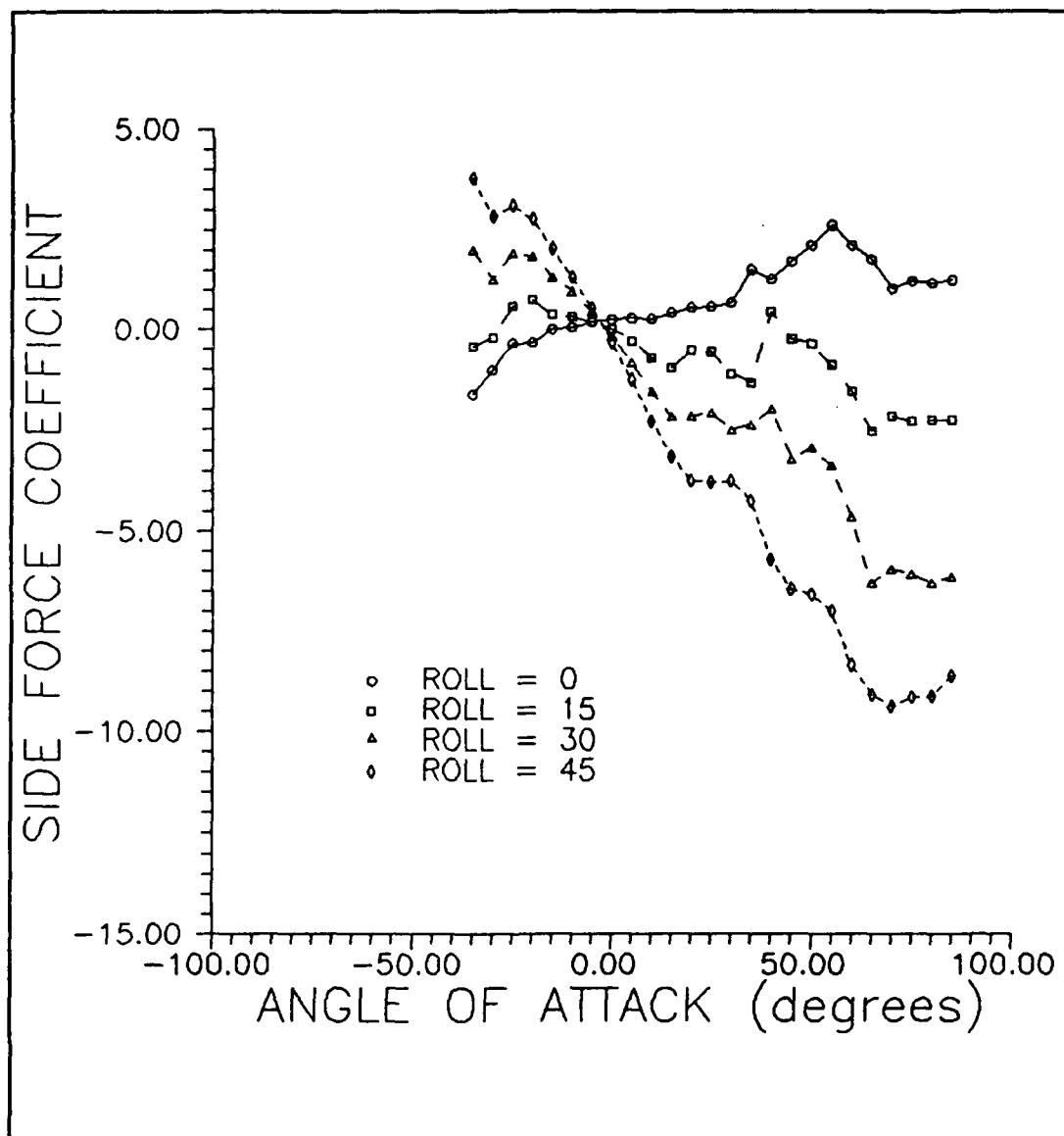
Figure 145. Side Force Coefficient (Roll)

150
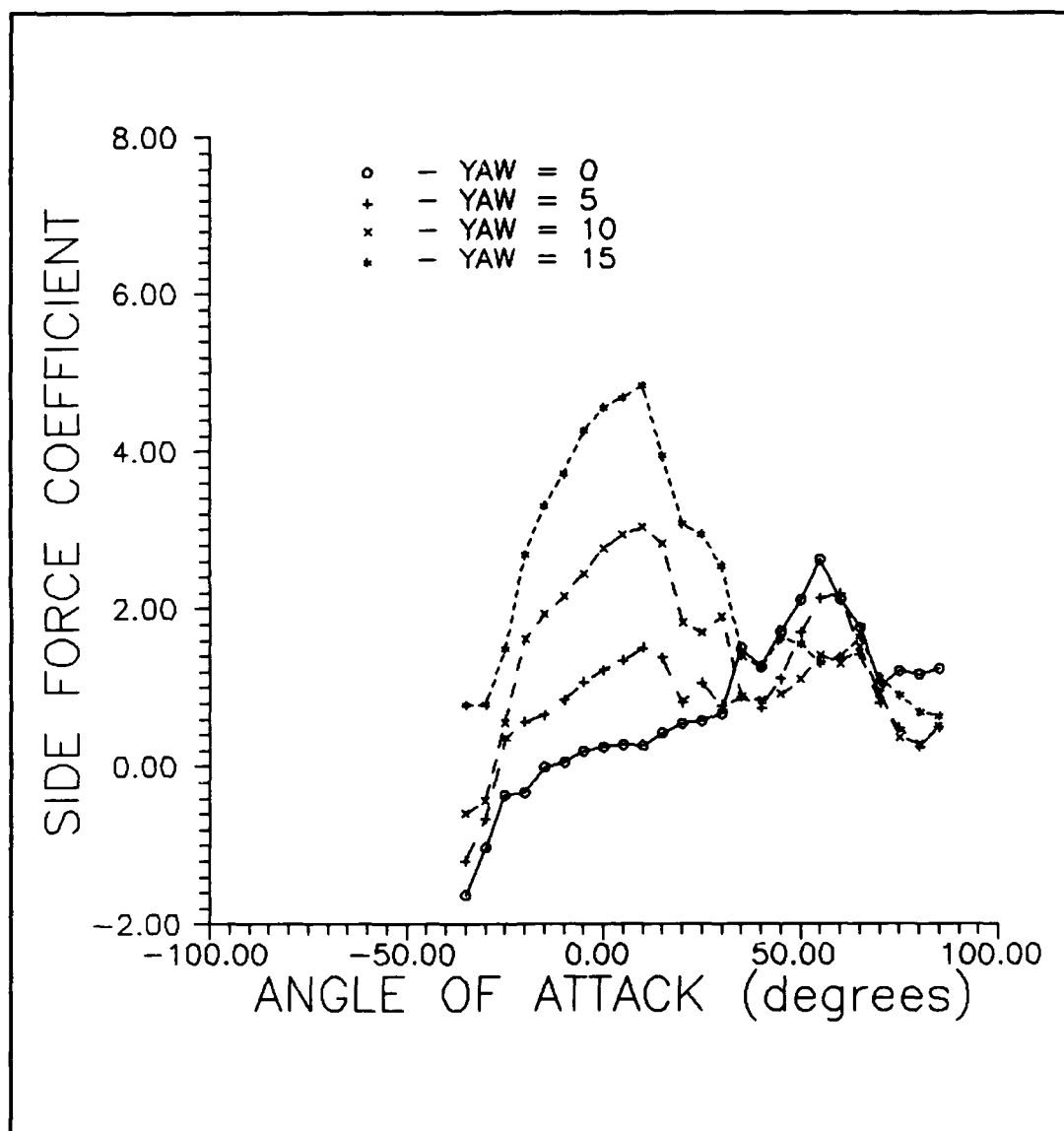
Figure 146. Side Force Coefficient (Yaw)
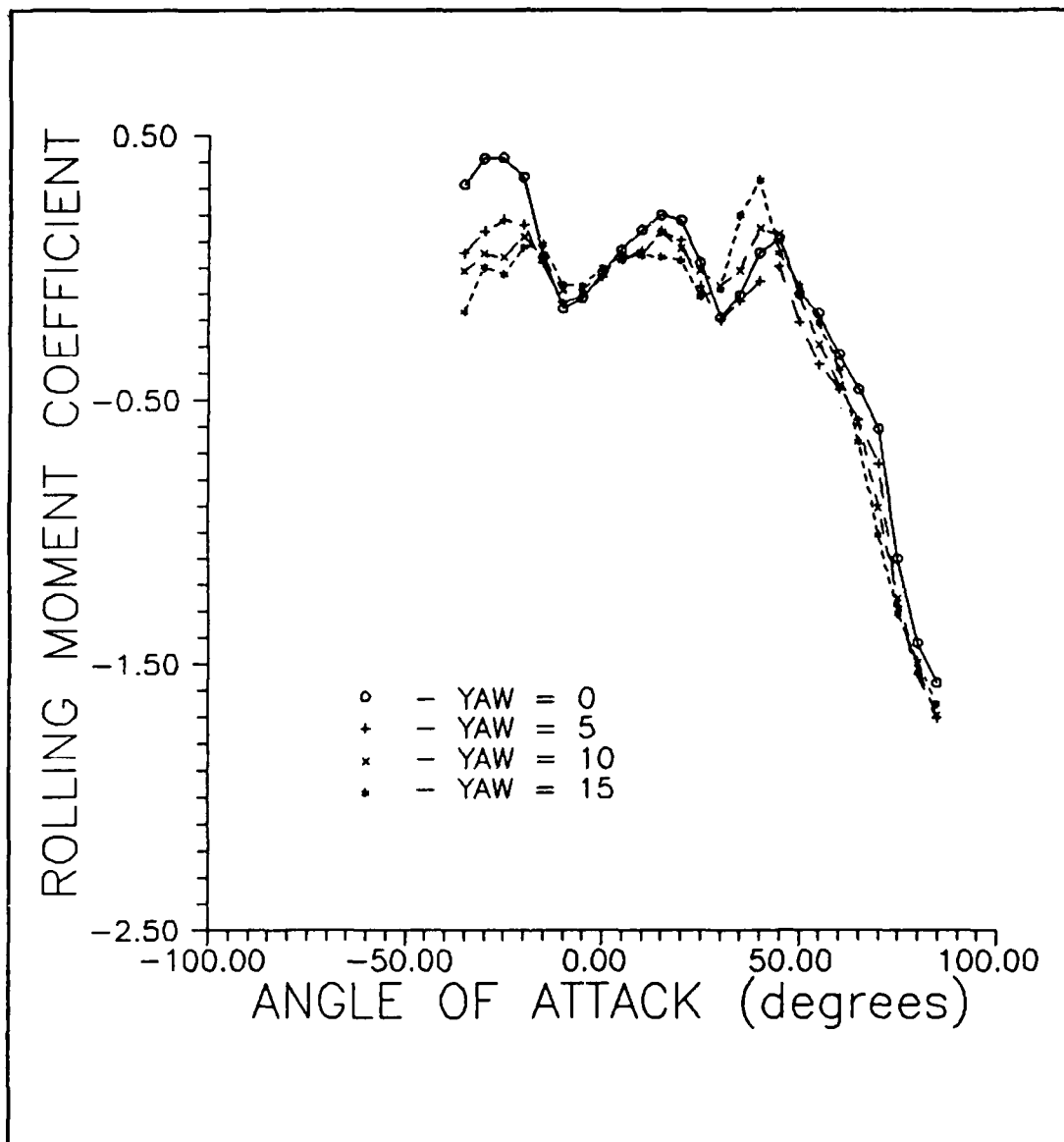
151
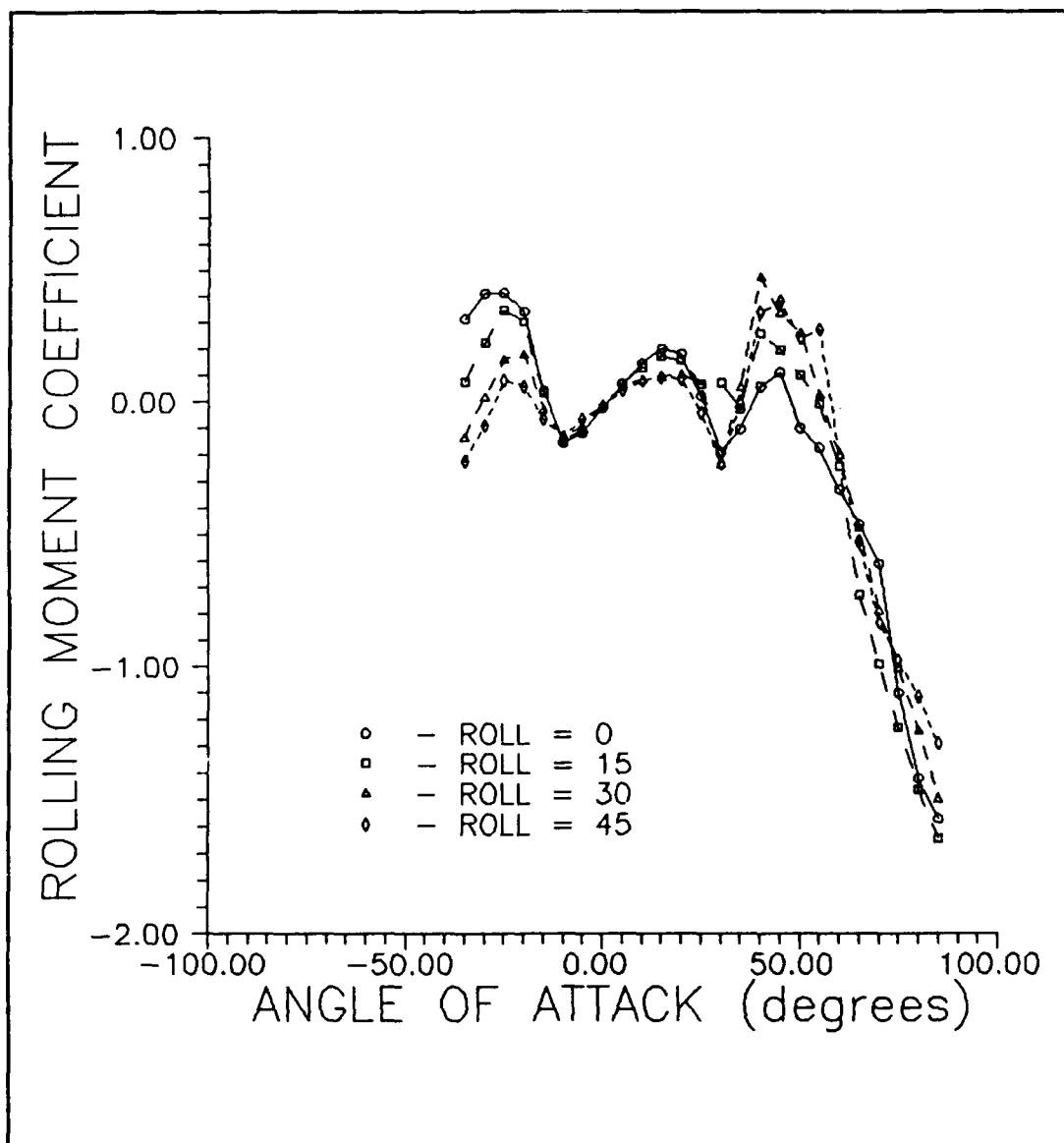
Figure 147. Rolling Moment Coefficient (Roll)

152

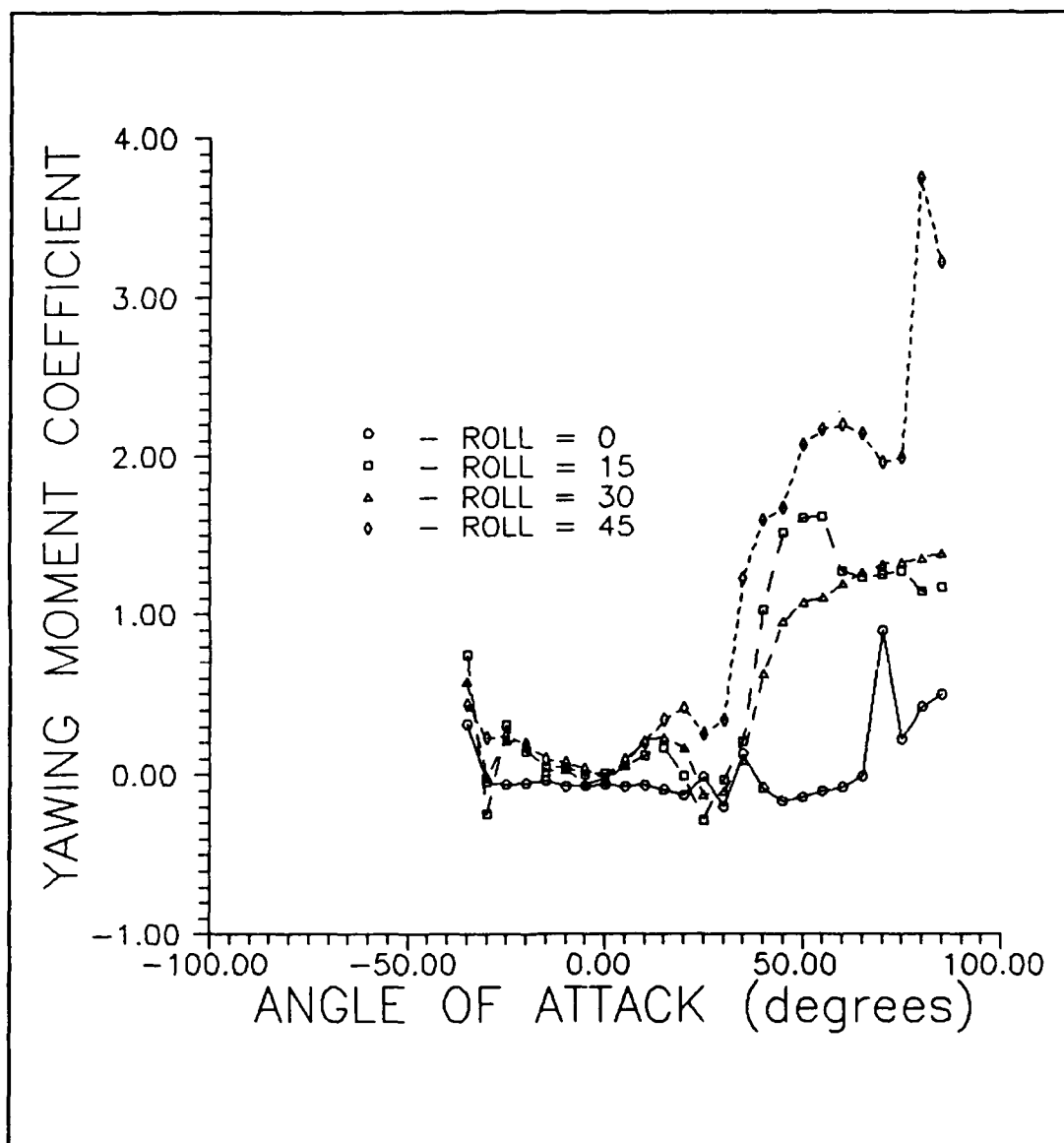**Figure 148.** Rolling Moment Coefficient (Yaw)

Figure 149. Yawing Moment Coefficient (Roll)
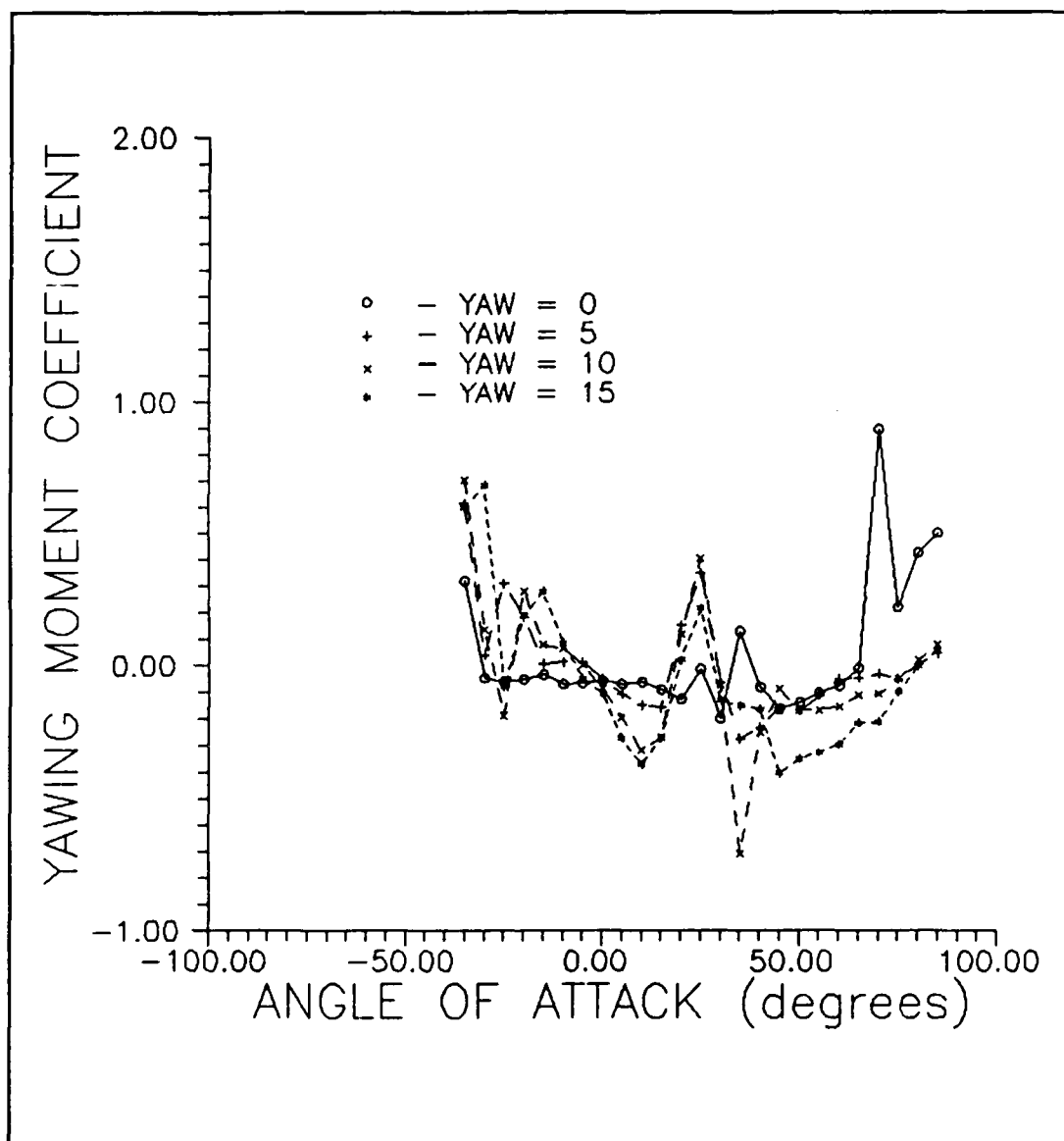
154

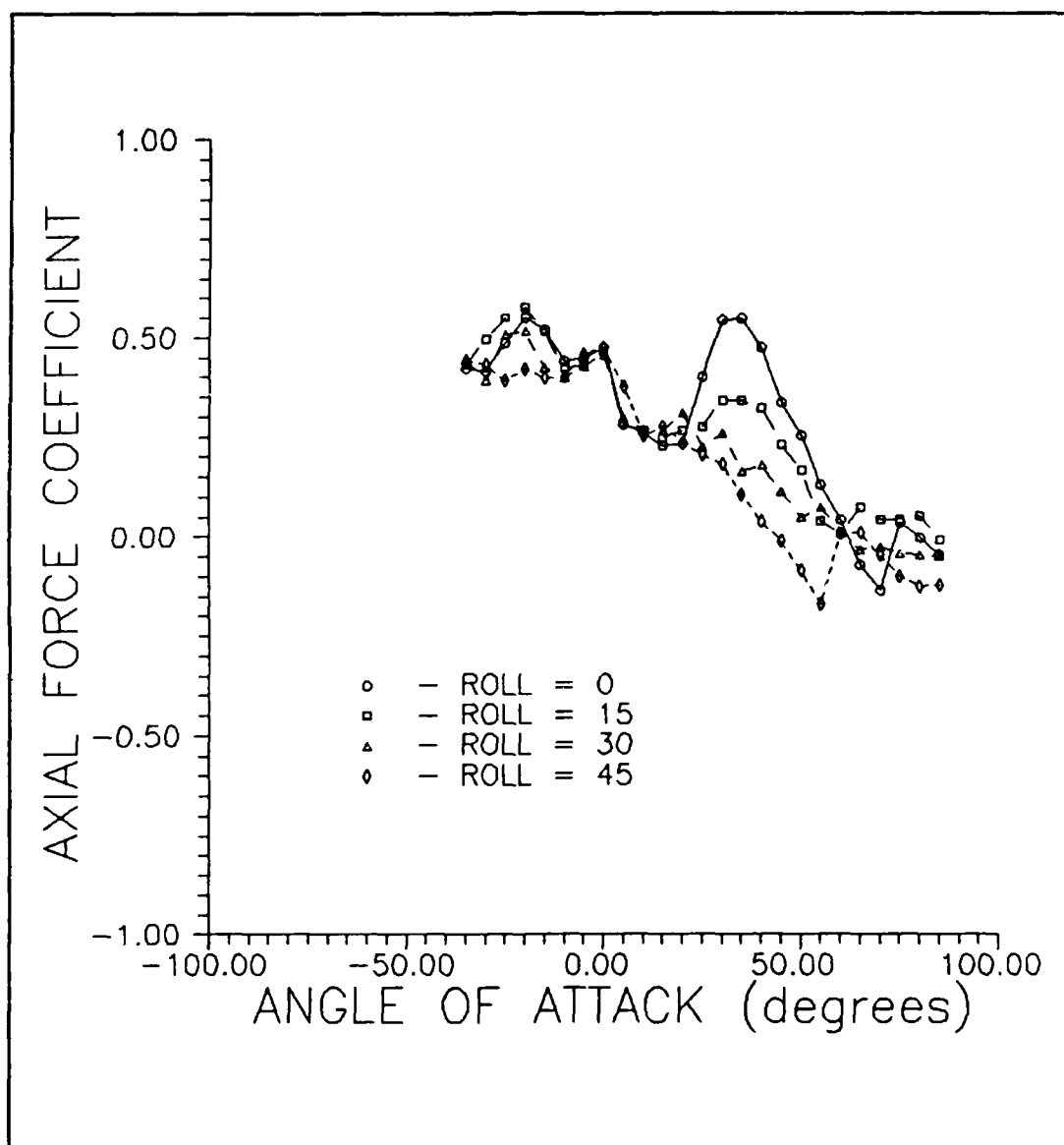**Figure 150.** Yawing Moment Coefficient (Yaw)
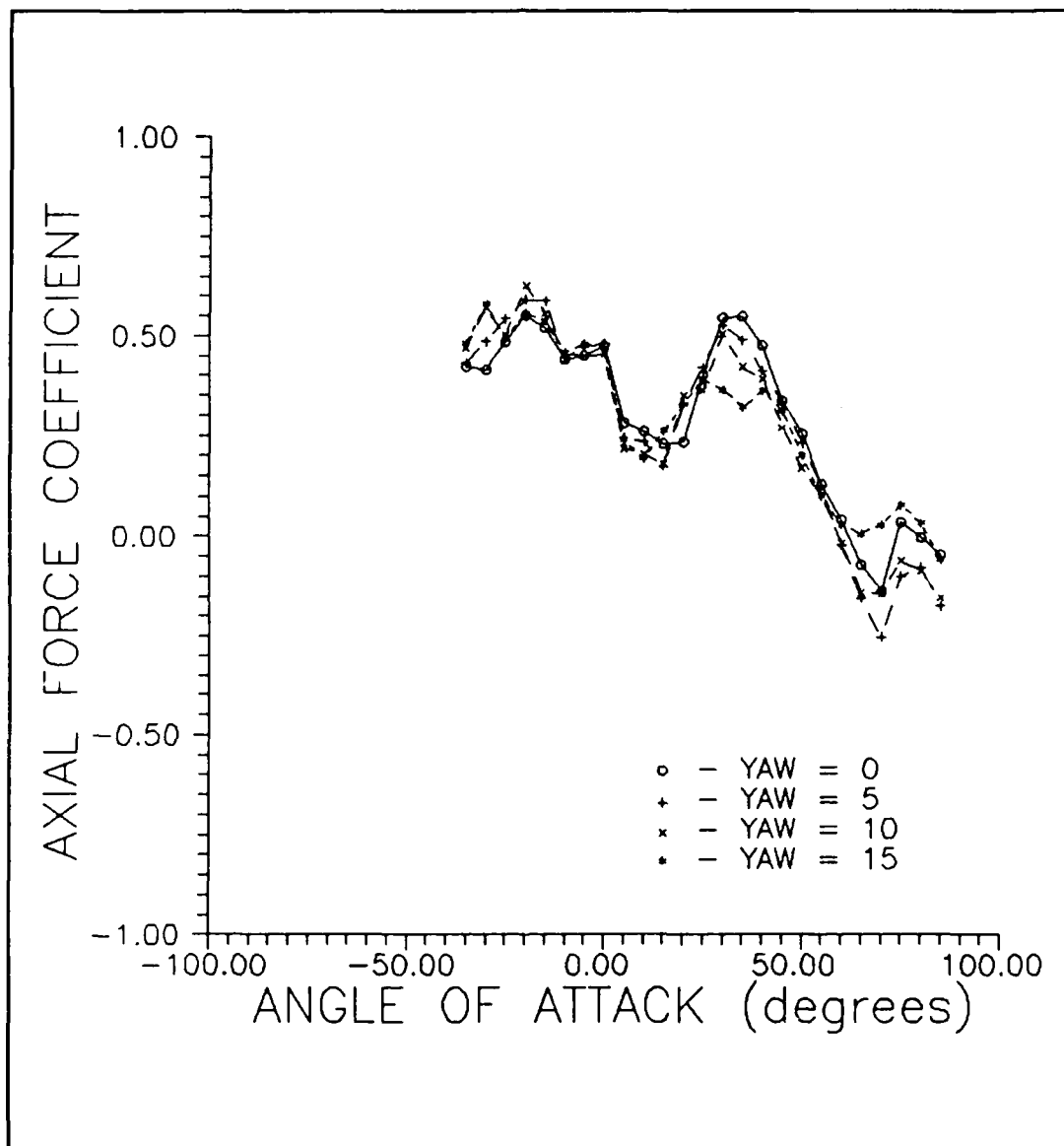
155

Figure 151. Axial Force Coefficient (Roll)

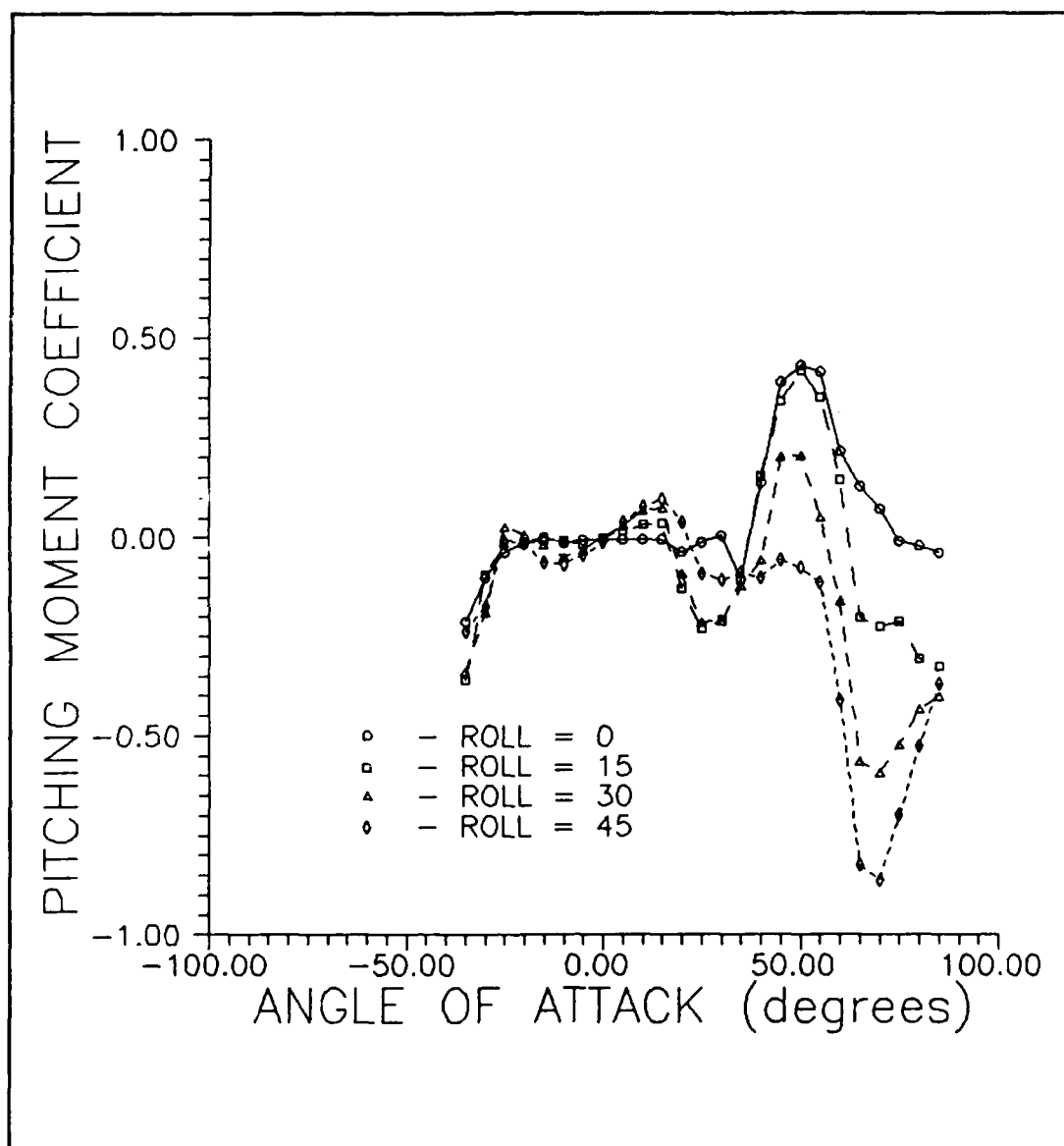**Figure 152.** Axial Force Coefficient (Yaw)

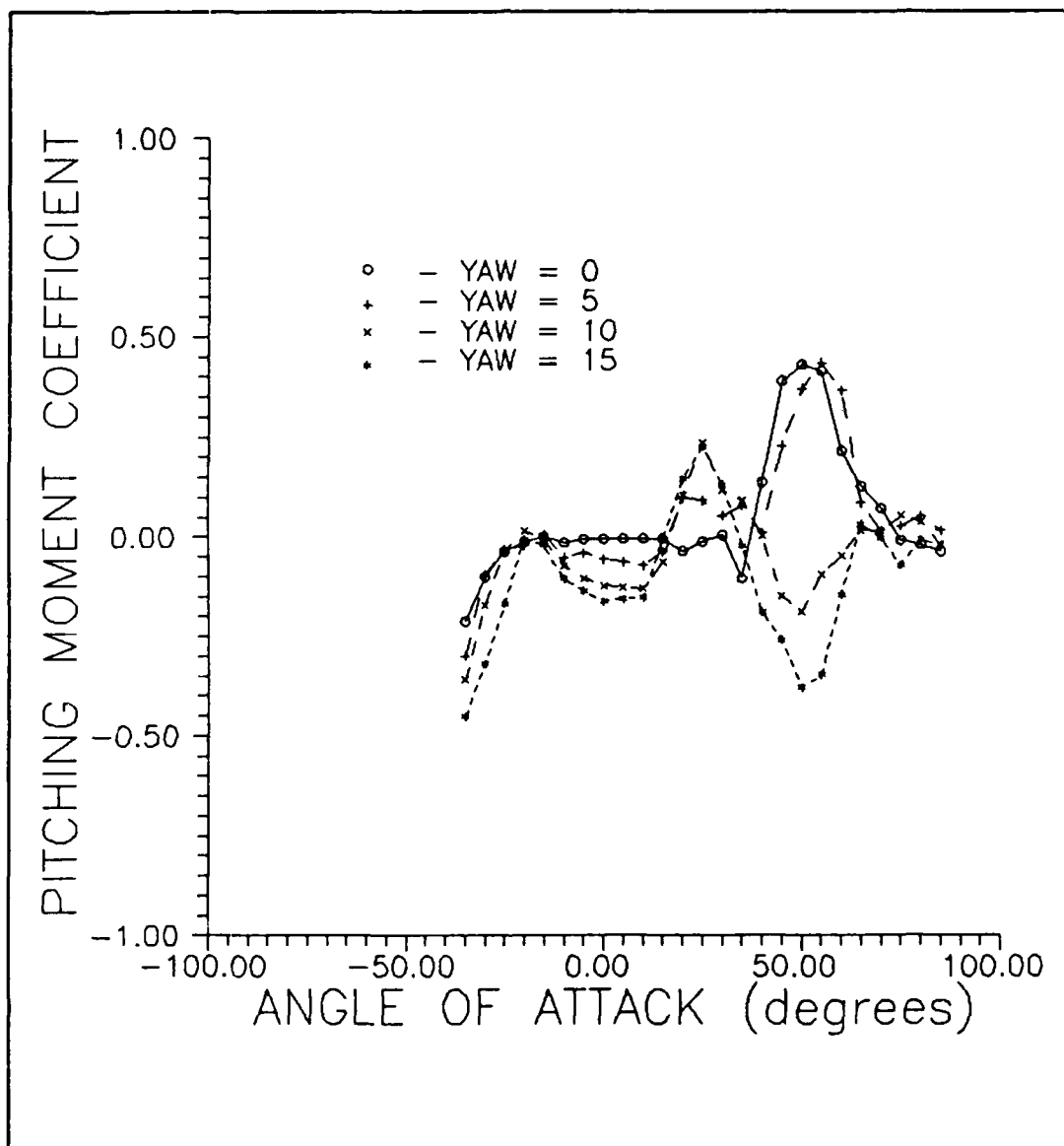**Figure 153.** Pitching Moment Coefficient (Roll)

Figure 154. Pitching Moment Coefficient (Yaw)

159

INITIAL DISTRIBUTION LIST

1. Defense Technical Information Center   2
   Cameron Station
   Alexandria, Virginia   22304-6145

2. Library, Code 0142   2
   Naval Postgraduate School
   Monterey, California   93943-5002

3. S. K. Hebbar, Code 67Hb   11
   Department of Aeronautics and Astronautics
   Naval Postgraduate School
   Monterey, California   93943-5000

4. E. R. Wood, Chairman   1
   Department of Aeronautics and Astronautics
   Naval Postgraduate School
   Monterey, California   93943-5000

5. RADM R. C. Austin, Superintendent   1
   Naval Postgraduate School
   Monterey, California   93943-5000

6. M. F. Platzer, Code 67Pr   1
   Department of Aeronautics and Astronautics
   Naval Postgraduate School
   Monterey, California   93943-5000

7. D. H. Leedy   3
   Naval Plant Representative Office
   Grumman Corporation
   Bethpage, New York   11714-3593

8. J. King, Code 67Jk   1
   Department of Aeronautics and Astronautics
   Naval Postgraduate School
   Monterey, California   93943-5000

9. D. P. Bence   1
   Chief, Applied Aerodynamics Branch
   NASA Ames Research Center (M.S. 227-6)
   Moffet Field, California   94035

10. S. Davis   1
    Chief, Fluid Mechanics Laboratory
    NASA Ames Research Center (M.S. 260-1)
    Moffet Field, California   94035

11. D. L. Antani   1
    Northrop Corporation
    Aircraft Division, Department 3811/82
    One Northrop Avenue
    Hawthorne, California   90250

12. G. Ericson   1
    Mail Stop 294
    NASA Langley Research Center
    Hampton, Virginia   23665

13. Naval Air Systems Command   1
    Attn: Tom Momiyama
    Code 931
    Washington, DC   20361-9320

14. Naval Air Systems Command   1
    Attn: Harry Berman, Program Manager
    AIR 931K
    Washington, DC   20361-9320

15. Office of Naval Research   1
    Attn: Spiro Lekoudis, Program Manager
    Code 1132F
    800 North Quincy Street
    Arlington, Virginia   22217-5000

16. David Taylor, NRSDC, Code 8   1
    Attn: Jim Nichols
    Aviation and Surface Effects Department
    Bethesda, Maryland   20084